

# Quantum Chemical Calculations of EPR Parameters using Density Functional Methods

Dissertation  
zur Erlangung des Doktorgrades  
der Naturwissenschaften

Vorgelegt beim Fachbereich 14  
der Johann Wolfgang Goethe-Universität  
in Frankfurt am Main

von  
Jörg Fritscher  
aus Fulda

Frankfurt 2006  
(D 30)

Vom Fachbereich Chemische und Pharmazeutische Wissenschaften der  
Johann Wolfgang Goethe-Universität Frankfurt als Dissertation angenommen.

Dekan: Prof. Dr. Harald Schwalbe

Gutachter: Prof. Dr. Thomas F. Prisner  
Prof. Dr. Martin Kaupp  
Prof. Dr. Harald Schwalbe

Datum der Disputation: 14.09.2006





*“The fact is, there has been a split of chemistry into two schools since the intrusion of the Arrhenic faith, rather it should be said, the addition of a new class of worker into our profession – people without knowledge of the laboratory arts and with sufficient mathematics at their command to be led astray by curvilinear agreements; without the ability to criticise, still less of giving any chemical interpretation. The fact is, the physical chemists never use their eyes and are most lamentably lacking in chemical culture. It is essential to cast out from our midst, root and branch, this physical element and return to our laboratories.”*

H. ARMSTRONG, 1936

*“I think that what could be an elegant piece of work has been turned into an inconclusive paper with no impact.”*

REVIEWER 67, DECEMBER 2004

*“I have an old belief that a good observer really means a good theorist.”*

CHARLES DARWIN, 1860



Meiner Familie



# Abstract

One of the most important tasks in *chemistry* and especially in *structural biology* has always been the elucidation of three-dimensional molecular structures – either of small molecules or large biopolymers. Among the (bio)physical methods to acquire structural data at atomic resolution *electron paramagnetic resonance* (EPR) spectroscopy is the most valuable technique for obtaining structural information about many different kinds of paramagnetic species. In biological systems, either paramagnetic metal ions/clusters, transient paramagnetic intermediates in electron transfer processes or artificially attached stable spin labels can be found.

The usual approach to interpret EPR spectra is to perform simulations based on the so-called *spin Hamiltonian* (SH). This means that the well-defined numerical parameters (tensors) in the SH representing different types of interaction are obtained by fitting the experimental data. The SH parameters include electronic *g*-values, hyperfine coupling (HFC) and quadrupole coupling (QC) constants, zero-field splittings and constants to describe exchange and dipolar interactions between electron spin systems. However, since the SH only contains spin degrees of freedom, a direct translation of the SH EPR parameters into structural information is not straightforward. Therefore, methods to predict such SH interaction parameters starting from molecular structures are required.

In this thesis it was investigated whether quantum chemical calculations of EPR parameters based on *density functional theory* (DFT) methods may be employed to overcome these problems thus enabling a correlation of experimental EPR data with molecular structure. It was the central goal of this work to point out the potential of a fruitful interplay between quantum chemistry and experiment and to study how both can benefit from each other.

For this purpose DFT methods were applied to a variety of *organic radical* or *transition metal* systems to calculate different EPR parameters.

Using the ‘broken symmetry’ formalism it was possible to compute the exchange coupling constant for a nitroxide biradical and furthermore decompose the exchange mechanism in different through-bond and through-space interactions.

Spin density distributions,  $^{14}\text{N}$  and  $^1\text{H}$  HFC constants as well as dipole moments and polarizabilities were computed for a number of aromatic nitroxides to examine their properties and select promising candidates which may serve as DNA-intercalating spin labels.

Systematic investigations of the influence of hydrogen bond geometry on the  $^{14}\text{N}$  QC parameters for imidazole–water and methylimidazole–benzosemiquinone complexes lead to the conclusion that especially the imidazole amino nitrogen QC parameters are very sensitive probes of the bond geometry, in particular of the hydrogen bond length. The results of this study may be applied to biological systems, e.g. to gain structural information about quinone binding sites.

Moreover, quantum chemical methods were applied to elucidate the structure of a nitrogen-centered radical intermediate in the inhibition process of ribonucleotide reductase (RNR). It was possible to find a molecular structure in accordance with all experimentally available data, thus revealing the long-sought structure of the  $\text{N}^\bullet$  radical and providing evidence for the trapping of a 3'-ketonucleotide in the reduction process catalyzed by RNR.

To test the capability of modern DFT methods to predict  $g$ - and molybdenum HFC tensors for  $\text{Mo}^{\text{V}}$  complexes, validation studies were carried out. Comparison of computed EPR parameters of a number of  $\text{Mo}^{\text{V}}$  compounds with corresponding experimental values showed that  $g$ - and HFC tensors could be predicted in good accuracy, although some systematic errors of the computational methods have to be considered for such heavy  $4d^1$  transition metal systems.

Furthermore, DFT calculations on a  $\text{Mn}^{2+}$  binding site model of the hammerhead ribozyme allowed to conclude that the structure of the binding site as studied by EPR spectroscopy in frozen solution is very likely to be identical to the site found occupied by  $\text{Mn}^{2+}$  in crystals.

Finally, computational methods were employed to aid in the structural characterization of the  $\text{Mn}^{2+}$  binding site in Ras (rat sarcoma protein) by providing accurate starting parameters for spectral simulations and furthermore helping to interpret the experimental data.

In conclusion, it was demonstrated in this thesis that the combination of sophisticated experimental and quantum chemical methods represents a powerful approach in the field of EPR spectroscopy and that it may be essential to employ EPR parameter computations to extract the full information content from EPR spectra. Therefore, great potential lies in future applications of DFT methods to the large number of systems where detailed and reliable experimental data is available but where an unequivocal correlation of these data with structural information is still lacking.

# Contents

<b>1</b>	<b>Zusammenfassung</b>	<b>1</b>
	References . . . . .	5
<b>2</b>	<b>Introduction</b>	<b>7</b>
	2.1 Background and Motivation . . . . .	7
	2.2 Objectives of this Work . . . . .	13
	2.3 Publications and Conference Contributions . . . . .	15
	References . . . . .	21
<b>3</b>	<b>Theory of Electron Paramagnetic Resonance Parameters</b>	<b>29</b>
	3.1 The Spin Hamiltonian Concept . . . . .	29
	3.2 Non-Relativistic Quantum Theory . . . . .	34
	3.3 Relativistic Quantum Theory . . . . .	35
	3.4 The Breit–Pauli Hamiltonian . . . . .	42
	3.5 Effective Hamiltonians and Perturbation Theory . . . . .	49
	3.6 Sum-Over-States Perturbation Expressions for EPR Parameters . . . . .	51
	3.7 Calculation of Electric Field Gradients and Quadrupole Couplings . . . . .	57
	3.8 Calculation of Exchange Interactions . . . . .	58
	3.9 Computational Approaches to EPR Parameters . . . . .	59
	References . . . . .	63
<b>4</b>	<b>Computational Methods</b>	<b>67</b>
	4.1 Hartree–Fock Approximation and Electron Correlation . . . . .	67
	4.2 Coupled Cluster Methods . . . . .	71
	4.3 Density Functional Theory . . . . .	73
	4.4 Exchange–Correlation Functionals . . . . .	79
	4.5 Basis Sets . . . . .	81
	4.6 Computational Chemistry Program Packages . . . . .	85

---

References . . . . .	85
<b>5 Summary of Results and Discussion</b>	<b>91</b>
5.1 Organic Radicals in Model Systems . . . . .	92
5.1.1 Theoretical Investigation of the Exchange Coupling Mechanisms for a Nitroxide Biradical . . . . .	92
5.1.2 Spin Density Distributions and Hyperfine Couplings for Aromatic Nitroxides . . . . .	96
5.1.3 Influence of Hydrogen Bond Geometry on Quadrupole Coupling Parameters of Imidazole Complexes . . . . .	100
5.2 Organic Radicals in Biological Systems . . . . .	103
5.2.1 Structure of the Nitrogen-Centered Radical Formed During Inactivation of RNR by N <sub>3</sub> UDP . . . . .	103
5.3 Transition Metals in Model Complexes . . . . .	109
5.3.1 Computational Studies of <i>g</i> -Tensors and Molybdenum Hyperfine Couplings for Paramagnetic Molybdenum Complexes . . . . .	109
5.4 Transition Metals in Biological Systems . . . . .	122
5.4.1 Structural Characterization of a Mn <sup>2+</sup> Binding Site in the Hammerhead Ribozyme . . . . .	122
5.4.2 Structural Characterization of the Metal Binding Site in Ras125 . . . . .	125
References . . . . .	128
<b>6 Publications</b>	<b>139</b>
6.1 Synthesis, Structure and Magnetic Properties of a Novel Nitroxide Biradical. Theoretical Investigation of the Exchange Mechanisms . . . . .	141
6.2 Synthesis of Novel Aromatic Nitroxides as Potential DNA Intercalators. An EPR Spectroscopic and DFT Computational Study . . . . .	145
6.3 Structural Investigations of a High-Affinity Mn <sup>II</sup> Binding Site in the Hammerhead Ribozyme by EPR Spectroscopy and DFT Calculations. Effects of Neomycin B on Metal-Ion Binding . . . . .	149
6.4 Influence of Hydrogen Bond Geometry on Quadrupole Coupling Parameters: A Theoretical Study of Imidazole-Water and Imidazole-Semiquinone Complexes . . . . .	153
6.5 Structure of the Nitrogen-Centered Radical Formed During Inactivation of <i>E. coli</i> Ribonucleotide Reductase by 2'-Azido-2'-deoxyuridine-5'-diphosphate: Trapping of the 3'-Ketonucleotide . . . . .	157

---

6.6	High-Frequency 94 GHz ENDOR Characterization of the Metal Binding Site in Wild-Type Ras•GDP and Its Oncogenic Mutant G12V in Frozen Solution . . . . .	161
6.7	Computational Studies of EPR Parameters for Paramagnetic Molybdenum Complexes. I. Method Validation on Small and Medium-Sized Systems . . . . .	165
6.8	Computational Studies of EPR Parameters for Paramagnetic Molybdenum Complexes. II. Larger Mo <sup>V</sup> Systems Relevant to Molybdenum Enzymes . . . . .	169
<b>7</b>	<b>General Conclusions</b>	<b>173</b>
	References . . . . .	175
<b>A</b>	<b>Abbreviations</b>	<b>179</b>
<b>B</b>	<b>Constants and Conversion Factors</b>	<b>183</b>
	<b>Acknowledgment</b>	<b>185</b>
	<b>Lebenslauf</b>	<b>187</b>



*“Die Maschine wird alles tun können,  
sie wird alle Probleme, die man ihr  
stellt, lösen können, aber sie wird  
niemals ein Problem zu stellen  
vermögen.”*

A. EINSTEIN, 1879–1955

# Chapter 1

## Zusammenfassung

Eine der wichtigsten Aufgaben der *Chemie* und besonders der *Strukturbiologie* ist es, dreidimensionale molekulare Strukturen von kleinen Molekülen oder großen Biopolymeren aufzuklären. Unter den (bio)physikalischen Methoden zur Strukturuntersuchung mit atomarer Auflösung ist die *elektronenparamagnetische Resonanzspektroskopie* (EPR-Spektroskopie) [1–5] das wichtigste Werkzeug, um strukturelle Informationen über viele verschiedene Arten von paramagnetischen Spezies zu gewinnen. In biologischen Systemen findet man paramagnetische Metallionen oder Metallcluster, transiente paramagnetische Intermediate in Elektronentransferprozessen oder künstlich angebrachte Spinlabel [1–4, 6].

Zur Analyse von EPR-Spektren versucht man in der Regel, diese mit Hilfe des sogenannten *Spin-Hamiltonoperators* (SH-Operators) zu simulieren. Dies bedeutet, dass man die im SH-Operator definierten numerischen Parameter (Tensoren), die verschiedene physikalische Wechselwirkungen repräsentieren, durch Anpassung an die experimentellen Daten bestimmt. Zu den SH-Parametern gehören elektronische  $g$ -Werte, Hyperfeinwechselwirkungs- (HFC) und Quadrupolkopplungskonstanten (QC-Konstanten), Nullfeldaufspaltungen und Konstanten, die die Austausch- und dipolaren Wechselwirkungen zwischen Elektronenspins beschreiben. Da der SH-Operator allerdings nur Spinfreiheitsgrade und das äußere Magnetfeld beinhaltet, ist eine direkte Übersetzung der SH-EPR-Parameter in Strukturinformationen oft schwierig. Aus diesem Grund benötigt man Methoden, um die SH-Parameter ausgehend von molekularen Strukturen vorhersagen zu können.

In dieser Arbeit wurde daher untersucht, ob quantenchemische Berechnungen von EPR-Parametern [7–9], die auf *Dichtefunktionaltheorie* (DFT) basieren,

verwendet werden können, um die beschriebenen Probleme zu lösen und eine Korrelation zwischen experimentellen EPR-Daten und molekularer Struktur zu erreichen. Das zentrale Ziel dieser Arbeit war es, das große Potential des Zusammenspiels von Quantenchemie und Experiment herauszustellen und zu untersuchen, wie beide Methoden voneinander profitieren können.

Zu diesem Zweck wurden DFT-Methoden auf verschiedene paramagnetische Systeme angewendet, um deren EPR-Eigenschaften zu berechnen. Die untersuchten Systeme können grob in *organische Radikale* und *Übergangsmetallkomplexe* eingeteilt werden, wobei diese beiden Systemklassen weiter in Modellsysteme und biologische Systeme unterteilt werden können. Die Studien, die im Rahmen dieser Arbeit an Vertretern der einzelnen Systemklassen durchgeführt wurden, werden im Folgenden kurz beschrieben.

Unter Verwendung des ‘Broken-Symmetry’-Formalismus war es möglich, die Austauschwechselwirkungskonstante für ein Nitroxidbiradikal in guter Übereinstimmung mit EPR- und magnetischen Messungen zu berechnen [10]. Außerdem konnte die Wechselwirkung im Detail analysiert und mit Hilfe von Rechnungen an verschiedenen Modellsystemen in Anteile, die durch den Raum bzw. durch Bindungen vermittelt werden, aufgeteilt werden. Diese Art des Einblicks in die physikalischen Prozesse, die zu den beobachteten magnetischen Eigenschaften führen, kann auf experimentellem Weg oft gar nicht oder nur sehr schwierig erhalten werden. Daher stellt die Möglichkeit solcher Analysen einen Vorteil quantenchemischer Methoden dar.

In einem weiteren Projekt wurden für eine Reihe von aromatischen Nitroxiden Spindichteverteilungen,  $^{14}\text{N}$ - und  $^1\text{H}$ -HFC-Konstanten sowie Dipolmomente und Polarisierbarkeiten vorhergesagt, um deren strukturelle, elektronische und magnetische Eigenschaften zu untersuchen und solche Verbindungen herauszusortieren, die als DNA-interkalierende Spinlabel geeignet sein könnten [11]. Auch in diesem Fall war die Übereinstimmung der berechneten EPR-Parameter mit den experimentell gefundenen Werten gut.

Mittels systematischer Untersuchungen des Einflusses von Wasserstoffbrückengeometrien auf  $^{14}\text{N}$ -QC-Parameter an Imidazol–Wasser- und Methylimidazol–Benzosemichinon-Systemen [12] konnte herausgefunden werden, dass insbesondere die Aminostickstoff-QC-Parameter sehr empfindliche Indikatoren für die Geometrie der Wasserstoffbrückenbindung sind. Besonders großen Einfluss auf die QC-Parameter hat hierbei die Länge der Wasserstoffbrücke. Die Ergebnisse dieser Studie können auch auf biologische Systeme angewandt werden, z.B. um

Einblicke in die Struktur von Chinonbindungstaschen zu gewinnen. Es ist zudem anzumerken, dass theoretische Methoden eine einfache Möglichkeit bieten, solche systematischen Abhängigkeiten zwischen Moleküleigenschaften und strukturellen Parametern zu untersuchen, um allgemeingültige Korrelationen zu finden, die dann zur Unterstützung der Interpretation neuer experimenteller Daten dienen können. Experimentell ist es oft ungleich schwieriger und aufwendiger (wenn nicht sogar unmöglich), geeignete Modellsysteme zu synthetisieren und zu charakterisieren.

Im Zusammenhang mit der Anwendung von DFT-Methoden auf organische Radikale in biologischen Systemen wurden quantenchemische Berechnungen verwendet, um die Struktur eines stickstoffzentrierten Radikalintermediats des Inhibitionsprozesses von Ribonukleotidreduktase (RNR) aufzuklären [13]. Bei der Inkubation von RNR mit 2'-N<sub>3</sub>UDP findet eine Inaktivierung des Enzyms statt, die einhergeht mit der Bildung eines unbekanntes Radikals N<sup>•</sup>. Trotz intensiver experimenteller Bemühungen konnte während der letzten 20 Jahre keine eindeutige Zuordnung einer molekularen Struktur zu den vorhandenen experimentellen Daten über N<sup>•</sup> getroffen werden. In dieser Arbeit war es nun möglich, eine Molekülstruktur zu finden, deren berechnete Eigenschaften in Übereinstimmung mit den verfügbaren experimentellen Daten sind, und die daher der lange gesuchten Struktur des N<sup>•</sup>-Radikals entspricht. Dazu wurden im Wesentlichen <sup>17</sup>O- und <sup>14</sup>N-HFC-Konstanten für eine große Anzahl von Modellsystemen verschiedener Konstitution und Konformation berechnet und mit EPR-Resultaten verglichen. Diese Strukturaufklärung lieferte gleichzeitig wichtige Hinweise für das Auftreten eines 3'-Ketonukleotids im Reduktionsprozess, der von RNR katalysiert wird, und damit eine Bestätigung des von Stubbe et al. postulierten Reaktionsmechanismus (vgl. Ref. 13 und Referenzen darin).

In weiteren Projekten wurde untersucht, ob moderne DFT-Methoden geeignet sind, *g*- und Molybdän-HFC-Tensoren für Mo<sup>V</sup>-Komplexe vorherzusagen [14, 15]. Im Rahmen dieser Validierungsstudien wurden die EPR-Parameter für eine Reihe von Mo<sup>V</sup>-Spezies berechnet und mit experimentellen Daten verglichen. Zu den untersuchten Komplexen gehören auch viele größere Modellkomplexe, die synthetisiert worden waren, um die Eigenschaften von Molybdänbindungstaschen in Molybdoenzymen wie Sulfit-Oxidase oder Xanthin-Oxidase nachzubilden. Da für Molybdän keine Basissätze existierten, die speziell zur Berechnung von EPR-Parametern geeignet waren, wurde zunächst ein geeigneter Basissatz entwickelt, der dann als Standardbasis in allen weiteren Rechnungen verwendet wer-

den konnte. Für die Mo<sup>V</sup>-Komplexe wurde anschließend die Abhängigkeit der EPR-Parameter vom verwendeten Funktional und insbesondere vom Anteil der Beimischung von exaktem Hartree-Fock-Austausch untersucht. Desweiteren wurden auch Einflüsse von Spinbahnkorrekturen auf die HFC-Konstanten sowie von relativistischen Effekten höherer Ordnung auf die  $g$ -Werte bestimmt. Für einige der Komplexe wurden zudem die Beiträge einzelner Molekülorbitale sowie der Metall- / Liganden-Spinbahnkopplungen zum  $g$ -Tensor im Detail analysiert. Die Ergebnisse haben insgesamt gezeigt, dass sowohl  $g$ - und HFC-Werte als auch die relativen und absoluten Orientierungen der jeweiligen Tensoren unter Verwendung von Funktionalen mit 30–40% exaktem Austausch mit zufriedenstellender bis guter Genauigkeit vorhergesagt werden können – auch wenn einige systematische Fehler der theoretischen Methoden bei der Behandlung schwerer 4d<sup>1</sup>-Übergangsmetallsysteme berücksichtigt werden müssen. So spielen z.B. bei der Berechnung der  $\Delta g_{11}$ -Komponenten Spinbahneffekte höherer Ordnung eine Rolle, was dazu führt, dass diese Komponenten in nicht-relativistischen Rechnungen nicht ausreichend negativ sind. Zudem müssen für eine präzise Vorhersage der HFC-Konstanten Spinbahnkorrekturen berücksichtigt werden. Insgesamt zeigen die Validierungsstudien, dass DFT-Methoden im Prinzip in der Lage sind, auch solche komplizierten Übergangsmetallsysteme zu behandeln, und unterstreichen, dass zukünftige Anwendungen auf biologisch relevante Molybdänsysteme vielversprechend sind.

DFT-Rechnungen konnten in dieser Arbeit auch dazu eingesetzt werden, um zu zeigen, dass die Struktur der Mn<sup>2+</sup>-Bindungstasche im Hammerhead-Ribozym, die mittels EPR-Spektroskopie in gefrorener Lösung untersucht worden war, sehr wahrscheinlich identisch ist mit der Struktur der Bindungstasche, die in Kristallen gefunden worden war. Dazu wurden die HFC- und QC-Parameter für ein strukturelles Modell basierend auf der Hammerhead-Kristallstruktur berechnet und mit den experimentellen EPR-Daten verglichen [16]. Da beide Sätze von EPR-Parametern sehr ähnlich waren, konnte gefolgert werden, dass auch die dazugehörigen Strukturen sehr ähnlich sein müssen und somit die Bindungstaschengometrie in Lösung derjenigen im Kristall gleicht.

Schließlich war es in einem anderen Projekt möglich, mit Hilfe quantenchemischer Methoden die strukturelle Charakterisierung der Mn<sup>2+</sup>-Bindungsstelle in Ras ('rat sarcoma protein') zu unterstützen [17]. Hier sollte untersucht werden, ob sich die Ligandensphäre des Metallions im Wildtyp-Ras von der in der onkogenen G12V-Mutante unterscheidet bzw. ob im Wildtyp-Protein ein Wasserli-

gand durch eine Aminosäure oder ein Phosphation ersetzt wird. Ausgehend von Kristallstrukturmodellen von Ras wurden  $^{13}\text{C}$ -HFC-Rechnungen verwendet, um genaue Startparameter für die Simulation der Spektren zu erhalten und experimentelle Daten zu interpretieren. Damit konnte gezeigt werden, dass keine weitere Aminosäure im Wildtyp-Protein koordiniert ist. Weiterhin wurde in Ref. 17 auch ausgeschlossen, dass ein freies Phosphation an das  $\text{Mn}^{2+}$  gebunden ist.

Zusammengefasst wurden in dieser Arbeit verschiedene EPR-Parameter ( $g$ -Tensoren, HFC- und QC-Tensoren sowie Austauschwechselwirkungen) für ein breitgefächertes Spektrum paramagnetischer Spezies mittels DFT-Methoden berechnet. Für all die verschiedenen Projekte war es möglich, theoretische Methoden so einzusetzen, dass die Verbindung zwischen experimentellen spektroskopischen Daten und strukturellen Informationen hergestellt werden konnte. Weiterhin wurden in vielen Fällen tiefere Einblicke in die physikalischen Grundlagen und Mechanismen, die den Wechselwirkungen zu Grunde liegen, gewonnen.

In dieser Arbeit wurde demonstriert, dass die Kombination von modernen experimentellen und quantenchemischen Techniken eine leistungsfähige Methode im Zusammenhang mit der EPR-Spektroskopie darstellt und dass es unabdingbar sein kann, quantenchemische EPR-Parameterberechnungen durchzuführen, um den kompletten Informationsgehalt von EPR-Spektren auszuschöpfen. Aus diesem Grund liegt ein großes Potential in zukünftigen Anwendungen von DFT-Methoden auf die vielen (biologischen) Systeme, für die zwar detaillierte und zuverlässige experimentelle Daten vorliegen, bei denen aber eindeutige Korrelationen dieser Daten mit strukturellen Informationen noch immer fehlen.

## References

- [1] Berliner, L. J., Ed.; *Biological Magnetic Resonance*; volume 14 Plenum Press: New York, 1998.
- [2] Berliner, L. J., Ed.; *Biological Magnetic Resonance*; volume 19 Plenum Press: New York, 2001.
- [3] Grinberg, O.; Berliner, L. J., Eds.; *Biological Magnetic Resonance*; volume 22 Plenum Press: New York, 2004.
- [4] Bennati, M.; Prisner, T. F. *Rep. Prog. Phys.* **2005**, *68*, 411–448.

- [5] Schweiger, A.; Jeschke, G. *Principles of Pulse Electron Paramagnetic Resonance*; Oxford University Press: Oxford, 2001.
- [6] Stubbe, J.; van der Donk, W. *Chem. Rev.* **1998**, *98*, 705–762.
- [7] Kaupp, M.; Malkin, V. G.; Bühl, M., Eds.; *Calculation of NMR and EPR Parameters*; Wiley-VCH: Weinheim, 2004.
- [8] Neese, F.; Solomon, E. I. In *Magnetism: Molecules to Materials IV*; Miller, J. S.; Drillon, M., Eds.; Wiley-VCH: 2002.
- [9] Kaupp, M. In *EPR of Free Radicals in Solids – Trends in Methods and Applications*, Vol. 10; Lund, A.; Shiotani, M., Eds.; Springer: 2003.
- [10] Fritscher, J.; Beyer, M.; Schiemann, O. *Chem. Phys. Lett.* **2002**, *364*, 393–401.
- [11] Beyer, M.; Fritscher, J.; Feresin, E.; Schiemann, O. *J. Org. Chem.* **2003**, *68*, 2209–2215.
- [12] Fritscher, J. *Phys. Chem. Chem. Phys.* **2004**, *6*, 4950–4956.
- [13] Fritscher, J.; Artin, E.; Wnuk, S.; Bar, G.; Robblee, J. H.; Kacprzak, S.; Kaupp, M.; Griffin, R. G.; Bennati, M.; Stubbe, J. *J. Am. Chem. Soc.* **2005**, *127*, 7729–7738.
- [14] Fritscher, J.; Hrobárik, P.; Kaupp, M. *J. Phys. Chem. B* **2007**, *Computational Studies of EPR Parameters for Paramagnetic Molybdenum Complexes. I. Method Validation on Small and Medium-Sized Systems*, accepted.
- [15] Fritscher, J.; Hrobárik, P.; Kaupp, M. *Inorg. Chem.* **2007**, *Computational Studies of EPR Parameters for Paramagnetic Molybdenum Complexes. II. Larger Mo<sup>V</sup> Systems Relevant to Molybdenum Enzymes*, submitted.
- [16] Schiemann, O.; Fritscher, J.; Kisseleva, N.; Sigurdsson, S. T.; Prisner, T. F. *ChemBioChem* **2003**, *4*, 1057–1065.
- [17] Bennati, M.; Hertel, M. M.; Fritscher, J.; Prisner, T. F.; Weiden, N.; Hofweber, R.; Spörner, M.; Horn, G.; Kalbitzer, H.-R. *Biochemistry* **2006**, *45*, 42–50.

*“We are perhaps not far removed  
from the time when we shall be able  
to submit the bulk of chemical  
phenomena to calculation.”*

J. L. GAY-LUSSAC, 1778–1850

# Chapter 2

## Introduction

### 2.1 Background and Motivation

One of the most important tasks in *chemistry* and especially in *structural biology* has always been the elucidation of three-dimensional molecular structures – either of small molecules or large biopolymers. One of the main reasons for this interest is the structure–function paradigm of biology [1–3] stating that a specific function of a protein is determined by its unique three-dimensional structure. For the purpose of acquiring different sorts of structural data a number of (bio)physical methods [4–15] such as X-ray crystallography, mass spectrometry, circular dichroism, optical rotary dispersion, optical spectroscopies (e.g. infra-red or UV/Vis), Raman spectroscopy, Mössbauer spectroscopy, electron microscopy as well as magnetic resonance techniques (NMR and EPR) have become readily available. Among those, X-ray crystallography [9, 10], nuclear magnetic resonance (NMR) spectroscopy [11] and electron paramagnetic resonance (EPR) spectroscopy [12–16] are particularly useful methods to gain global or local three-dimensional structure information at atomic resolution. Each of the different methods has its own advantages and drawbacks but EPR spectroscopy is the most valuable technique to obtain structural information about many different kinds of paramagnetic species. In biological systems, either paramagnetic metal ions/clusters, transient paramagnetic intermediates in electron transfer processes or artificially attached stable spin labels can be found [8, 12–15, 17]. Due to several reasons, which will be specified later on in this chapter, the interpretation of EPR spectra is not always straightforward thus rendering it often difficult to extract structural information from the experimental data. In this thesis it will

be investigated whether quantum chemical calculations of EPR parameters [18] can be employed to overcome these problems. Before describing more specific objectives of this work, a brief introduction to the historical development of EPR spectroscopy and of theoretical methods to compute EPR interaction parameters will be given in the following.

The first observation of magnetic resonance was reported by Zavoisky [19] in 1945. In the following years electron paramagnetic resonance (EPR) spectroscopy progressed quickly as a means of studying transition metal ions in crystals and very soon it was observed that the EPR resonance line may contain hyperfine structure due to coupling of the magnetic moment of the unpaired electron(s) to the nuclear magnetic moment of the metal centers (e.g. for a  $\text{Cu}^{\text{II}}$  complex in 1949 [20]) or the coordinating ligand atoms (e.g. for  $\text{IrCl}_6^{2-}$  in 1953 [21]). About the same time also organic chemists working with aromatic  $\pi$ -radicals and inorganic chemists studying metal-free radicals started using EPR techniques. The first EPR spectrum of such a  $\pi$ -radical exhibiting a rich structure caused by proton hyperfine coupling (HFC) was reported in 1953 [22] and an EPR study of  $(\text{SO}_3)_2(\text{NO})^{2-}$  was published in 1952 [23]. In the period from the 1960s to the 1980s continuous wave (CW) EPR was developed into a routine technique for investigating paramagnetic species and CW EPR spectrometers became commercially available from various companies. Already in 1958 the first electron spin echo was observed by Blume [24] and subsequently pulse EPR techniques were developed in the 1960s mainly in the laboratories of Mims [25–29]. However, due to technical demands pulsed EPR techniques only became more commonly available in the 1980s when sufficiently fast and affordable electronic devices had been developed (see e.g. Refs. 16, 30). The first electron–nuclear double resonance (ENDOR) experiment was carried out by Feher in 1956 [31, 32], but, as for the other EPR techniques, it took considerable time for this method to be widely used.

Since the late 1980s pulsed EPR techniques have become more and more commonly available and today a variety of advanced methods are used. Electron–nuclear double resonance (ENDOR) [27] experiments are applied to obtain precise information about small nuclear hyperfine coupling (HFC) tensors (yielding e.g. electron–nuclear distances) or quadrupole coupling (QC) tensors. Electron–electron double resonance (ELDOR) [33, 34] experiments are employed to acquire data about electron–electron interactions (leading e.g. to reliable electron–electron distances up to about 80 Å [35, 36]). Electron spin-echo envelope

modulation (ESEEM) [25] experiments, two-dimensional correlation methods [37, 38] (e.g. hyperfine sublevel correlation HYSCORE [39]) and high-field (high-frequency) EPR spectroscopy [40–42] also belong to the repertoire of the modern EPR spectroscopist. The latter method is especially useful for measuring  $g$ -tensors to a high accuracy, to enhance spectral resolution (e.g. in field-swept EPR or ENDOR experiments) or to employ orientation-selective spectra to extract orientational information.

Nowadays EPR spectroscopy is one of the major sources of structural and dynamical information for paramagnetic species [16, 43–48]. The wide range of application includes e.g. paramagnetic defects and impurities in crystals and glasses, organic (e.g. nitroxides or free radical intermediates in organic reactions) or inorganic (e.g. transition metal catalysts) molecules as well as paramagnetic centers in biomolecules [12, 15, 49–51] like proteins / enzymes, DNA or RNA / ribozymes. In these biologically relevant macromolecules such stable or transient paramagnetic species can be metal ions or clusters (e.g.  $\text{Mn}^{\text{II}}$ ,  $\text{Mo}^{\text{V}}$ ,  $\text{Cu}^{\text{II}}$  or iron–sulfur clusters), organic cofactors (e.g. quinone radicals), substrate or amino acid radicals (e.g. nucleotide, glycyI or tyrosyl radicals) as well as artificially attached spin labels (e.g. nitroxides) [12, 15, 17, 49–51].

Since the early days of EPR spectroscopy it has always been an important issue and a challenge to interpret experimental data and to extract the full information content from EPR spectra. Naturally, it is of utmost importance to correlate the experimentally found EPR parameters with molecular and electronic structure parameters. Thus, suitable theoretical models are needed to fulfill this task and at that point quantum chemical methods come into play.

The usual approach to interpret EPR spectra is to perform simulations based on the so-called *effective spin Hamiltonian* (SH) – a concept that is described in more detail in Section 3.1. This means that the well-defined numerical parameters (tensors) in the SH representing different types of interaction are obtained by fitting the experimental data. The SH parameters include electronic  $g$ -values, HFC and QC constants, zero-field splittings (ZFS) and constants to describe exchange and dipolar interactions between electron spin systems (cf. Section 3.1). However, since the SH only contains spin degrees of freedom, a direct translation of the SH EPR parameters into structural information is not straightforward. Therefore, methods to predict such SH interaction parameters starting from molecular structures are required. First developments in this field by Pryce [52, 53] and Abragam and Pryce [54–57] employed perturbation theory within the framework of crystal

field theory to treat metal complexes. Later, these theories were extended to account for metal–ligand covalency to consider delocalization of spin density onto ligand atoms (cf. Refs. 55, 56, 58, 59) and to account for configuration interaction (CI) of the ground term with excited terms to describe the isotropic HFC contributions of the metals [55, 56]. An easier solution to account for core shell spin polarization is to use spin-unrestricted self-consistent field (SCF) approaches [60]. Watson and Freeman employed UHF (unrestricted Hartree–Fock) calculations to develop the idea that s-shell spin polarization effects are responsible for the isotropic metal HFC constants [61–63].

A similar problem in the context of interpretation of isotropic HFC constants arose for the treatment of  $\pi$ -radicals. Here, the observed HFC constants were correctly assigned to ring protons but within a framework of a simple molecular orbital (MO) approach it was not possible to explain the spin density at the position of the protons located in a nodal plane of the MO carrying the unpaired electron. Weissman [64], McConnell and Chesnut [65–67], Jarrett [68] and Bersohn [69] accounted for the proton spin density by either using valence bond (VB) theory together with the  $\sigma$ – $\pi$  exchange interaction concept or by using MO theory including the admixture of excited configurations involving the C–H bond into the ground state. These approaches led to the result that the proton spin density is proportional to the spin density at the adjacent carbon atom but possesses a negative sign – a proportionality known as the famous McConnell equation [65–67]. The McConnell equation was extended in various forms later on [67, 70]. Furthermore, it was found that this spin polarization of the C–H bond also induces spin density at the carbon nucleus and the so-called Karplus–Fraenkel equation [71] was formulated. Similarly, another important relation between the isotropic HFC constant of a proton bound to a carbon in  $\beta$ -position to an aromatic radical and its orientation with respect to the ring was established (*hyperconjugation*) [72].

Early calculations of spin distributions were based on HMO (Hückel molecular orbital) theory or semiempirical CNDO or INDO (complete or intermediate neglect of differential overlap) molecular orbital approaches [73–76] and later spin-unrestricted Hartree–Fock (UHF) calculations were performed. However, the *ab initio* UHF method lead to rather disappointing results for isotropic HFC values [77, 78]. For a long time almost all the computational studies were devoted to the isotropic HFC constants. One of the reasons for this was that most EPR experiments were carried out in fluid solution and neither anisotropic HFC values

nor anisotropic  $g$ -tensors were measured. In cases where experimental anisotropic HFC tensors were available, it was found that the dipolar part of the HFC tensor was rather easy to predict for organic radicals [79]. For organic radicals the deviations of the  $g$ -values from the free electron  $g$ -value are very small and were therefore usually not considered in the quantum chemical studies.

In the period between the 1970s and the 1990s several computational works revealed that only the most sophisticated and accurate *ab initio* methods (e.g. high-level multi-reference configuration interaction (MRCI) or coupled cluster CCSD(T) calculations) in combination with large and flexible basis sets were able to yield quantitative agreement with experiment for the isotropic HFC constants in organic radicals [79]. When density functional (DFT) methods [80] became available in the 1990s it was found that these methods – provided the use of a suitable functional and basis set – could predict isotropic HFC values for many radicals in an accuracy comparable to the high-level *ab initio* results [79, 81–83] but requiring much less computational resources. However, despite all the improvements brought about by the use of DFT methods, the computation of isotropic (and anisotropic) HFC constants for transition metal complexes still remains a challenge [84, 85]. Only very recently treatments incorporating spin-orbit (SO) coupling contributions to the HFC tensor within a DFT framework were developed [85–88]. These corrections give rise to a non-traceless tensor (i.e. representing an isotropic and an anisotropic contribution) and are especially important for transition metals or heavier ligand nuclei.

Although computational quantum chemistry was mostly concerned with the treatment of isotropic HFC constants in the past, the theory of the other SH parameters made significant progress since the first approaches by Abragam and Pryce. In 1965 McWeeny presented a rigorous derivation of the SH starting from the microscopic Breit–Pauli terms as described by Bethe and Salpeter [89]. He ended up with a convenient sum-over-states (SOS) theory that is described in more detail in Refs. 90 and 91. Harriman wrote a comprehensive monograph on the theoretical background of EPR parameters in 1978 providing a detailed analysis of the relativistic origin of all SH parameters [92].

However, although such general formulations were developed, the main interest was focused on methods being applicable within the MO framework. Among those, one of the most famous works is the SOS  $g$ -tensor theory of Stone [93] which was extended to third-order perturbation expressions [94] and later for orbitally degenerate ground states [95]. Stone’s theory was used during the 1970s

for the interpretation of  $g$ -tensors of organic radicals and transition metal complexes [96, 97]. For the following 20 years very little progress was achieved in the field of  $g$ -tensor calculations until Lushington and Grein reported *ab initio*  $g$ -tensor predictions based on ROHF (restricted open Hartree–Fock) level SOS methods and further extended their works using the accurate MRCI methodology [98–101]. Little later Vahtras et al. chose a different way to avoid problems inherent to SOS treatments of the  $g$ -tensor (e.g. convergence difficulties) by employing linear response theory within their multi-configurational approach [102, 103].

The latest developments in the field of  $g$ -tensor calculations [18, 104, 105] are mainly DFT approaches (cf. Section 4.3) which may be attributed to the general success of the application of DFT in chemistry. In the late 1990s several groups have started to use DFT methods for the prediction of  $g$ -tensors following two different routes. One possibility is to apply second-order perturbation theory to standard, non-relativistic Kohn–Sham wave functions (cf. Section 3.6) [106–111], and the second technique uses wave functions from spin–orbit coupled DFT equations and subsequently applies first-order perturbation theory to compute magnetic-field effects [112–115].

As might already be inferred from the description of the historical development of EPR spectroscopy and theories for the calculation of spin Hamiltonian parameters, the progress in the experimental methods has, to some extent, inspired the design of new computational methods. This is particularly important for advances in the field of  $g$ -tensor calculations since the development of high-field EPR techniques lead to an tremendously increased availability of precise  $g$ -tensor data for a wide range of systems.

Considering all the above-mentioned developments of theoretical methods for the computation of SH parameters one can say that the principal interactions dominating EPR spectra are theoretically well understood. This is completely true from a qualitative point of view, however, there are a number of cases where the quantitative accuracy of the quantum chemical predictions is still far from reasonable. Concerning the HFC values the main goal for the future will be to deal with the complicated Fermi contact term and possibly also to improve SO correction calculations to be able to reproduce the isotropic HFC constants with DFT or efficient *ab initio* methods and not only with the best available *ab initio* approaches. In the case of the  $g$ -tensor the main problem of DFT seems to be the treatment of transition metal complexes. For the prediction of quadrupole couplings (QC) current DFT methods are well suited whereas the theory for

the calculation of zero-field splittings (ZFS) is still at the very beginning and requires more development. Most of these points are discussed in depth in Ref. 18. Besides the  $g$ -, HFC and QC as well as the ZFS tensors another important SH parameter is the electron–electron exchange interaction between two unpaired electrons. A computation of this interaction can be performed within the Kohn–Sham framework employing the so-called *broken symmetry (BS) formalism* (cf. Section 6.1) although it might be suitable from a rigorous theoretical point of view to use multi-determinantal approaches for this purpose [116, 117].<sup>1</sup>

However, for many of the species studied in this work and in general for models of biological relevance, DFT is the method of choice due to the size of the systems. DFT methods exhibit a good predictive power in EPR parameter calculations while using a moderate amount of computational resources. Since the DFT methods are almost fully developed from the technical side and are being implemented in commonly available quantum chemical program packages, they can readily be applied to current research problems.

In conclusion, the rapid progress and enhanced accuracy in the quantum chemical prediction of EPR parameters achieved recently together with the increasing amount of precise and detailed experimental EPR data for important biological systems provide a strong motivation for an application of state-of-the-art computational methods to aid in the interpretation of EPR data.

## 2.2 Objectives of this Work

Following the argumentation in the preceding section, it seems to be a very promising approach to employ modern DFT methods for the calculation of EPR parameters thus providing an important link between EPR spectroscopy and molecular structure information. It is the central goal of this work to point out the potential of a fruitful interplay between quantum chemistry and experiment and to study how both can benefit from each other.

Subsequent to this introduction including background information, motivation and aims of this work as well as a summary of publications and conference contributions, a theoretical overview of the spin Hamiltonian concept, the calculation of SH parameters from first principles (both in Chapter 3) and the computational

---

<sup>1</sup>For a more elaborate overview over the historical aspects of EPR and the calculation of EPR spin Hamiltonian parameters see also Chapter 3 in Ref. 18.

methods that have been used in this work (Chapter 4) will be given.

One aim of this thesis is to use DFT methods to address several different aspects in the computation of EPR parameters, thereby demonstrating their power but also revealing their drawbacks and limitations. These aspects are described in the following and references to results presented in later chapters are given. All computations were either targeted to deal with systems that have been studied experimentally but where some interpretation help from theory was required or where deeper insight was sought or validation was necessary.

Theoretical studies open up the possibility to gain *insight into the mechanisms (physical origin) of the interactions* studied by EPR spectroscopy – an information which is often very difficult to obtain experimentally. Therefore, the mechanisms governing the exchange interaction in a nitroxide biradical [118] (Section 6.1) as well as the various MO and atomic SO contributions to the  $g$ -shifts of  $\text{Mo}^{\text{V}}$  complexes [119, 120] (Sections 6.7 and 6.8) were analyzed in detail.

Another advantage of quantum chemistry is that it allows to easily carry out *systematic studies* of the interdependency of specific structural parameters and the EPR properties of a molecule or complex. Such type of data is difficult to obtain experimentally except for some rare cases where suitable model systems are available. In this context the influence of hydrogen bond geometry on the quadrupole coupling parameters for imidazole–water or imidazole–semiquinone complexes was investigated [121] (Section 6.4). Results from systematic studies may be used later on to interpret EPR data and to translate it ‘back’ into structural information.

Besides these ‘rather theoretical’ aspects (study of interaction mechanisms and of systematic trends), quantum chemical methods may of course also be directly employed to *predict molecular structures in accordance with experimental data* thus providing the link between EPR spectroscopy and structural information. This direct interaction between experiment and theory may be considered the most important task of applied computational chemistry in the field of EPR spectroscopy. The obtained structural data about paramagnetic centers and intermediates in biological systems does often lead to a deeper insight into reaction mechanisms and catalytic functionalities. In this work the EPR properties of small aromatic nitroxide radicals [122] (Section 6.2) and of metal or substrate binding pockets of biomolecules [123–125] (Sections 6.3, 6.5 and 6.6) were studied. The aim of the calculations on the binding site models was to elucidate the general structure of these sites or of the paramagnetic substrate intermediates

studied by EPR spectroscopy.

In cases where the systems to be treated are more complicated from a theoretical point of view (e.g. transition metals, other heavier elements or systems with another type of complicated electronic structure) *validation studies* are required to test the computational methods before drawing extensive conclusions. One objective of this thesis was to carry out such a validation study for Mo<sup>V</sup> complexes to investigate whether state-of-the-art DFT methods are able to predict *g*-tensors and molybdenum HFC constants for these 4d<sup>1</sup> systems [119, 120] (Sections 6.7 and 6.8).

In conclusion, it shall be demonstrated how DFT calculations can help to understand EPR properties in more detail and aid in the interpretation of EPR experiments thus enabling the extraction of the full information content encoded in the EPR spectra.

A more specific explanation of the aims of the individual research projects and the resulting conclusions can be found in the corresponding sections of Chapters 5 and 6, where all results are summarized (Chapter 5) and presented as manuscripts of the publications that have originated from these doctoral studies (Chapter 6).

Finally, some general conclusions are drawn in Chapter 7 and the thesis ends with appendices containing abbreviations, constants and conversion factors, an acknowledgment and the author's curriculum vitae.

## 2.3 Publications and Conference Contributions

All publications are presented explicitly in Chapter 6. Most parts of this work have also been presented as talks or poster contributions<sup>2</sup> on conferences or meetings.

### Publications

*“Synthesis, crystal structure and magnetic properties of a novel nitroxide biradical. Theoretical investigation of the exchange mechanisms”*

Jörg Fritscher, Mario Beyer, Olav Schiemann *Chem. Phys. Lett.* **2002**, *364*, 393–401.

---

<sup>2</sup>Usually the first author is the presenting author.

*“Synthesis of Novel Aromatic Nitroxides as Potential DNA Intercalators. An EPR Spectroscopical and DFT Computational Study”*

Mario Beyer, Jörg Fritscher, Emiliano Feresin, Olav Schiemann *J. Org. Chem.* **2003**, *68*, 2209–2215.

*“Structural Investigation of a High-Affinity Mn<sup>II</sup> Binding Site in the Hammerhead Ribozyme by EPR Spectroscopy and DFT Calculations. Effects of Neomycin B on Metal–Ion Binding”*

Olav Schiemann, Jörg Fritscher, Natalja Kisseleva, Snorri Th. Sigurdsson, Thomas F. Prisner *ChemBioChem* **2003**, *4*, 1057–1065.

*“Influence of hydrogen bond geometry on quadrupole coupling parameters: A theoretical study of imidazole–water and imidazole–semiquinone complexes”*

Jörg Fritscher *Phys. Chem. Chem. Phys.* **2004**, *6*, 4950–4956.

*“Structure of the Nitrogen-Centered Radical Formed During Inactivation of E. coli Ribonucleotide Reductase by 2'-Azido-2'-deoxyuridine-5'-diphosphate: Trapping of the 3'-Ketonucleotide”*

Jörg Fritscher, Erin Artin, Stanislaw Wnuk, Galit Bar, John H. Robblee, Sylwia Kacprzak, Martin Kaupp, Robert G. Griffin, Marina Bennati, JoAnne Stubbe *J. Am. Chem. Soc.* **2005**, *127*, 7729–7738.

*“High-Frequency 94 GHz ENDOR Characterization of the Metal Binding Site in Wild-Type Ras•GDP and Its Oncogenic Mutant G12V in Frozen Solution”*

Marina Bennati, Melanie M. Hertel, Jörg Fritscher, Thomas F. Prisner, Norbert Weiden, Roland Hofweber, Michael Spörner, Gudrun Horn, Hans-Robert Kalbitzer *Biochemistry* **2006**, *45*, 42–50.

*“Computational Studies of EPR Parameters for Paramagnetic Molybdenum Complexes. I. Method Validation on Small and Medium-Sized Systems”*

Jörg Fritscher, Peter Hrobárik, Martin Kaupp *J. Phys. Chem. B* **2007**, accepted.

*“Computational Studies of EPR Parameters for Paramagnetic Molybdenum Complexes. II. Larger Mo<sup>V</sup> Systems Relevant to Molybdenum Enzymes”*

Jörg Fritscher, Peter Hrobárik, Martin Kaupp *Inorg. Chem.* **2007**, submitted.

## Talks

*“Quantenchemische Rechnungen als Werkzeug zur Interpretation von EPR-Spektren”*

Jörg Fritscher *Stipendiatentreffen des Fonds der Chemischen Industrie*, Darmstadt (Merck AG), 2001.

*“Quantum Chemistry and Structural Biology – DFT Calculations of EPR Parameters”*

Jörg Fritscher *Seminar of the DFG Sonderforschungsbereich 472 Molecular Bioenergetics*, Frankfurt a. M., 2002.

*“Quantum Chemical Calculations of EPR Parameters – Theoretical Foundations of EPR”*

Jörg Fritscher *Winter Seminar of the Institut für Physikalische und Theoretische Chemie (J.W.G. University)*, Hirschegg, 2003.

*“Quantum Chemical Calculations of EPR Parameters – Theory and Application”*

Jörg Fritscher *Winter Seminar of the Institut für Physikalische und Theoretische Chemie (J.W.G. University)*, Hirschegg, 2004.

*“Structure of the N<sup>•</sup> Radical Intermediate Formed During Reaction of Class I RNR with Inhibitor N<sub>3</sub>UDP”*

Jörg Fritscher *26<sup>th</sup> GDCh Magnetic Resonance Meeting*, Aachen, 2004.

*“Structure of the N<sup>•</sup> Radical Intermediate Formed During Reaction of Class I RNR with Inhibitor N<sub>3</sub>UDP”*

Jörg Fritscher *Meeting of the DFG Schwerpunktprogramm 1071 Radicals in Enzymatic Catalysis*, Marburg, 2005.

*“Quantum Chemical Calculation of EPR Parameters: Theory and Application”*

Jörg Fritscher *Seminar of the Institut für Physikalische und Theoretische Chemie (J.W.G. University)*, Frankfurt a. M., 2005.

*“Structure of the Nitrogen-Centered Radical Formed during Inactivation of E. coli Ribonucleotide Reductase by N<sub>3</sub>UDP: Trapping of the 3'-Ketonucleotide”*

Jörg Fritscher *Ernst Award Lecture, 27<sup>th</sup> GDCh Magnetic Resonance Meeting*, Mainz, 2005.

## Poster Contributions

*“EPR-spektroskopische und theoretische Untersuchungen an Nitroxiden”*

J. Fritscher, O. Schiemann, T. F. Prisner *Magnetische-Resonanz-Tagung*, Hirschegg, 2000.

*“Calculations of HFC and QC Tensors as a Tool for Correlating EPR Data with Molecular Structure”*

J. Fritscher, F. MacMillan, O. Schiemann, T. F. Prisner *14<sup>th</sup> ISMAR Conference (International Society of Magnetic Resonance)*, Rhodes, Greece, 2001.

*“Calculations of HFC and QC Tensors as a Tool for Correlating EPR Data with Molecular Structure”*

J. Fritscher, F. MacMillan, O. Schiemann, T. F. Prisner *GDCh-Jahrestagung*, Würzburg, 2001.

*“DFT Studies on the pH-Dependence of the <sup>14</sup>N Hyperfine Coupling of Imidazoline and Imidazolidine Nitroxides and on the Exchange Coupling in a Bisnitroxide”*

O. Schiemann, N. Skuridin, J. Fritscher, T. F. Prisner, V. V. Khramtsov *6<sup>th</sup> Voevodsky Conference*, Novosibirsk, Russia, 2002.

*“Calculations of Molybdenum EPR Parameters – Relevance for the Structure of Polysulfide Reductase”*

J. Fritscher, T. F. Prisner, M. Kaupp *2<sup>nd</sup> International Conference on Quantum Bioinorganic Chemistry (QBIC-2)*, Örenäs Castle, Sweden, 2002.

*“Calculations of Molybdenum EPR Parameters – Relevance for the Structure of Polysulfide Reductase”*

J. Fritscher, T. F. Prisner, M. Kaupp *6<sup>th</sup> European Conference on Bioinorganic Chemistry (EUROBIC6)*, Lund, Sweden, 2002.

*“Structural Characterization of a Mn<sup>2+</sup> Binding Site in a Hammerhead Ribozyme by Pulsed EPR and DFT”*

O. Schiemann, J. Fritscher, A. Weber, N. Kisseleva, T. F. Prisner *24<sup>th</sup> GDCh Magnetic Resonance Meeting*, Bremen, 2002.

*“Structural Characterization of a Mn<sup>2+</sup> Binding Site in a Hammerhead Ribozyme by Pulsed EPR and DFT”*

J. Fritscher, O. Schiemann, A. Weber, N. Kisseleva, T. F. Prisner *European EPR School*, Retie, Belgium, 2002.

*“Calculation of Molybdenum EPR Parameters – A Validation of DF Methods for a 4d Transition Metal”*

J. Fritscher, M. Kobus, O. Frolow, T.F. Prisner, M. Kaupp *25<sup>th</sup> GDCh Magnetic Resonance Meeting*, Leipzig, 2003.

*“Structure and Localization of the High-Affinity Mn(II) Binding Site in the Hammerhead Ribozyme and Development of a Nanometer Distance Ruler for RNA/DNA”*

O. Schiemann, J. Fritscher, N. Kisseleva, T.F. Prisner *8<sup>th</sup> Annual Meeting of the RNA Society*, Vienna, Austria, 2003.

*“Structure and Localization of the High-Affinity Mn(II) Binding Site in the Hammerhead Ribozyme and Development of a Nanometer Distance Ruler for RNA/DNA”*

O. Schiemann, J. Fritscher, N. Kisseleva, T.F. Prisner *4<sup>th</sup> European Biophysics Congress*, Alicante, Spain, 2003.

*“Aromatic Nitroxides – Potential Intercalators for Ribonucleic Acids”*

B. Bode, J. Fritscher, M. Beyer, E. Feresin, O. Schiemann *Conference on RNA-Structure, Function and Ligand Interaction*, Frankfurt, 2003.

*“Structure and Localization of the High-Affinity Mn(II) Binding Site in the Hammerhead Ribozyme”*

N. Kisseleva, J. Fritscher, T.F. Prisner, O. Schiemann *Conference on RNA-Structure, Function and Ligand Interaction*, Frankfurt, 2003.

*“Calculation of Molybdenum EPR Parameters for Mo<sup>V</sup> Model Complexes – Validation and Application to Biological Systems”*

J. Fritscher, P. Hrobarik, M. Kobus, T.F. Prisner, M. Kaupp *7<sup>th</sup> European Conference on Bioinorganic Chemistry (EUROBIC7)*, Garmisch-Partenkirchen, 2004.

*“Structure of the Radical Intermediate Formed During Reaction of Class I RNR with the Mechanism-Based Inhibitor (<sup>3</sup>-<sup>17</sup>O)N<sub>3</sub>UDP by EPR Spectroscopy (9 and 140 GHz) and DFT Calculations”*

J. Fritscher, J. Antonic, G. Bar, J. Robblee, S. Wnuk, S. Kacprzak, M. Kaupp, R. G. Griffin, J. Stubbe, M. Bennati *7<sup>th</sup> European Conference on Bioinorganic Chemistry (EUROBIC7)*, Garmisch-Partenkirchen, 2004.

*“Structural Characterization of Mn<sup>2+</sup> Binding Sites in the Minimal and Extended Hammerhead Ribozyme”*

O. Schiemann, N. Kisseleva, J. Fritscher, T.F. Prisner *7<sup>th</sup> European Conference on Bioinorganic Chemistry (EUROBIC7)*, Garmisch-Partenkirchen, 2004.

*“Calculation of Molybdenum EPR Parameters for Mo<sup>V</sup> Model Complexes – Validation and Application to Biological Systems”*

J. Fritscher, P. Hrobarik, M. Kobus, T. F. Prisner, M. Kaupp *26<sup>th</sup> GDCh Magnetic Resonance Meeting, Aachen, 2004.*

*“Structure of the Radical Intermediate Formed During Reaction of Class I RNR with the Mechanism-Based Inhibitor (*3*-<sup>17</sup>O)N<sub>3</sub>UDP by EPR Spectroscopy (9 and 140 GHz) and DFT Calculations”*

J. Fritscher, J. Antonic, G. Bar, J. Robblee, S. Wnuk, S. Kacprzak, M. Kaupp, R. G. Griffin, J. Stubbe, M. Bennati *26<sup>th</sup> GDCh Magnetic Resonance Meeting, Aachen, 2004.*

*“Structural Characterization of Mn<sup>2+</sup> Binding Sites in the Minimal and Extended Hammerhead Ribozyme”*

O. Schiemann, N. Kisseleva, J. Fritscher, T. F. Prisner *26<sup>th</sup> GDCh Magnetic Resonance Meeting, Aachen, 2004.*

*“Structural Characterization of Mn<sup>2+</sup> Binding Sites in the Minimal and Extended Hammerhead Ribozyme”*

N. Kisseleva, J. Fritscher, A. Khvorova, E. Westhof, O. Schiemann *Gordon Research Conference on Nucleic Acids, Newport, USA, 2004.*

*“High-Field ENDOR studies of the catalytic site in Ras”*

M. M. Hertel, T. F. Prisner, N. Weiden, J. Fritscher, R. Hofweber, M. Spoerner, H.-R. Kalbitzer, M. Bennati *First European Conference on Chemistry for Life Sciences, Rimini, Italy, 2005.*

*“Calculation of EPR Parameters for Mo<sup>V</sup> Model Complexes – Validation of Density Functional Methods”*

J. Fritscher, P. Hrobarik, T. F. Prisner, and M. Kaupp *Bunsentagung, Frankfurt a. M., 2005.*

*“Structure of the Radical Intermediate Formed During Reaction of Class I RNR with the Mechanism-Based Inhibitor (*3*-<sup>17</sup>O)N<sub>3</sub>UDP by EPR Spectroscopy (9 and 140 GHz) and DFT Calculations”*

J. Fritscher, E. Artin, G. Bar, J. Robblee, S. Wnuk, S. Kacprzak, M. Kaupp, R. G. Griffin, J. Stubbe, M. Bennati *European EPR School, Naurod (Wiesbaden), 2005.*

*“High-Field ENDOR studies of the catalytic site in Ras”*

M. M. Hertel, T. F. Prisner, N. Weiden, J. Fritscher, R. Hofweber, M. Spoerner,

- H.-R. Kalbitzer, M. Bennati *European EPR School*, Naurod (Wiesbaden), 2005.
- “*Structure of the Radical Intermediate Formed During Reaction of Class I RNR with the Mechanism-Based Inhibitor ( $3\text{-}^{17}\text{O}$ ) $\text{N}_3\text{UDP}$  by EPR Spectroscopy (9 and 140 GHz) and DFT Calculations*”
- J. Fritscher, E. Artin, G. Bar, J. Robblee, S. Wnuk, S. Kacprzak, M. Kaupp, R. G. Griffin, J. Stubbe, M. Bennati *27<sup>th</sup> GDCh Magnetic Resonance Meeting*, Mainz, 2005.
- “*High-Field ENDOR studies of the catalytic site in Ras*”
- M. M. Hertel, T. F. Prisner, N. Weiden, J. Fritscher, R. Hofweber, M. Spoerner, H.-R. Kalbitzer, M. Bennati *27<sup>th</sup> GDCh Magnetic Resonance Meeting*, Mainz, 2005.

## References

- [1] Moulton, J.; Melamud, E. *Curr. Opin. Struct. Biol.* **2000**, *10*, 384–389.
- [2] Wright, P. E.; Dyson, H. J. *J. Mol. Biol.* **1999**, *293*, 321–331.
- [3] Uversky, V. N. *Cell. Mol. Life Sci.* **2003**, *60*, 1852–1871.
- [4] Hammes, G. G. *Spectroscopy for the Biological Sciences*; Wiley-Interscience: 2005.
- [5] Que, L., Ed.; *Physical Methods in Bioinorganic Chemistry: Spectroscopy and Magnetism*; University Science Books: 2000.
- [6] Solomon, E. I.; Hodgson, K. O., Eds.; *Spectroscopic Methods in Bioinorganic Chemistry*; American Chemical Society: 1998.
- [7] Lottspeich, F.; Zorbas, H., Eds.; *Bioanalytik*; Spektrum Akademischer Verlag: 1998.
- [8] Neuberger, A.; van Deenen, L. L. M., Eds.; *Modern Physical Methods in Biochemistry*; volume 11A of *New Comprehensive Biochemistry* Elsevier: Amsterdam, 1985.
- [9] Drenth, J. *Principles of Protein X-Ray Crystallography*; Springer: 1999.

- 
- [10] McRee, D. E. *Practical Protein Crystallography*; Academic Press: 1999.
- [11] Cavanagh, J.; Fairbrother, W. J.; III, A. G. P.; Skelton, N. J. *Protein NMR Spectroscopy – Principles and Practice*; Academic Press: San Diego, 1996.
- [12] Berliner, L. J., Ed.; *Biological Magnetic Resonance*; volume 14 Plenum Press: New York, 1998.
- [13] Berliner, L. J., Ed.; *Biological Magnetic Resonance*; volume 19 Plenum Press: New York, 2001.
- [14] Grinberg, O.; Berliner, L. J., Eds.; *Biological Magnetic Resonance*; volume 22 Plenum Press: New York, 2004.
- [15] Bennati, M.; Prisner, T. F. *Rep. Prog. Phys.* **2005**, *68*, 411–448.
- [16] Schweiger, A.; Jeschke, G. *Principles of Pulse Electron Paramagnetic Resonance*; Oxford University Press: Oxford, 2001.
- [17] Stubbe, J.; van der Donk, W. *Chem. Rev.* **1998**, *98*, 705–762.
- [18] Kaupp, M.; Malkin, V. G.; Bühl, M., Eds.; *Calculation of NMR and EPR Parameters*; Wiley-VCH: Weinheim, 2004.
- [19] Zavoisky, E. *J. Phys. USSR* **1945**, *9*, 211–245.
- [20] Penrose, R. P. *Nature* **1949**, *163*, 992.
- [21] Owen, J.; Stevens, K. H. W. *Nature (London)* **1953**, *171*, 836.
- [22] Weissman, S. I.; Townsend, J.; Paul, D. E.; Pake, G. E. *J. Chem. Phys.* **1953**, *21*, 2227–2228.
- [23] Pake, G. E.; Townsend, J.; Weissman, S. I. *Phys. Rev.* **1952**, *85*, 682–683.
- [24] Blume, R. J. *Phys. Rev.* **1958**, *109*, 1867–1873.
- [25] Mims, W. B.; Nassau, K.; McGee, J. D. *Phys. Rev.* **1961**, *123*, 2059–2069.
- [26] Mims, W. B. *Phys. Rev.* **1964**, *133*, A835–A840.
- [27] Mims, W. B. *Proc. Roy. Soc. (London) A* **1965**, *283*, 452–457.

- [28] Mims, W. B. *Phys. Rev. B* **1972**, *5*, 2409–2419.
- [29] Davies, E. R. *Phys. Lett. A* **1974**, *47*, 1–2.
- [30] Mims, W. B.; Peisach, J. In *Advanced EPR: Applications in Biology and Biochemistry*; Hoff, A. J., Ed.; Elsevier: Amsterdam, 1989.
- [31] Feher, G. *Phys. Rev.* **1956**, *103*, 834–835.
- [32] Feher, G. *Phys. Rev.* **1959**, *114*, 1219–1244.
- [33] Milov, A. D.; Ponomarev, A. B.; Tsvetkov, Y. D. *Chem. Phys. Lett.* **1984**, *110*, 67–72.
- [34] Milov, A. D.; Salikhov, K. M.; Shirov, M. D. *Fiz. Tverd. Tela* **1981**, *23*, 975–982.
- [35] Jeschke, G. *ChemPhysChem* **2002**, *3*, 927–932.
- [36] Jeschke, G. *Macromol. Rapid. Commun.* **2002**, *23*, 227–246.
- [37] Merks, R. P. J.; de Beer, R. J. *Phys. Chem.* **1979**, *83*, 3319–3322.
- [38] Gorcester, J.; Freed, J. H. *J. Chem. Phys.* **1986**, *85*, 5375–5377.
- [39] Höfer, P.; Grupp, A.; Nebenführ, H.; Mehring, M. *Chem. Phys. Lett.* **1986**, *132*, 279–282.
- [40] Grinberg, O. A.; Dubinski, A. A.; Lebedev, Y. S. *Russ. Chem. Rev.* **1983**, *52*, 850–865.
- [41] Weber, R. T.; Disselhorst, J. A.; Prevo, J. M.; Schmidt, J.; Wenckebach, W. T. *J. Magn. Reson.* **1989**, *81*, 129–144.
- [42] Prisner, T. F. *Adv. Magn. Opt. Res.* **1997**, *20*, 245–299.
- [43] Abragam, A. *The Principles of Nuclear Magnetism*; Oxford University Press: Oxford, New York, 1961.
- [44] Gordy, W. *Theory and Applications of Electron Spin Resonance*; volume XV of *Techniques of Chemistry* John Wiley & Sons: New York, 1980.
- [45] Weltner, W. *Magnetic Atoms and Molecules*; Dover Publications: New York, 1983.

- [46] Mabbs, F. E.; Collison, D. *Electron Paramagnetic Resonance of d Transition Metal Compounds*; Elsevier Science: Amsterdam, 1992.
- [47] Atherton, N. M. *Principles of Electron Spin Resonance*; Ellis Horwood PTR Prentice Hall: New York, 1993.
- [48] Weil, J. A.; Bolton, J. R.; Wertz, J. E. *Electron Paramagnetic Resonance – Elementary Theory and Practical Applications*; Wiley: New York, 1994.
- [49] Berliner, L. J.; Reuben, J., Eds.; *Biological Magnetic Resonance*; volume 8 Plenum Press: New York, 1989.
- [50] Prisner, T.; Rohrer, M.; MacMillan, F. *Annu. Rev. Phys. Chem.* **2001**, *52*, 279–313.
- [51] Bennati, M.; Lendzian, F.; Schmittel, M.; Zipse, H. *Biol. Chem.* **2005**, *386*, 1007–1022.
- [52] Pryce, M. H. L. *Proc. Phys. Soc. A* **1950**, *63*, 25–29.
- [53] Pryce, M. H. L. *Phys. Rev.* **1950**, *80*, 1107–1108.
- [54] Abragam, A.; Horowitz, J.; Pryce, M. H. L. *Proc. Roy. Soc. (London) A* **1955**, *230*, 169–187.
- [55] Abragam, A.; Pryce, M. H. L. *Proc. Roy. Soc. (London) A* **1951**, *205*, 135–153.
- [56] Abragam, A.; Pryce, M. H. L. *Proc. Roy. Soc. (London) A* **1951**, *206*, 173–191.
- [57] Abragam, A.; Pryce, M. H. L. *Proc. Phys. Soc. A* **1950**, *63*, 409–411.
- [58] Stevens, K. H. W. *Proc. Roy. Soc. (London) A* **1953**, *219*, 542–555.
- [59] Owen, J.; Thornley, J. H. M. *Rep. Prog. Phys.* **1966**, *29*, 675–728.
- [60] Pople, J. A.; Nesbet, R. K. *J. Chem. Phys.* **1954**, *22*, 571–572.
- [61] Watson, R. E.; Freeman, A. J. *Phys. Rev.* **1961**, *123*, 2027–2047.
- [62] Freeman, A. J.; Watson, R. E. In *Magnetism. Vol. II*; Rado, G. T.; Suhl, H., Eds.; Academic Press: New York, 1965.

- [63] Watson, R. E.; Freeman, A. J. In *Hyperfine Interactions*; Freeman, A. J.; Frankel, R. B., Eds.; Academic Press: New York, 1967.
- [64] Weissman, S. I. *J. Chem. Phys.* **1956**, *25*, 890–891.
- [65] McConnell, H. M. *J. Chem. Phys.* **1956**, *24*, 764–766.
- [66] McConnell, H. M. *J. Chem. Phys.* **1958**, *28*, 1188–1192.
- [67] McConnell, H. M.; Chesnut, D. B. *J. Chem. Phys.* **1958**, *28*, 107–117.
- [68] Jarrett, H. S. *J. Chem. Phys.* **1956**, *25*, 1289–1290.
- [69] Bersohn, R. *J. Chem. Phys.* **1956**, *24*, 1066–1070.
- [70] McLachlan, A. D.; Dearman, H. H.; Lefebvre, R. *J. Chem. Phys.* **1960**, *33*, 65–70.
- [71] Karplus, M.; Fraenkel, G. K. *J. Chem. Phys.* **1961**, *35*, 1312–1323.
- [72] Heller, C.; McConnell, H. M. *J. Chem. Phys.* **1960**, *32*, 1535–1539.
- [73] McLachlan, A. D. *Mol. Phys.* **1959**, *2*, 271–284.
- [74] McLachlan, A. D. *Mol. Phys.* **1960**, *3*, 233–252.
- [75] Pople, J. A.; Beveridge, D. L.; Dobosh, P. A. *J. Chem. Phys.* **1967**, *47*, 2026–2033.
- [76] Beveridge, D. L.; McIver, J. W. *J. Chem. Phys.* **1970**, *54*, 4681–4690.
- [77] Chipman, D. M. *J. Chem. Phys.* **1979**, *71*, 761–768.
- [78] Chipman, D. M. *J. Chem. Phys.* **1983**, *78*, 4785–4786.
- [79] Engels, B.; Eriksson, L. A.; Lunell, S. *Adv. Quant. Chem.* **1996**, *27*, 297–369.
- [80] Parr, R. G.; Yang, W. *Density-Functional Theory of Atoms and Molecules*; Oxford University Press: New York, 1989.
- [81] Ishii, N.; Shimizu, T. *Phys. Rev. A* **1993**, *48*, 1691–1694.
- [82] Barone, V.; Adamo, C.; Russo, N. *Chem. Phys. Lett.* **1993**, *212*, 5–11.

- [83] Malkin, V. G.; Malkina, O. L.; Eriksson, L. A.; Salahub, D. R. In *Modern Density Functional Theory: A Tool for Chemistry*, Vol. 2; Seminario, J. M.; Politzer, P., Eds.; Elsevier Science: Amsterdam, 1995.
- [84] Munzarová, M.; Kaupp, M. *J. Phys. Chem. A* **1999**, *103*, 9966–9983.
- [85] Neese, F. *J. Chem. Phys.* **2003**, *118*, 3939–3948.
- [86] van Lenthe, E.; van der Avoird, A.; Wormer, P. E. S. *J. Chem. Phys.* **1998**, *108*, 4783–4796.
- [87] Arbuznikov, A. V.; Vaara, J.; Kaupp, M. *J. Chem. Phys.* **2004**, *120*, 2127–2139.
- [88] Remenyi, C.; Reviakine, R.; Arbuznikov, A. V.; Vaara, J.; Kaupp, M. *J. Phys. Chem. A* **2004**, *108*, 5026–5033.
- [89] McWeeny, R. *J. Chem. Phys.* **1965**, *42*, 1717–1725.
- [90] McWeeny, R. *Spins in Chemistry*; Academic Press: New York, 1970.
- [91] McWeeny, R. *Methods of Molecular Quantum Mechanics*; Academic Press: London, 1992.
- [92] Harriman, J. E. *Theoretical Foundations of Electron Spin Resonance*; Academic Press: New York, 1978.
- [93] Stone, A. J. *Proc. Roy. Soc. (London) A* **1963**, *271*, 424–434.
- [94] Atkins, P. W.; Jamieson, A. M. *Mol. Phys.* **1967**, *14*, 425–431.
- [95] Moss, R. E.; Perry, A. J. *Mol. Phys.* **1971**, *22*, 789–798.
- [96] Keijzers, C. P.; de Vries, H. J. M.; van der Avoird, A. *Inorg. Chem.* **1972**, *11*, 1338–1343.
- [97] Keijzers, C. P.; de Boer, E. *Mol. Phys.* **1974**, *29*, 1007–1020.
- [98] Lushington, G. H.; Bündgen, P.; Grein, F. *Int. J. Quant. Chem.* **1995**, *55*, 377–392.
- [99] Lushington, G. H.; Grein, F. *Theor. Chim. Acta* **1996**, *93*, 259–267.

- [100] Lushington, G. H.; Grein, F. *Int. J. Quant. Chem.: Quant. Chem. Symp.* **1996**, *30*, 467–472.
- [101] Lushington, G. H.; Grein, F. *J. Chem. Phys.* **1997**, *106*, 3292–3300.
- [102] Vahtras, O.; Minaev, B.; Ågren, H. *Chem. Phys. Lett.* **1997**, *281*, 186–192.
- [103] Engström, M.; Vahtras, O.; Ågren, H. *Chem. Phys. Lett.* **2000**, *328*, 483–491.
- [104] Neese, F.; Solomon, E. I. In *Magnetism: Molecules to Materials IV*; Miller, J. S.; Drillon, M., Eds.; Wiley-VCH: 2002.
- [105] Kaupp, M. In *EPR of Free Radicals in Solids – Trends in Methods and Applications*, Vol. 10; Lund, A.; Shiotani, M., Eds.; Springer: 2003.
- [106] Schreckenbach, G.; Ziegler, T. *J. Phys. Chem. A* **1997**, *101*, 3388–3399.
- [107] Schreckenbach, G.; Ziegler, T. *Theor. Chem. Acc.* **1998**, *99*, 71–82.
- [108] Patchkovskii, S.; Ziegler, T. *J. Phys. Chem A* **2001**, *105*, 5490–5497.
- [109] Malkina, O. L.; Vaara, J.; Schimmelpfennig, B.; Munzarová, M.; Malkin, V. G.; Kaupp, M. *J. Am. Chem. Soc.* **2000**, *122*, 9206–9218.
- [110] Kaupp, M.; Reviakine, R.; Malkina, O. L.; Arbuznikov, A.; Schimmelpfennig, B.; Malkin, V. G. *J. Comp. Chem.* **2002**, *23*, 794–803.
- [111] Neese, F. *J. Chem. Phys.* **2001**, *115*, 11080–11096.
- [112] van Lenthe, E.; Wormer, P. E. S.; van der Avoird, A. *J. Chem. Phys.* **1997**, *107*, 2488–2498.
- [113] Jayatilaka, D. *J. Chem. Phys.* **1998**, *108*, 7587–7594.
- [114] Neyman, K. M.; Ganyushin, D. I.; Matveev, A. V.; Nasluzov, V. A. *J. Phys. Chem. A* **2002**, *106*, 5022–5030.
- [115] Malkin, I.; Malkina, O. L.; Malkin, V. G.; Kaupp, M. *J. Chem. Phys.* **2005**, *123*, 244103.
- [116] Illas, F.; de P. R. Moreira, I.; de Graaf, C.; Barone, V. *Theor. Chem. Acc.* **2000**, *104*, 265–272.

- [117] Neese, F. *J. Phys. Chem. Solids* **2004**, *65*, 781–785.
- [118] Fritscher, J.; Beyer, M.; Schiemann, O. *Chem. Phys. Lett.* **2002**, *364*, 393–401.
- [119] Fritscher, J.; Hrobárik, P.; Kaupp, M. *J. Phys. Chem. B* **2007**, *Computational Studies of EPR Parameters for Paramagnetic Molybdenum Complexes. I. Method Validation on Small and Medium-Sized Systems*, accepted.
- [120] Fritscher, J.; Hrobárik, P.; Kaupp, M. *Inorg. Chem.* **2007**, *Computational Studies of EPR Parameters for Paramagnetic Molybdenum Complexes. II. Larger Mo<sup>V</sup> Systems Relevant to Molybdenum Enzymes*, submitted.
- [121] Fritscher, J. *Phys. Chem. Chem. Phys.* **2004**, *6*, 4950–4956.
- [122] Beyer, M.; Fritscher, J.; Feresin, E.; Schiemann, O. *J. Org. Chem.* **2003**, *68*, 2209–2215.
- [123] Schiemann, O.; Fritscher, J.; Kisseleva, N.; Sigurdsson, S. T.; Prisner, T. F. *ChemBioChem* **2003**, *4*, 1057–1065.
- [124] Fritscher, J.; Artin, E.; Wnuk, S.; Bar, G.; Robblee, J. H.; Kacprzak, S.; Kaupp, M.; Griffin, R. G.; Bennati, M.; Stubbe, J. *J. Am. Chem. Soc.* **2005**, *127*, 7729–7738.
- [125] Bennati, M.; Hertel, M. M.; Fritscher, J.; Prisner, T. F.; Weiden, N.; Hofweber, R.; Spörner, M.; Horn, G.; Kalbitzer, H.-R. *Biochemistry* **2006**, *45*, 42–50.

*“The Spin Hamiltonian is a convenient resting place during the long trek from fundamental theory to the squiggles of an oscilloscope” and it is “the last outpost in our land of theoretical physics.”*

J. S. GRIFFITH, 1964

## Chapter 3

# Theory of Electron Paramagnetic Resonance Parameters

This chapter provides a short introduction about the theoretical foundations of EPR parameters. First, the concept of a spin Hamiltonian will be introduced followed by a schematic description how the spin Hamiltonian parameters can be calculated from first principles starting from relativistic quantum mechanics and employing second-order perturbation theory to introduce relativistic effects into non-relativistic wave functions. In-depth information can especially be found in Refs. 1–8 as well as Refs. 9–15 and further references will only be given in special cases.

### 3.1 The Spin Hamiltonian Concept

An important intermediate in the interpretation of most EPR experiments is the *effective spin Hamiltonian* (c.f. also Section 2.1 and references therein).<sup>1</sup> It is essentially a model which allows experimental data to be summarized in terms of a small number of parameters. The eigenfunctions and eigenvalues of the spin Hamiltonian (SH) determine the energy levels of the system, or at least those aspects of interest for an EPR experiment.

The SH (or EPR) parameters, which describe the various interactions in a system, occur in sets or arrays commonly called tensors, although some of them may not actually transform properly as tensors. In solution EPR only the isotropic

---

<sup>1</sup>Here, only the static spin Hamiltonian will be considered, i.e. any dynamic / relaxation effects are excluded from the discussion.

average of each tensor  $\mathbf{T}$ , namely  $\frac{1}{3}\text{Tr}\{\mathbf{T}\}$ , is relevant due to random and rapid tumbling of the molecules. In single crystal EPR, the various tensor components can be obtained separately whereas spectra obtained from polycrystalline powders or frozen solutions are superpositions of many single-crystal-like spectra for molecules in all possible orientations. Therefore, their analysis requires the use of anisotropic parameters (tensors). The SH is thus a concept used to simulate and analyze EPR spectra as well as to understand and design EPR experiments.

**SH Eigenstates** The SH operates on a manifold of electron–nuclear spin states  $|SM, \mathbf{M}^{(I)}\rangle$ .

$$|SM, \mathbf{M}^{(I)}\rangle = |SM\rangle \otimes \prod_{A=1}^{N_A} |I^{(A)}M^{(A)}\rangle \quad (3.1)$$

where  $N_A$  is the number of magnetic nuclei,  $|SM\rangle$  is a function that exists in the space spanned by the spin variables of the electron spin and  $|I^{(A)}M^{(A)}\rangle$  represents the nuclear spin degrees of freedom for nucleus  $A$ . For a spin  $S$  there are  $2S + 1$  values of  $M$  and for a spin  $I^{(A)}$  there are  $2I^{(A)} + 1$  possible values of  $M^{(A)}$ . The dimension of the electron spin space is usually chosen to correspond to the true value of the total spin of the ground state configuration. However, sometimes an *effective spin quantum number* is defined by requiring that  $2S_{\text{eff}} + 1$  equals the number of electronic states important for the experimental situation. Therefore, one frequently refers to a *fictitious spin*.

The set of functions  $|SM, \mathbf{M}^{(I)}\rangle$  provides a complete, orthonormal set of functions in which the eigenfunctions of the SH can be expanded. An exact solution to the Schrödinger equation with the model SH

$$\hat{\mathcal{H}}_{\text{SH}}\Theta = E\Theta \quad (3.2)$$

can be found by diagonalizing the matrix representation of the SH in the basis of the states  $|SM, \mathbf{M}^{(I)}\rangle$

$$(\hat{\mathcal{H}}_{\text{SH}})_{K,L} = \langle SM_K, \mathbf{M}_K^{(I)} | \hat{\mathcal{H}}_{\text{SH}} | SM_L, \mathbf{M}_L^{(I)} \rangle. \quad (3.3)$$

The SH eigenfunctions can be expressed by

$$\Theta_I = \sum_J p_{IJ} |SM_J, \mathbf{M}_J^{(I)}\rangle \quad (3.4)$$

where the matrix  $\mathbf{p}$  collects the expansion coefficients that are the normalized eigenvectors of the matrix  $\hat{\mathcal{H}}_{\text{SH}}$ .

**General Form of the SH** In the most general sense a spin Hamiltonian can be defined as a Hermitian operator containing only electron and nuclear spin operators and (coupling or interaction) parameters that have to be properly chosen to reproduce the observed set of energy levels. In practice the SH is assumed to be of the form

$$\hat{\mathcal{H}}_{\text{SH}} = \sum_{i,j} \mathbf{v}^i \cdot \mathbf{T}^{ij} \cdot \mathbf{v}^j \quad (3.5)$$

where  $\mathbf{v}^i$ ,  $\mathbf{v}^j$  are vectors – either the spin vector operators  $\hat{\mathbf{S}}$  or  $\hat{\mathbf{I}}$  or the magnetic field vector  $\mathbf{B}$ , and  $\mathbf{T}^{ij}$  is a parameter set (tensor,  $3 \times 3$  Cartesian matrix) parametrizing the various interactions. The tensors describe the orientation dependence of the interactions, but are independent of field strength or spin operators.

**Specific Terms of the SH** Electrons and nuclei with a non-zero spin possess magnetic dipole moments that may interact with each other as well as with an external magnetic field. For a free electron the magnetic dipole moment is

$$\hat{\boldsymbol{\mu}}_e = -\beta_e g_e \hat{\mathbf{S}} \quad (3.6)$$

where  $\beta_e$  is the Bohr magneton ( $1.3316 \times 10^{-4}$  MHz T<sup>-1</sup>),  $g_e$  is the free-electron  $g$ -value ( $g_e = 2.002319 \dots$ ) and  $\hat{\mathbf{S}}$  is the vector operator for the electron spin. A nucleus with spin  $I$  has the magnetic moment

$$\hat{\boldsymbol{\mu}}_N = \beta_N g_N \hat{\mathbf{I}} \quad (3.7)$$

where  $\beta_N$  is the nuclear magneton ( $7.2521 \times 10^{-8}$  MHz T<sup>-1</sup>),  $g_N$  is the nuclear  $g$ -value and  $\hat{\mathbf{I}}$  is the vector operator for the nuclear spin.

The total SH that will be used in this thesis describing the various interactions of the magnetic moments with the external magnetic field and with each other can be summarized as

$$\begin{aligned} \hat{\mathcal{H}}_{\text{SH}} = & \beta_e \mathbf{B} \mathbf{g} \hat{\mathbf{S}} + \sum_A^{N_A} \hat{\mathbf{S}} \mathbf{A}^{(A)} \hat{\mathbf{I}}^{(A)} + \sum_A^{N_A} \hat{\mathbf{I}}^{(A)} \mathbf{Q}^{(A)} \hat{\mathbf{I}}^{(A)} \\ & + \hat{\mathbf{S}} \mathbf{D} \hat{\mathbf{S}} - \beta_N \sum_A^{N_A} g_N^{(A)} \mathbf{B} \hat{\mathbf{I}}^{(A)}. \end{aligned} \quad (3.8)$$

The first term represents the *electron Zeeman effect* (the interaction of the net spin magnetic moment with the external magnetic field  $\mathbf{B}$ ) and the second term

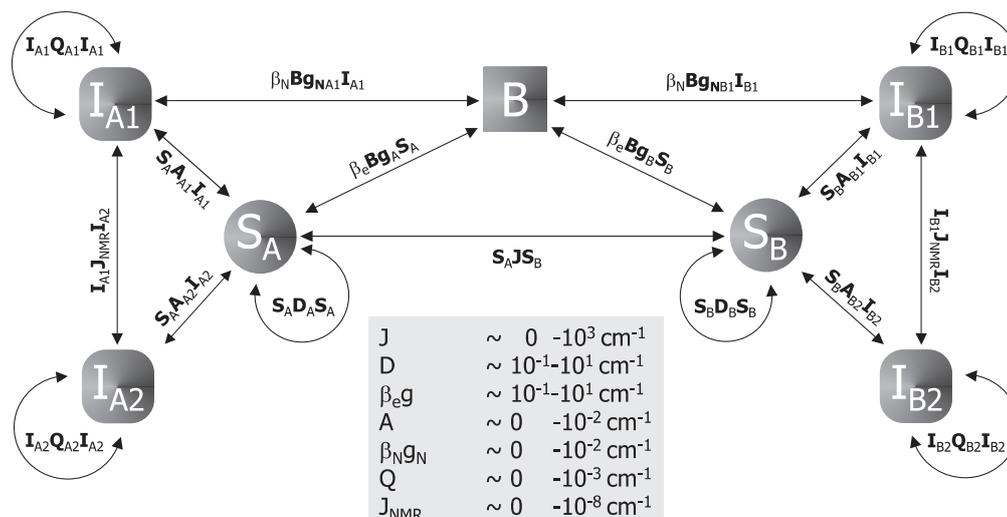


**Figure 3.1** Overview of different interactions within a spin system consisting of two electron spins  $S_A$  and  $S_B$ , each coupled to two nuclear spins  $I_{A(B)1}$  and  $I_{A(B)2}$ , in a magnetic field  $\mathbf{B}$ . The corresponding spin Hamiltonian terms and a comparison of the absolute magnitudes of the various couplings are given. Figure freely adapted from F. Neese.

describes the *hyperfine interaction* between the magnetic moment of the electron and the nuclear spin magnetic moments. The third term accounts for the *nuclear quadrupole interaction* for nuclei with  $I > \frac{1}{2}$ . The last two terms represent the *zero-field splitting* (ZFS) and the interaction of the nuclear spin magnetic moments with the external field (*nuclear Zeeman effect*). In reality,  $g_N^{(A)}$  is not a scalar nor is it equal to the free atom value (as assumed above), but also a tensor corresponding to the *chemical shift anisotropy* which is of importance in NMR spectroscopy. However, these deviations are too small to be explicitly considered here in the context of EPR spectra. Moreover, *NMR spin-spin coupling* ( $J_{\text{NMR}}$ ) has also been neglected in Eq. 3.8. In this thesis only the first three terms of the SH, namely the electron Zeeman effect as well as the hyperfine and quadrupole coupling terms, are dealt with.

In the case of two paramagnetic centers an additional *electron-electron exchange interaction* may occur that can be described by the following term in the SH

$$\hat{\mathcal{H}}_J = -2J \hat{\mathbf{S}}_A \hat{\mathbf{S}}_B. \quad (3.9)$$

It should be noted, that there may also be anisotropic contributions to the exchange coupling due to spin-orbit coupling effects. *Dipolar interactions* between

electrons may play an important role if the paramagnetic centers are spatially separated from each other in a way that the exchange coupling becomes very small. All electron–electron interactions can be included in the SH terms

$$\hat{\mathcal{H}}_{\text{el-el}} = \hat{\mathbf{S}}_A \mathbf{J} \hat{\mathbf{S}}_B + \hat{\mathbf{S}}_A \mathbf{d} \hat{\mathbf{S}}_B \quad (3.10)$$

where  $\mathbf{J}$  represents the sum of the isotropic and anisotropic exchange coupling and  $\mathbf{d}$  is the dipole–dipole coupling tensor.

Figure 3.1 displays an overview of the different interactions in a spin system of two electron and four nuclear spins, together with the corresponding SH terms and a comparison of the absolute magnitudes of the various coupling parameters.

In summary, the EPR parameters that are of importance in the following are the  $g$ -tensor  $\mathbf{g}$ , the hyperfine coupling tensors  $\mathbf{A}^{(A)}$ , the quadrupole coupling tensors  $\mathbf{Q}^{(A)}$  and the (isotropic) exchange coupling constant  $J$ .

One can calculate an isotropic  $g$ -value  $g_{\text{iso}}$  from the  $g$ -tensor by taking one third of the tensor trace. Often the  $g$ -values are expressed as  $g$ -shifts  $\Delta g_{ii}$  (in ppm) relative to the free electron value  $g_e$ .

$$\Delta g_{ii} = g_{ii} - g_e \quad (3.11)$$

The HFC tensors can be split into an isotropic ( $A_{\text{iso}}$ ) and an anisotropic part. Neglecting spin–orbit effects, the isotropic part corresponds to the so-called *Fermi contact interaction* and the anisotropic part relates to the *dipolar interaction* tensor ( $\mathbf{T}$ ). SO coupling may add further isotropic and anisotropic corrections (cf. also Sections 6.7 and 6.8). The QC tensor is a traceless tensor that may therefore be expressed (in its diagonal form) using only two parameters: the QC constant  $\chi$  and the asymmetry parameter  $\eta$  (see also Section 3.7).

**SH Parameters and Molecular Structure** Frequently it is possible to establish empirical correlations relating SH parameter values to structural or other chemically interesting information (cf. also Section 2.1). Examples for this are the *McConnell relation* or the *point-dipole approximation* that is often successfully applied to obtain spin–spin distances from dipolar coupling constants (from  $\mathbf{T}$  or  $\mathbf{d}$  tensors). However, since a SH contains solely operators for an effective electronic spin and for nuclear spins, the external magnetic field and numerical parameters, i.e. only spin degrees of freedom, in general no direct structural information can be acquired from the SH. All structural dependence is encoded

in the EPR parameters and it is not straightforward to extract this information and correlate measured EPR parameters with electronic / molecular structure. To overcome this problem and provide a link between experiment and structure, a relation of the SH parameters to the total electronic wave function of a system is necessary. This implies a recourse to the complicated underlying physics, but on the other hand leads to a deeper understanding of the physical meaning of the different EPR parameters.

In the next sections it will be outlined how these parameters can be computed using quantum mechanics.

## 3.2 Non-Relativistic Quantum Theory

The main goal in non-relativistic quantum mechanics in the *Born–Oppenheimer* (BO) approximation (‘frozen’ nuclei) is to solve the time-independent *Schrödinger equation*

$$\hat{\mathcal{H}}_{\text{BO}}\Psi_i(\mathbf{x}_1, \dots, \mathbf{x}_N; \mathbf{R}_1, \dots, \mathbf{R}_M) = E_i\Psi_i(\mathbf{x}_1, \dots, \mathbf{x}_N; \mathbf{R}_1, \dots, \mathbf{R}_M) \quad (3.12)$$

with the Hamilton operator (given in atomic units)

$$\begin{aligned} \hat{\mathcal{H}}_{\text{BO}} &= \hat{T}_e + \hat{V}_{Ne} + \hat{V}_{ee} + \hat{V}_{NN} \\ &= \sum_{i=1}^N \left( -\frac{1}{2} \nabla_i^2 \right) + \sum_{A=1}^M \sum_{i=1}^N \left( -\frac{Z_A}{r_{iA}} \right) + \sum_{i<j}^N \left( \frac{1}{r_{ij}} \right) + \sum_{A<B}^M \left( \frac{Z_A Z_B}{R_{AB}} \right) \end{aligned} \quad (3.13)$$

where  $N$  and  $M$  are the total number of electrons and nuclei, respectively, and  $Z_A$  is the charge of nucleus  $A$ .  $\mathbf{x}_i$  represents the spatial ( $\mathbf{r}_i$ ) and spin ( $\sigma_i$ ) degrees of freedom for the  $i$ th electron. The first term of  $\hat{\mathcal{H}}_{\text{BO}}$  is the kinetic energy of the electrons, the second term is the nucleus–electron attraction and the third term is the electron–electron repulsion. The last term is the internuclear repulsion and is a constant for a given nuclear configuration (nuclear coordinates enter the wave function as parameters not variables).

Since the Schrödinger equation can only be solved exactly for very simple cases, in general approximate methods have to be employed and two approaches are commonly used: the *variational principle* and *perturbation theory*.

Due to the *Pauli principle* the total wave function  $\Psi$  must be antisymmetric in the coordinates of the electrons. Furthermore, it should be an eigenfunction of the  $\hat{S}^2$  and  $\hat{S}_z$  operators since both commute with the Born–Oppenheimer

Hamiltonian which does not explicitly contain spin variables. Following these considerations, a set of many-electron wave functions  $\{|\alpha SM\rangle\}$  can be introduced that either exactly or approximately diagonalizes the Hamilton operator. Here,  $S$  and  $M$  are the spin quantum numbers and  $\alpha$  represents the spatial symmetry ( $|0SM\rangle$  is the ground state configuration and excited configurations are  $|\alpha SM\rangle$  with  $\alpha = 1, 2, \dots$ ). Each of the functions  $|\alpha SM\rangle$  is  $2S + 1$ -fold degenerate with the energy of state  $|\alpha SM\rangle$  being  $E_\alpha$ . The  $2S + 1$  components ( $M = -S, \dots, S$ ) will be referred to as *magnetic sublevels*.

However, in non-relativistic quantum mechanics ‘spin’ is not accounted for from first principles and it has to be postulated that the electron possesses an intrinsic spin connected with a magnetic moment. Moreover, the Born–Oppenheimer Hamiltonian yields degenerate magnetic sublevels and is therefore not suitable to describe magnetic resonance experiments where transitions between these levels are observed. These deficiencies emphasize the need for a new theory that includes the magnetic field as well as further interactions between the particles and the particles and the magnetic field.

### 3.3 Relativistic Quantum Theory

In this section a quantum theory including effects of *special relativity* [16] and a *uniform magnetic field* will be introduced. The spin-dependent terms in the Hamiltonian which are necessary for the description of magnetic interactions arise directly from such a theory and there is no need to ‘artificially’ include spin.

**The Dirac Equation** In order to probe the relativistic behaviour of electrons, Dirac applied Einstein’s relationship between the total energy  $E$ , momentum  $\mathbf{p}$  and rest mass  $m$  of a free particle

$$\begin{aligned}\frac{E^2}{c^2} &= \mathbf{p} \cdot \mathbf{p} + m^2 c^2 \\ E &= \pm c \sqrt{\mathbf{p}^2 + m^2 c^2}.\end{aligned}\tag{3.14}$$

A substitution of the physical observables  $E$  and  $\mathbf{p}$  by quantum mechanical operators leads to a relativistic version of a free particle Schrödinger equation

$$-\frac{\hbar}{i} \frac{\partial \Psi}{\partial t} = \pm c \sqrt{-\hbar^2 \nabla^2 + m^2 c^2} \Psi.\tag{3.15}$$

However, it is not clear how such an operator involving the square root would be interpreted. Therefore, to obtain a linear equation Dirac used the following expression for the energy

$$E = \sqrt{\mathbf{p}^2 c^2 + m^2 c^4} = \boldsymbol{\alpha} \cdot \mathbf{p}c + \beta mc^2 \quad (3.16)$$

where  $\boldsymbol{\alpha}$  and  $\beta$  have to be chosen such that when this equation is squared one arrives back at Equation 3.14. Clearly,  $\beta$  has to be some scalar and  $\boldsymbol{\alpha} = (\alpha_x, \alpha_y, \alpha_z)$  has to be a vector so that both terms on the right hand side are scalars. This may only be satisfied if the following conditions hold:

$$\alpha_i^2 = \beta^2 = 1 \quad (3.17)$$

and

$$\boldsymbol{\alpha}\beta + \beta\boldsymbol{\alpha} = 0 \quad (3.18)$$

$$\alpha_x \alpha_y + \alpha_y \alpha_x = \alpha_y \alpha_z + \alpha_z \alpha_y = \alpha_x \alpha_z + \alpha_z \alpha_x = 0. \quad (3.19)$$

This means that the squares of the corresponding operators  $\hat{\boldsymbol{\alpha}}$  and  $\hat{\beta}$  have to be equal to the identity operator, and all components of  $\hat{\boldsymbol{\alpha}}$  and  $\hat{\beta}$  have to anticommute with each other. Provided these conditions can be met, Equation 3.16 is a valid way of writing the energy and the corresponding energy operator can be written as

$$\sqrt{-\hbar^2 c^2 \nabla^2 + m^2 c^4} = \frac{\hbar c}{i} \nabla \cdot \hat{\boldsymbol{\alpha}} + \hat{\beta} mc^2. \quad (3.20)$$

The described algebraic behaviour is impossible for ordinary real numbers representing  $\hat{\alpha}_i$  and  $\hat{\beta}$ . However, a solution to that problem can be found if these entities are taken as  $4 \times 4$  matrices.

$$\hat{\alpha}_x = \begin{pmatrix} 0 & 0 & 0 & 1 \\ 0 & 0 & 1 & 0 \\ 0 & 1 & 0 & 0 \\ 1 & 0 & 0 & 0 \end{pmatrix} = \begin{pmatrix} 0 & \hat{\sigma}_x \\ \hat{\sigma}_x & 0 \end{pmatrix} \quad (3.21)$$

$$\hat{\alpha}_y = \begin{pmatrix} 0 & 0 & 0 & -i \\ 0 & 0 & i & 0 \\ 0 & -i & 0 & 0 \\ i & 0 & 0 & 0 \end{pmatrix} = \begin{pmatrix} 0 & \hat{\sigma}_y \\ \hat{\sigma}_y & 0 \end{pmatrix} \quad (3.22)$$

$$\hat{\alpha}_z = \begin{pmatrix} 0 & 0 & 1 & 0 \\ 0 & 0 & 0 & -1 \\ 1 & 0 & 0 & 0 \\ 0 & -1 & 0 & 0 \end{pmatrix} = \begin{pmatrix} 0 & \hat{\sigma}_z \\ \hat{\sigma}_z & 0 \end{pmatrix} \quad (3.23)$$

$$\hat{\beta} = \begin{pmatrix} 1 & 0 & 0 & 0 \\ 0 & 1 & 0 & 0 \\ 0 & 0 & -1 & 0 \\ 0 & 0 & 0 & -1 \end{pmatrix} = \begin{pmatrix} \hat{I}_2 & 0 \\ 0 & -\hat{I}_2 \end{pmatrix} \quad (3.24)$$

These are the so-called *Dirac matrices* where  $\hat{I}_2$  is the  $2 \times 2$  identity matrix and the  $\hat{\sigma}_i$  are the *Pauli spin matrices*.

$$\hat{\sigma}_x = \begin{pmatrix} 0 & 1 \\ 1 & 0 \end{pmatrix} \quad \hat{\sigma}_y = \begin{pmatrix} 0 & -i \\ i & 0 \end{pmatrix} \quad \hat{\sigma}_z = \begin{pmatrix} 1 & 0 \\ 0 & -1 \end{pmatrix} \quad (3.25)$$

Due to the  $4 \times 4$  nature of the operators, the relativistic wave function has to be a four component function of the form

$$\Psi(\mathbf{r}, t) = \begin{pmatrix} \psi_1(\mathbf{r}, t) \\ \psi_2(\mathbf{r}, t) \\ \psi_3(\mathbf{r}, t) \\ \psi_4(\mathbf{r}, t) \end{pmatrix}. \quad (3.26)$$

Therefore, Dirac's relativistic version of the Schrödinger equation

$$-\frac{\hbar}{i} \frac{\partial}{\partial t} \Psi - \left( \frac{\hbar c}{i} \nabla \cdot \hat{\boldsymbol{\alpha}} + \hat{\beta} m c^2 \right) \Psi = 0 \quad (3.27)$$

is a matrix equation involving a set of four linear partial differential equations. The *Dirac equation* [13, 17] always yields four independent solutions for any given electronic state  $\Psi(\mathbf{r}, t)$  which all have been shown to be physically meaningful. Of the four solutions, only two correspond to the normal electronic behaviour. The other two were found to describe a particle with properties identical to the electron except for an opposite charge, the so-called positron.

A separation of time and space variables yields a wave function of the form

$$\Psi(\mathbf{r}, t) = \begin{pmatrix} \psi_1(\mathbf{r}) \\ \psi_2(\mathbf{r}) \\ \psi_3(\mathbf{r}) \\ \psi_4(\mathbf{r}) \end{pmatrix} e^{-iEt/\hbar} \quad (3.28)$$

and substituting this into the time-dependent Dirac equation and doing the time differentiation gives the time-independent Dirac equation

$$\left(\frac{\hbar c}{i}\nabla \cdot \hat{\boldsymbol{\alpha}} + \hat{\beta}mc^2\right)\Psi(\mathbf{r}) = E\Psi(\mathbf{r}). \quad (3.29)$$

**Introduction of a Magnetic Field** When a free electron is treated in a field-free environment, it may be described equally by the two independent electronic solutions of the Dirac equation corresponding to electronic states of equal energy and spatial distribution. However, in the presence of a magnetic field, these two states become energetically non-degenerate in Dirac formalism.

A uniform magnetic field  $\mathbf{B}$  can be introduced by using field-dependent operators for momentum and energy

$$\begin{aligned} \hat{\mathbf{p}} = \frac{\hbar}{i}\nabla &\rightarrow \hat{\boldsymbol{\pi}} = \frac{\hbar}{i}\nabla + \frac{e}{c}\mathbf{A} \\ -\frac{\hbar}{i}\frac{\partial}{\partial t} &\rightarrow -\frac{\hbar}{i}\frac{\partial}{\partial t} + e\phi \end{aligned} \quad (3.30)$$

where  $\mathbf{A}$  and  $\phi$  are the vector and scalar potentials corresponding to the external field. Moreover, the magnetic flux density is  $\mathbf{B} = \nabla \times \mathbf{A}$  and for a uniform field the vector potential takes the form  $\mathbf{A} = \frac{1}{2}\mathbf{B} \times \mathbf{r}$ . Using the operator substitutions the *field-dependent Dirac equation*

$$-\frac{\hbar}{i}\frac{\partial}{\partial t}\Psi - \left(c\hat{\boldsymbol{\pi}} \cdot \hat{\boldsymbol{\alpha}} + \hat{\beta}mc^2 - e\phi\right)\Psi = 0 \quad (3.31)$$

can be obtained.

**Pauli Reduction to the Non-Relativistic Limit** Although the Dirac equation is not difficult to derive, it is essentially impossible to solve exactly except in the most simple systems. It is possible, however, to obtain approximate solutions to the Dirac equation which still retain much of the vital information contained in the original formalism. For this purpose various techniques have been developed, e.g. the *Foldy–Wouthuysen transformation* [18] and the *partitioning approach* which is also referred to as *method of the large component* or *Pauli reduction*. The latter formalism will now be applied to a free electron in a magnetic field.

Since only the two electronic solutions of Equation 3.31 are of interest for EPR, it is generally desirable to reduce the  $4 \times 4$  set of equations to a  $2 \times 2$

system. To accomplish this task,  $\Psi$  may be expressed in terms of two two-row spinors ('upper' and 'lower' spinors)

$$\Psi = \begin{pmatrix} \psi_u \\ \psi_l \end{pmatrix} \quad (3.32)$$

where

$$\psi_u = \begin{pmatrix} \psi_1 \\ \psi_2 \end{pmatrix} \quad \psi_l = \begin{pmatrix} \psi_3 \\ \psi_4 \end{pmatrix}. \quad (3.33)$$

For  $\hat{\alpha}$  and  $\hat{\beta}$  one obtains accordingly

$$\hat{\alpha} = \begin{pmatrix} \hat{0} & \hat{\sigma} \\ \hat{\sigma} & \hat{0} \end{pmatrix} \quad \hat{\beta} = \begin{pmatrix} \hat{I}_2 & \hat{0} \\ \hat{0} & \hat{I}_2 \end{pmatrix} \quad (3.34)$$

where  $\hat{0}$  is the  $2 \times 2$  zero matrix and  $\hat{\sigma} = (\hat{\sigma}_x, \hat{\sigma}_y, \hat{\sigma}_z)$  involves the Pauli spin matrices.

If these  $2 \times 2$  submatrices are used, the Dirac equation reads

$$\begin{pmatrix} mc^2 - e\phi - \hat{E} & c\hat{\sigma} \cdot \hat{\pi} \\ c\hat{\sigma} \cdot \hat{\pi} & -mc^2 - e\phi - \hat{E} \end{pmatrix} \begin{pmatrix} \psi_u \\ \psi_l \end{pmatrix} = 0 \quad (3.35)$$

where  $\hat{E}$  can be thought of either as the eigenvalue of the Dirac Hamiltonian or as the operator  $-\hbar/i(\partial/\partial t)$ . A partitioning of the total energy  $E$  into the portion arising from the rest mass  $mc^2$  and all additional energy  $\epsilon$

$$E = \epsilon + mc^2 \quad (3.36)$$

leads to the following equations

$$\begin{pmatrix} e\phi - \epsilon & c\hat{\sigma} \cdot \hat{\pi} \\ c\hat{\sigma} \cdot \hat{\pi} & -2mc^2 - e\phi - \epsilon \end{pmatrix} \begin{pmatrix} \psi_u \\ \psi_l \end{pmatrix} = 0. \quad (3.37)$$

In a stationary state with  $\phi \equiv 0$  the second equation can be formally solved to give

$$\psi_l = \frac{c\hat{\sigma} \cdot \hat{\pi}}{\epsilon + 2mc^2} \psi_u. \quad (3.38)$$

The presence of  $2mc^2$  in the denominator justifies the description of  $\psi_l$  as the 'small' components. Substituting the expression for  $\psi_l$  allows to write an equation in terms of  $\psi_u$

$$\frac{c^2(\hat{\sigma} \cdot \hat{\pi})^2}{\epsilon + 2mc^2} \psi_u = \epsilon \psi_u. \quad (3.39)$$

To obtain an equation linear in  $\epsilon$  the denominator must be simplified by assuming that the total energy is dominated by the rest mass (*non-relativistic limit*:  $E \approx mc^2 \gg \epsilon$ ). With the approximation  $\epsilon + 2mc^2 \approx 2mc^2$ , which is called the *first Pauli limit*, it is possible to write

$$\frac{1}{2m}(\hat{\boldsymbol{\sigma}} \cdot \hat{\boldsymbol{\pi}})^2 \psi_u = \epsilon \psi_u. \quad (3.40)$$

When the relations

$$(\hat{\boldsymbol{\sigma}} \cdot \hat{\boldsymbol{\pi}})^2 = \hat{\boldsymbol{\pi}}^2 + i\hat{\boldsymbol{\sigma}} \cdot \hat{\boldsymbol{\pi}} \times \hat{\boldsymbol{\pi}} \quad (3.41)$$

and

$$\begin{aligned} \hat{\boldsymbol{\pi}} \times \hat{\boldsymbol{\pi}} &= \frac{e}{c}(\hat{\mathbf{p}} \times \mathbf{A} + \mathbf{A} \times \hat{\mathbf{p}}) \\ &= \frac{e}{c}(-\mathbf{A} \times \hat{\mathbf{p}} - i\hbar \nabla \times \mathbf{A} + \mathbf{A} \times \hat{\mathbf{p}}) \\ &= \frac{e\hbar}{ic} \nabla \times \mathbf{A} = \frac{e\hbar}{ic} \mathbf{B} \end{aligned} \quad (3.42)$$

are employed one finds

$$\begin{aligned} \frac{1}{2m}(\hat{\boldsymbol{\sigma}} \cdot \hat{\boldsymbol{\pi}})^2 \psi_u &= \frac{1}{2m} \left( \hat{\boldsymbol{\pi}}^2 + \frac{e\hbar}{c} \hat{\boldsymbol{\sigma}} \cdot \mathbf{B} \right) \psi_u \\ &= \left( \frac{\hat{\boldsymbol{\pi}}^2}{2m} + \beta_e \hat{\boldsymbol{\sigma}} \cdot \mathbf{B} \right) \psi_u = \epsilon \psi_u. \end{aligned} \quad (3.43)$$

which is identical to the expression suggested by Pauli as an empirical incorporation of spin into non-relativistic quantum theory [19]. Therefore, the process described above is also referred to as *Pauli reduction*. The first term is simply that which appears in the non-relativistic quantum mechanical treatment of a (spinless) charged particle in a magnetic field. The second term describes the interaction of the electron spin magnetic moment with the field.

Taking  $\mathbf{B}$  to be oriented along the  $z$ -direction ( $\mathbf{B} = (0, 0, B)$ ) and expanding  $\hat{\sigma}_z$  leads to

$$\begin{pmatrix} \frac{\hat{\boldsymbol{\pi}}^2}{2m} + \beta_e B & 0 \\ 0 & \frac{\hat{\boldsymbol{\pi}}^2}{2m} - \beta_e B \end{pmatrix} \begin{pmatrix} \psi_1 \\ \psi_2 \end{pmatrix} = \epsilon \begin{pmatrix} \psi_1 \\ \psi_2 \end{pmatrix} \quad (3.44)$$

which has two non-trivial solutions

$$\psi_1 \propto |n, l, m_l\rangle \quad \text{and} \quad \psi_2 \equiv 0 \quad (3.45)$$

with

$$\epsilon = (2n + 2)\beta_e B + \frac{l^2 \hbar^2}{2m} \quad (3.46)$$

or

$$\psi_1 \equiv 0 \quad \text{and} \quad \psi_2 \propto |n, l, m_l\rangle \quad (3.47)$$

with

$$\epsilon = 2n\beta_e B + \frac{l^2 \hbar^2}{2m}. \quad (3.48)$$

From these solutions the evidence of an intrinsic magnetic moment becomes clear. In a magnetic field, the two electronic states with identical spatial distribution possess different energies, meaning that the degeneracy of the magnetic sublevels has been lifted. The energy difference amounts to

$$\Delta\epsilon = 2\beta_e B \approx g_e \beta_e B \quad \text{with} \quad g_e \approx 2.0023193\dots \quad (3.49)$$

which is approximately the Zeeman splitting. The deviation of the electron  $g$ -factor given by Dirac theory from the ‘true’  $g_e$  is rather small and due to some approximations. Two aspects essential to Dirac theory but leading to error are the treatment of the electromagnetic field classically rather than quantum mechanically and the neglect of states involving several electrons or positrons. These aspects are more correctly included in *quantum electrodynamics* which yields even better agreement with experimental observations. However, some radiative corrections can easily be included into relativistic quantum mechanics, e.g. by simply substituting  $\hat{\sigma} = 2\hat{S}$  with  $\hat{\sigma} = g_e \hat{S}$ .

In summary, by reducing the Dirac equation to the first Pauli limit ( $\epsilon + 2mc^2 \approx 2mc^2$ ) it could be demonstrated how the Dirac equation describes an electronic spin magnetic moment. To make more accurate approximations, one expresses the denominator in Equation 3.39 as a Taylor series

$$\begin{aligned} \frac{1}{\epsilon + 2mc^2} &= \frac{1}{2mc^2} \left(1 + \frac{\epsilon}{2mc^2}\right)^{-1} \\ &= \frac{1}{2mc^2} \left(1 - \frac{\epsilon}{2mc^2} + \left(\frac{\epsilon}{2mc^2}\right)^2 - \dots\right). \end{aligned} \quad (3.50)$$

This allows to derive analogues of the Pauli equation to any desired accuracy by keeping more terms in the expansion. Taking the first two terms (*second Pauli limit*) results in an approximate Dirac equation which explicitly accounts for spin-orbit coupling, the Darwin term and a relativistic correction to the kinetic energy (see also below).

### 3.4 The Breit–Pauli Hamiltonian

**Extension to Many-Electron Systems** The results developed thus far have applied to one-electron systems. In order to treat more interesting systems such as molecules it is, however, necessary to extend the theory to include interactions of electrons with nuclei and with other electrons. One approach would be to use quantum electrodynamics which is a many-electron theory capable of dealing with relativistic effects. Since such calculations are very difficult, it is more useful to seek for an approximate theory.

Using the Born–Oppenheimer (clamped nuclei) approximation, Coulombic electron–nuclear interactions can be incorporated into the static potential  $\phi$  while any nuclear magnetic moment  $\beta_N$  may be included empirically into a many-electron theory. However, accounting for electron–electron interactions is much more difficult.

An obvious starting point for a many-electron relativistic theory is to treat each electron as an independent Dirac particle and include interactions separately. For an  $N$ -electron system one may then write

$$\hat{\mathcal{H}} = \sum_{j=1}^N \hat{\mathcal{H}}_j + \sum_{j=1}^N \sum_{\substack{k=1 \\ k \neq j}}^N \hat{\mathcal{H}}_{jk} \quad (3.51)$$

where  $\hat{\mathcal{H}}_j$  represents the Dirac operators and  $\hat{\mathcal{H}}_{jk}$  models the interelectronic interactions. In the field-dependent version  $\hat{\mathcal{H}}_j$  becomes

$$\hat{\mathcal{H}}_j = c \left( \hat{\boldsymbol{\pi}}_j \cdot \hat{\boldsymbol{\alpha}}_j + \hat{\beta}_j m c - \frac{e}{c} \phi_j \right) \quad (3.52)$$

with the electronic charge  $e$  and the static potential  $\phi_j$  which is experienced by electron  $j$ . The indices for the Dirac matrices are introduced to keep the nomenclature consistent although the matrices have their usual form.

If the electron–electron interaction were simply the Coulomb interaction,  $\hat{\mathcal{H}}$  would be

$$\hat{\mathcal{H}} = \sum_{j=1}^N \hat{\mathcal{H}}_j + \sum_{j=1}^N \sum_{\substack{k=1 \\ k \neq j}}^N \frac{e^2}{r_{jk}}. \quad (3.53)$$

Unfortunately, this Hamiltonian does not satisfy the *Lorentz invariance criterion* of special relativity [16, 20] because of the instantaneous character of the Coulomb interaction. Relativity limits the propagation of coupling forces between electrons

to the speed of light. Quantum electrodynamics (QED), which deals with photonic exchange between electrons, can be used to approximate the interactions to any desired accuracy. In general, however, the QED expansion is truncated at second order resulting in the following Hamiltonian (ignoring interactions that involve three or more particles)

$$\hat{\mathcal{H}} = \sum_{j=1}^N \hat{\mathcal{H}}_j + \sum_{j=1}^N \sum_{\substack{k=1 \\ k \neq j}}^N \left( \frac{e^2}{r_{jk}} + \hat{B}_{jk} + \mathcal{O}(mc^2\alpha^5) \right) \quad (3.54)$$

where  $\mathcal{O}(mc^2\alpha^5)$  denotes higher-order terms,  $\alpha = e^2/(\hbar c)$  is the fine structure constant and

$$\hat{B}_{jk} = -\frac{e^2}{2r_{jk}} \left( \hat{\boldsymbol{\alpha}}_j \cdot \hat{\boldsymbol{\alpha}}_k + \frac{(\hat{\boldsymbol{\alpha}}_j \cdot \mathbf{r}_{jk})(\hat{\boldsymbol{\alpha}}_k \cdot \mathbf{r}_{jk})}{r_{jk}^2} \right) \quad (3.55)$$

is the *Breit operator* [21–23].

Using the Breit operator, an eigenvalue expression which represents a many-electron extension to the (two-electron) *Breit equation* can be derived.

$$\left( \sum_{j=1}^N \hat{\mathcal{H}}_j + \sum_{j=1}^N \sum_{\substack{k=1 \\ k \neq j}}^N \left( \frac{e^2}{r_{jk}} + \hat{B}_{jk} \right) \right) \Psi = -\frac{\hbar}{i} \frac{\partial}{\partial t} \Psi \quad (3.56)$$

As the Dirac equation, the Breit equation contains substantial information about the interaction of matter with electromagnetic radiation. However, due to the omission of higher-order QED terms it is still not fully Lorentz invariant and thus only applicable to systems with electrons moving much slower than the speed of light (as is the case for molecules). Moreover, it is a  $4N$  dimensional system and hence becomes impossibly complicated for all but the smallest systems.

**Breit–Pauli Approximation** Fortunately, it is possible to exploit much of the information content of the Breit formalism by reducing the equation to non-relativistic limits (since it is only valid for electrons with low velocities), in this case to the second Pauli limit (see above). The resulting *Breit–Pauli Hamiltonian* [2, 3] is correct to  $\frac{1}{c^2}$  (or  $\alpha^2$ , in atomic units) and able to provide at least approximate descriptions for all known interactions of a molecule with an electromagnetic field. It should be noted, that radiative corrections due to QED effects are incorporated into the Breit–Pauli (BP) Hamiltonian via the substitution  $-(e\hbar/2mc)\hat{\boldsymbol{\sigma}} \rightarrow -g_e\beta_e\hat{\mathbf{S}}$  with the accurate value of  $g_e = 2.0023193$ . In the

following those terms of the Breit–Pauli operator which may play a role for the calculation of EPR parameters are introduced.

For the sake of convenience atomic units will be used in the next parts of this chapter. Thus, the elementary charge  $e$ , the mass of the electron  $m$ , Planck's constant  $\hbar$  and the permittivity of free space  $4\pi\epsilon_0$  all take unit values. In the atomic unit system the speed of light equals the inverse of the fine structure constant

$$c = \alpha^{-1} = 137.03599\dots \quad (3.57)$$

and the Bohr and nuclear magnetons become

$$\beta_e = \frac{e\hbar}{2mc} = \frac{\alpha}{2} \approx 3.64868 \times 10^{-3} \quad (3.58)$$

and

$$\beta_N = \beta_e \frac{m}{m_p} = \frac{\alpha}{2} \frac{m}{m_p} \approx 1.98713 \times 10^{-6} \quad (3.59)$$

where the ratio of the proton and electron mass is  $m_p/m \approx 1836.15274$ .

**Zeeman Interaction Terms** The first Breit–Pauli term of interest is a one-electron term describing the interaction between the external magnetic field and the magnetic moment caused by the orbital motion of the electrons

$$\hat{\mathcal{H}}_{\text{LB}} = \frac{\alpha}{2} \sum_i \mathbf{B} \hat{\mathbf{l}}_i = \frac{\alpha}{2} \mathbf{B} \hat{\mathbf{L}} \quad (3.60)$$

which is called *orbital Zeeman* term. This term already arises in a non-relativistic Born–Oppenheimer theory including a magnetic field.

The coupling of the electron spin magnetic moment to the external magnetic field can be represented by the electron *spin Zeeman* operator

$$\hat{\mathcal{H}}_{\text{SB}} = \frac{\alpha g_e}{2} \sum_i \mathbf{B} \hat{\mathbf{s}}_i = \frac{\alpha g_e}{2} \mathbf{B} \hat{\mathbf{S}}. \quad (3.61)$$

In contrast to the orbital Zeeman operator it contains the ‘anomalous’ factor  $g_e$ . Furthermore, the relativistic treatment yields a ‘kinetic energy correction’ (*relativistic mass correction*) to the spin Zeeman energy of the form

$$\hat{\mathcal{H}}_{\text{SB}}^{\text{RMC}} = \frac{\alpha^3 g_e}{4} \sum_i \nabla_i \mathbf{B} \hat{\mathbf{s}}_i \quad (3.62)$$

which gives a correction of order  $\alpha^2$  to the  $g$ -tensor. In analogy to the electron Zeeman term one also finds a *nuclear Zeeman* operator

$$\hat{\mathcal{H}}_{\text{IB}} = \beta_N \sum_A g_N^{(A)} \mathbf{B} \hat{\mathbf{I}}_A. \quad (3.63)$$

**Spin–Orbit Coupling Terms** One term in the BP Hamiltonian which is of fundamental importance is the *spin–orbit coupling* (SOC) term. It describes the coupling of the electronic spin magnetic moment to the orbital magnetic moment of the same electron as well as of the other electrons. It can be written as

$$\hat{\mathcal{H}}_{\text{SO}} = \hat{\mathcal{H}}_{\text{SO}}^{(1)} + \hat{\mathcal{H}}_{\text{SO}}^{(2)} \quad (3.64)$$

with the one-electron part

$$\hat{\mathcal{H}}_{\text{SO}}^{(1)} = \frac{\alpha^2}{2} \sum_A \sum_i \frac{Z_A}{r_{iA}^3} \hat{\mathbf{l}}_i^A \hat{\mathbf{s}}_i \quad (3.65)$$

where  $\hat{\mathbf{l}}_i^A$  is the angular momentum of the  $i$ th electron relative to nucleus  $A$ .

$$\hat{\mathbf{l}}_i^A = (\mathbf{r}_i - \mathbf{R}_A) \times \hat{\mathbf{p}}_i \quad (3.66)$$

The two-electron part

$$\hat{\mathcal{H}}_{\text{SO}}^{(2)} = -\frac{\alpha^2}{2} \sum_i \hat{\mathbf{s}}_i \sum_{j \neq i} \frac{1}{r_{ij}^3} (\hat{\mathbf{l}}_i^j + 2\hat{\mathbf{l}}_j^i) \quad (3.67)$$

consists of two terms, where  $\hat{\mathbf{l}}_i^j$  is the angular momentum of electron  $i$  relative to electron  $j$ .

$$\hat{\mathbf{l}}_i^j = (\mathbf{r}_i - \mathbf{r}_j) \times \hat{\mathbf{p}}_i \quad (3.68)$$

The one-electron term  $\hat{\mathcal{H}}_{\text{SO}}^{(1)}$  has the familiar interpretation as discussed in standard quantum mechanics textbooks. The first term of the two-electron part  $\hat{\mathcal{H}}_{\text{SO}}^{(2)}$  arises from the movement of electron  $i$  in the Coulomb field of electron  $j$  and the second term is due to the coupling of the spin magnetic moment of electron  $i$  with the orbital current of electron  $j$ . The latter term is also called *spin–other orbit* (SOO) contribution.

Since the SO operator is a complicated two-electron operator that is quite difficult to handle computationally, often approximations to it are employed. One such approximation which is reasonable for atoms is to substitute the full SOC operator by an effective one-particle operator and to absorb the main effects of the two-electron part in the effective SOC constant  $\zeta'$ . This approach leads to good agreement with experiment for 2p and 3d elements.

A common approximation for molecules is the assumption that the two-electron term essentially provides a ‘screening’ of the nuclear charge and that

the overall behaviour of the SOC term is reasonably approximated by the one-electron term. Moreover, due to the  $r^{-3}$  dependence, the one-electron SOC is of rather local nature and it is a good approximation to consider only one-center matrix elements of this operator. Thus, one obtains an effective SOC operator of the form

$$\hat{\mathcal{H}}_{\text{SO}}^{\text{eff}} = \sum_A \sum_i \xi(r_{iA}) \hat{\mathbf{l}}_i^A \hat{\mathbf{s}}_i \quad (3.69)$$

where the function  $\xi(r_{iA})$  is usually written as

$$\xi(r_{iA}) = \frac{\alpha^2}{2} \frac{Z_{\text{eff}}^A}{r_{iA}^3}. \quad (3.70)$$

The *effective nuclear charges*  $Z_{\text{eff}}^A$  are semiempirical parameters that have to be determined by comparison with experimental data or results of more accurate computations.

However, the apparently simplest method to accurately approximate the full BP treatment of SOC is the *atomic-mean field* (AMFI) method of Hess and coworkers [24] which is inspired by the Hartree–Fock method where a two-body interaction (electron–electron repulsion) is approximated by a much simpler pseudo-single-particle operator. Finally, it should be mentioned that it is also possible to account for SOC effects using *effective core potentials*.

Thus far the momentum  $\hat{\mathbf{p}}$  rather than the gauge-invariant momentum  $\hat{\boldsymbol{\pi}}$  was used in the discussion of SOC. The use of  $\hat{\boldsymbol{\pi}}$  gives rise to one- and two-electron *gauge correction* terms to the SOC that lead to observable effects on  $g$ -values. To derive the correction to the effective one-electron operator in Equation 3.69, the expression for  $\hat{\boldsymbol{\pi}}$  has to be inserted instead of  $\hat{\mathbf{p}}$

$$\begin{aligned} \hat{\mathcal{H}}_{\text{SO}}^{\text{eff}} &= \sum_A \sum_i \xi(r_{iA}) \hat{\mathbf{l}}_i^A \hat{\mathbf{s}}_i \\ &= \sum_A \sum_i \xi(r_{iA}) (\mathbf{r}_{iA} \times \hat{\mathbf{p}}_i) \hat{\mathbf{s}}_i \\ &= \sum_A \sum_i \xi(r_{iA}) (\mathbf{r}_{iA} \times (\hat{\mathbf{p}}_i + \frac{1}{2}\alpha \mathbf{B} \times \mathbf{r}_i)) \hat{\mathbf{s}}_i. \end{aligned} \quad (3.71)$$

To obtain the correction to the SOC, terms involving  $\hat{\mathbf{p}}_i$  have to be dropped. The gauge-correction for the effective SOC operator can then be expressed as

$$\hat{\mathcal{H}}_{\text{SO}}^{\text{GC}} = \frac{\alpha}{2} \sum_A \sum_i \xi(r_{iA}) \{ (\hat{\mathbf{s}}_i \mathbf{B}) (\mathbf{r}_{iA} \mathbf{r}_i) - (\hat{\mathbf{s}}_i \mathbf{r}_i) (\mathbf{B} \mathbf{r}_{iA}) \} \quad (3.72)$$

where the vector identity  $\mathbf{a} \times (\mathbf{b} \times \mathbf{c}) = (\mathbf{a}\mathbf{b})\mathbf{c} - (\mathbf{a}\mathbf{c})\mathbf{b}$  has been used.

Finally, another aspect of SOC shall be briefly mentioned concerning the use of the ‘atom-like’ SOC operator

$$\hat{\mathcal{H}}_{\text{LS}} = \lambda \hat{\mathbf{L}} \hat{\mathbf{S}} \quad (3.73)$$

which can be derived in the context of *Russell–Saunders coupling* for atoms. This operator is only valid within a single atomic term. Since it is proportional to the total spin rather than incorporating the individual electron spins it will not have matrix elements between states of different total spin, in contrast to the more complete SOC operator. Furthermore, in molecules the total angular momentum  $\hat{\mathbf{L}}$  is not a good quantum number and the advantage of using  $\hat{\mathcal{H}}_{\text{LS}}$  instead of  $\hat{\mathcal{H}}_{\text{SO}}$  is less apparent. The ‘many-electron SOC constant’  $\lambda$  that is very useful in atomic spectroscopy is rather poorly defined in molecules where SOC of all atoms in the molecule should be considered.

**Electron Spin Coupling Terms** The direct *magnetic dipole–dipole coupling* leads to the BP Hamiltonian term

$$\hat{\mathcal{H}}_{\text{SS}}^{(\text{d})} = \frac{\alpha^2}{2} \sum_i \sum_{j \neq i} \frac{\hat{\mathbf{s}}_i \hat{\mathbf{s}}_j}{r_{ij}^3} - 3 \frac{(\hat{\mathbf{s}}_i \mathbf{r}_{ij})(\hat{\mathbf{s}}_j \mathbf{r}_{ij})}{r_{ij}^5}. \quad (3.74)$$

It is a two-electron effect which plays a role in ZFS computations and which is very difficult to calculate. Furthermore, an *electron–electron contact interaction* exists which leads, however, to no observable consequences [2] and can be omitted from the discussion.

**Electron–Nucleus Coupling Terms** Three different BP terms should be considered for the interaction of the nuclear magnetic moments with the electronic magnetic and orbital moment. The first term is due to the (classical) *magnetic dipole–dipole coupling* of the electron and nuclear magnetic moments

$$\hat{\mathcal{H}}_{\text{SI}}^{(\text{d})} = \frac{\alpha}{2} g_e \beta_N \sum_A g_n^{(A)} \sum_i \frac{\hat{\mathbf{s}}_i \hat{\mathbf{I}}^{(A)}}{r_{iA}^3} - 3 \frac{(\hat{\mathbf{s}}_i \mathbf{r}_{iA})(\hat{\mathbf{I}}^{(A)} \mathbf{r}_{iA})}{r_{iA}^5}. \quad (3.75)$$

The second term has no classical analogue and represents the *Fermi contact interaction* which depends on the electron spin density at the positions of the nuclei and may be formulated as

$$\hat{\mathcal{H}}_{\text{SI}}^{(\text{c})} = \frac{\alpha}{2} \frac{8\pi}{3} g_e \beta_N \sum_A g_n^{(A)} \sum_i \hat{\mathbf{s}}_i \hat{\mathbf{I}}^{(A)} \delta(r_{Ai}). \quad (3.76)$$

The last term arises from the interaction of the nuclear magnetic moment with the orbital moment of the electrons. This so-called *electron orbital–nucleus dipole* operator has the form

$$\hat{\mathcal{H}}_{\text{LI}} = \frac{\alpha}{2} \beta_N \sum_A g_n^{(A)} \sum_i \frac{\hat{\mathbf{I}}_i^A \hat{\mathbf{I}}^{(A)}}{r_{iA}^3}. \quad (3.77)$$

**Scalar Relativistic Terms** In addition to the magnetic terms discussed above there are two operators representing *scalar relativistic effects* that are of importance in the context of EPR parameter calculations. These operators do not have a direct influence of the SH parameters but their action leads to significant modification of the electron density and the electronic wave functions close to the nuclei. This is an important region since several of the magnetic operators have a dependence on  $r^{-3}$  and  $\delta(r)$ . Therefore, the scalar relativistic operators indirectly affect the EPR parameters.

The first operator arises from the variation of the electron mass with velocity for electrons that move close to the speed of light such as is the case for core electrons in heavy elements. This *mass-velocity* term may be formulated as

$$\hat{\mathcal{H}}_{\text{MV}} = -\frac{\alpha^2}{8} \sum_i \nabla^4. \quad (3.78)$$

The second scalar relativistic is the *Darwin* term

$$\hat{\mathcal{H}}_{\text{Darwin}} = \alpha^2 \frac{\pi}{2} \sum_A \sum_i Z_A \delta(r_{iA}) \quad (3.79)$$

which is thought to describe a ‘Zitterbewegung’ of the electron.

**Summary** In this section different correction terms have been introduced that have to be added to the Born–Oppenheimer Hamiltonian to describe the following SH parameters:  $g$ -tensors, hyperfine couplings and zero-field splittings. The latter will not be further discussed and for the approximate description of the other two properties all of the operators will be used in the form of one-electron operators. The calculation of quadrupole and exchange couplings will be briefly touched in Sections 3.7 and 3.8.

## 3.5 Effective Hamiltonians and Perturbation Theory

**Effective Hamiltonian Treatment** Of the various ways in which a spin Hamiltonian can be related to more fundamental theory, the method of *effective Hamiltonians* or method of partitioning will be used here [2, 6–8]. First, a zeroth-order model space that already contains the main physics of the system is defined and then an effective Hamiltonian is derived that approximately incorporates the effects of the additional terms in the Hamiltonian. The various terms of the effective Hamiltonian may finally be compared with the SH terms to express the SH parameters as matrix elements of the different perturbing operators over zeroth-order (non-relativistic) wave functions.

The treatment starts by assuming that the total Hamiltonian can be written as a sum of a major part and a perturbation

$$\hat{\mathcal{H}} = \hat{\mathcal{H}}_0 + \hat{\mathcal{H}}_1 \quad (3.80)$$

where  $\hat{\mathcal{H}}_0$  is the Born–Oppenheimer Hamiltonian and  $\hat{\mathcal{H}}_1$  stands for the sum of the various magnetic operators described in the preceding section. The set of states  $\{|\alpha SM\rangle\}$  is divided into two sets. The ‘*a*’ set  $\{|0SM\rangle\}$  of  $2S+1$  functions constituting the orbitally non-degenerate electronic ground state and the ‘*b*’ set  $\{|\alpha SM\rangle, \alpha = 1, 2, \dots\}$  of excited state wave functions. Any wave function can be expressed as a superposition of these states

$$\Psi = \sum_M c_M^a |0S_0M\rangle + \sum_{\alpha SM} c_{\alpha SM}^b |\alpha S_\alpha M_\alpha\rangle. \quad (3.81)$$

Using the variational principle the secular equations in matrix form can be obtained

$$\hat{\mathcal{H}}\mathbf{c} = E\mathbf{c} \quad (3.82)$$

where  $\mathbf{c}$  is the vector collecting the expansion coefficients and  $\hat{\mathcal{H}}$  is the complete Hamiltonian matrix with elements

$$\mathcal{H}_{\alpha SM, \alpha' S' M'} = \langle \alpha SM | \hat{\mathcal{H}} | \alpha' S' M' \rangle. \quad (3.83)$$

From this equation a partitioned version into ‘*a*’ and ‘*b*’ sets can be derived

$$\begin{pmatrix} \hat{\mathcal{H}}_{aa} & \hat{\mathcal{H}}_{ab} \\ \hat{\mathcal{H}}_{ba} & \hat{\mathcal{H}}_{bb} \end{pmatrix} \begin{pmatrix} \mathbf{c}^a \\ \mathbf{c}^b \end{pmatrix} = E \begin{pmatrix} \mathbf{c}^a \\ \mathbf{c}^b \end{pmatrix}. \quad (3.84)$$

Formally solving the second equation for  $\mathbf{c}^b$

$$\mathbf{c}^b = -(\hat{\mathcal{H}}_{bb} - \mathbf{I}E)^{-1} \hat{\mathcal{H}}_{ba} \mathbf{c}^a \quad (3.85)$$

and substituting the result into the first equation yields

$$\hat{\mathcal{H}}_{aa} \mathbf{c}^a - \hat{\mathcal{H}}_{ab} (\hat{\mathcal{H}}_{bb} - \mathbf{I}E)^{-1} \hat{\mathcal{H}}_{ba} \mathbf{c}^a = E \mathbf{c}^a \quad (3.86)$$

which is equivalent to the matrix representation of an eigenvalue equation of an effective Hamiltonian

$$\hat{\mathcal{H}}_{\text{eff}} \mathbf{c}^a = E \mathbf{c}^a \quad (3.87)$$

with

$$\hat{\mathcal{H}}_{\text{eff}} = \hat{\mathcal{H}}_{aa} - \hat{\mathcal{H}}_{ab} (\hat{\mathcal{H}}_{bb} - \mathbf{I}E)^{-1} \hat{\mathcal{H}}_{ba}. \quad (3.88)$$

The value of  $E$  in  $\hat{\mathcal{H}}_{\text{eff}}$  can be approximated by the unperturbed energy of the ground state  $E_0$ . Assuming that the basic set of states,  $\{|\alpha SM\rangle\}$ , diagonalizes  $\hat{\mathcal{H}}_0$ , the (diagonal) elements of the inverse term in  $\hat{\mathcal{H}}_{\text{eff}}$  can be written as

$$(\hat{\mathcal{H}}_{bb} - \mathbf{I}E_0)^{-1} \rightarrow (E_\alpha - E_0)^{-1} \equiv \Delta_\alpha^{-1}. \quad (3.89)$$

Thus the matrix elements of the effective Hamiltonian become

$$\begin{aligned} \langle 0SM | \hat{\mathcal{H}}_{\text{eff}} | 0SM' \rangle &= E_0 \delta_{MM'} + \langle 0SM | \hat{\mathcal{H}}_1 | 0SM' \rangle \\ &\quad - \sum_{\alpha S' M''} \Delta_\alpha^{-1} \langle 0SM | \hat{\mathcal{H}}_1 | \alpha S' M'' \rangle \langle \alpha S' M'' | \hat{\mathcal{H}}_1 | 0SM' \rangle \end{aligned} \quad (3.90)$$

where  $\Delta_\alpha > 0$ . The first term contains the unperturbed ground-state energy  $E_0$ , the second term represents first-order corrections and the last term of Equation 3.90 represents second-order contributions. The effective Hamiltonian matrix is of the same dimension as the SH matrix and contains the effect of the magnetic perturbations and the interactions of the ground state magnetic sublevels with the excited states up to second order. Higher-order correction terms can also be obtained, but they are seldom required.

Now, the link between the SH formalism and the quantum chemical treatment can be made by matching the SH parameters one by one with the matrix elements of the effective Hamiltonian. This procedure will be demonstrated in the following section where explicit expressions for the calculation of some EPR parameters will be presented.

**Rayleigh–Schrödinger Perturbation Theory** The method of an effective Hamiltonian is equivalent to standard *second-order Rayleigh–Schrödinger perturbation theory* using  $\hat{\mathcal{H}}_1$  as perturbation of the Born–Oppenheimer Hamiltonian  $\hat{\mathcal{H}}_0$ . Within this theory one finds for the energy including corrections up to second order the following *sum-over-states* (SOS) expression

$$\begin{aligned} \mathcal{E}_0 &= E_0^{(0)} + E_0^{(1)} + E_0^{(2)} \\ &= \langle \Psi_0^{(0)} | \hat{\mathcal{H}}_0 | \Psi_0^{(0)} \rangle + \langle \Psi_0^{(0)} | \hat{\mathcal{H}}_1 | \Psi_0^{(0)} \rangle + \sum_{j \neq 0} \frac{\langle \Psi_0^{(0)} | \hat{\mathcal{H}}_1 | \Psi_j^{(0)} \rangle \langle \Psi_j^{(0)} | \hat{\mathcal{H}}_1 | \Psi_0^{(0)} \rangle}{E_0^{(0)} - E_j^{(0)}}. \end{aligned} \quad (3.91)$$

Again, one chooses suitable BP terms as perturbations to first or second order, such that the corresponding correction terms exhibit the same dependence on the magnetic field and electron or nuclear spins as the SH term. To compute e.g.  $g$ -tensors one has to ensure that the first- and second-order contributions have a strictly linear dependence on  $\hat{\mathbf{S}}$  and  $\mathbf{B}$ . The energy correction terms may then be related to SH parameters.

### 3.6 Sum-Over-States Perturbation Expressions for EPR Parameters

**Matrix Elements of the SH** The matrix elements of the SH which are needed for comparison with the matrix elements of the effective Hamiltonian are straightforward to calculate employing standard quantum mechanical relations for angular momenta, such as

$$\hat{S}_z |SM\rangle = M |SM\rangle \quad (3.92)$$

$$\hat{S}_\pm |SM\rangle = (\hat{S}_x \pm i\hat{S}_y) |SM\rangle = \sqrt{(S \mp M)(S \pm M + 1)} |SM \pm 1\rangle \quad (3.93)$$

and similar equations for the nuclear spins.

For the *electron Zeeman* term one obtains the following matrix elements

$$\begin{aligned} \langle SM, \mathbf{M}^{(I)} | \beta_e \sum_{p,q=x,y,z} B_p g_{pq} \hat{S}_q | SM', \mathbf{M}'^{(I)} \rangle \\ = \delta_{\mathbf{M}^{(I)}, \mathbf{M}'^{(I)}} \beta_e \sum_{p,q=x,y,z} B_p g_{pq} \sigma_{MM'}^{S;q} \end{aligned} \quad (3.94)$$

with

$$\delta_{\mathbf{M}^{(I)}, \mathbf{M}'^{(I)}} = \prod_{A=1}^{N_A} \delta_{M^{(A)}, M'^{(A)}}. \quad (3.95)$$

This multidimensional Kronecker symbol returns zero whenever the nuclear spin quantum numbers  $M^{(A)}$  and  $M'^{(A)}$  for any magnetic nucleus  $A$  are different. The matrix elements  $\sigma_{MM'}^{S;p} = \langle SM | \hat{S}_p | SM' \rangle$  can be obtained using the angular momentum relations.

$$\sigma_{MM'}^{S;x} = \frac{1}{2} \left( \sqrt{(S-M')(S+M'+1)} \delta_{M-1, M'} + \sqrt{(S+M')(S-M'+1)} \delta_{M+1, M'} \right) \quad (3.96)$$

$$\sigma_{MM'}^{S;y} = \frac{i}{2} \left( \sqrt{(S-M')(S+M'+1)} \delta_{M-1, M'} + \sqrt{(S+M')(S-M'+1)} \delta_{M+1, M'} \right) \quad (3.97)$$

$$\sigma_{MM'}^{S;z} = \delta_{MM'} M \quad (3.98)$$

In a similar way, the matrix elements of the term representing the *hyperfine coupling* of the electron spin magnetic moment with nucleus  $A$  can be expressed as

$$\begin{aligned} \langle SM, \mathbf{M}^{(I)} | \sum_{p,q=x,y,z} \hat{S}_p A_{pq}^{(A)} \hat{I}_q^{(A)} | SM', \mathbf{M}'^{(I)} \rangle \\ = \delta_{\mathbf{M}^{(I)}, \mathbf{M}'^{(I)}}^A \sum_{p,q=x,y,z} A_{pq}^{(A)} \sigma_{MM'}^{S;p} \sigma_{M^{(A)} M'^{(A)}}^{(A);q} \end{aligned} \quad (3.99)$$

with the reduced Kronecker symbol

$$\delta_{\mathbf{M}^{(I)}, \mathbf{M}'^{(I)}}^A = \prod_{B \neq A} \delta_{M^{(B)}, M'^{(B)}} \quad (3.100)$$

which returns zero if two nuclear spin quantum numbers  $M^{(B)}$  and  $M'^{(B)}$  for a nucleus differ except when the nucleus is nucleus  $A$ .

***g*-Tensors** The *g*-tensor appears in the SH in a term that is linear in the electron spin and the magnetic field. Terms which involve the product of the spin magnetic moment and the magnetic field are therefore candidates for first-order contributions to the *g*-tensor in the sense of Equation 3.90. An inspection of the different BP terms reveals that such operators are the spin Zeeman operator  $\hat{\mathcal{H}}_{\text{SB}}$ , the relativistic mass correction  $\hat{\mathcal{H}}_{\text{SB}}^{\text{RMC}}$  and the gauge correction to the SOC,  $\hat{\mathcal{H}}_{\text{SO}}^{\text{GC}}$ .

These first-order contributions will be discussed before turning to second-order terms.

A comparison of the  $z$ -element of the electron Zeeman SH operator

$$\frac{\alpha}{2} \langle SS | g_{zz} B_z \hat{S}_z | SS \rangle = \frac{\alpha}{2} g_{zz} B_z S \quad (3.101)$$

with the matrix element of the  $z$ -component of  $\hat{\mathcal{H}}_{\text{SB}}$  (inserted as  $\hat{\mathcal{H}}_1$  into the first-order contribution term of Equation 3.90)

$$\langle 0SS | \hat{\mathcal{H}}_{\text{SB},z} | 0SS \rangle = \frac{\alpha g_e}{2} \langle 0SS | B_z \hat{S}_z | 0SS \rangle = \frac{\alpha g_e}{2} B_z S \quad (3.102)$$

reveals that

$$g_{zz}^{(SB)} = g_e \quad (3.103)$$

or more generally one finds

$$g_{\mu\nu}^{(SB)} = \delta_{\mu\nu} g_e \quad (3.104)$$

representing the familiar isotropic contribution of the free electron  $g$ -value to the  $g$ -tensor.

The relativistic mass correction  $\hat{\mathcal{H}}_{\text{SB}}^{\text{RMC}}$  similarly leads to

$$g_{zz}^{(\text{RMC})} = \frac{\alpha^2}{2} \frac{g_e}{S} \left\langle 0SS \left| \sum_i \hat{\nabla}_i^2 \hat{s}_{zi} \right| 0SS \right\rangle \quad (3.105)$$

or generally

$$g_{\mu\nu}^{(\text{RMC})} = \delta_{\mu\nu} \frac{\alpha^2}{2} \frac{g_e}{S} \left\langle 0SS \left| \sum_i \hat{\nabla}_i^2 \hat{s}_{zi} \right| 0SS \right\rangle. \quad (3.106)$$

This is also an isotropic contribution to the  $g$ -tensor of order  $\alpha^2$ . Due to the proportionality with the kinetic energy  $\hat{T}_i = -\frac{1}{2} \hat{\nabla}_i^2$  this term is frequently called a *kinetic energy correction*. However, it is a small contribution, usually of the order of a few hundred ppm.

The last first-order term to be considered here is due to the gauge correction to the SOC,  $\hat{\mathcal{H}}_{\text{SO}}^{\text{GC}}$ , and can be expressed as

$$g_{\mu\nu}^{(\text{GC})} = \frac{1}{S} \left\langle 0SS \left| \sum_{i,A} \xi(r_{iA}) \{ \mathbf{r}_{iA} \mathbf{r}_i - r_{iA,\mu} r_{i,\nu} \} \hat{s}_{zi} \right| 0SS \right\rangle. \quad (3.107)$$

This term is of comparable size as the kinetic energy correction ( $\xi(r_{iA})$  is of order  $\alpha^2$ ) and sometimes of different sign. Therefore, there may be cancellation between the two small first-order terms.

The most important second-order term is a cross term between the orbital Zeeman ( $\hat{\mathcal{H}}_{\text{LB}}$ ) and SOC ( $\hat{\mathcal{H}}_{\text{SO}}^{\text{eff}}$ ) terms. For its derivation it is important to notice that the orbital angular momentum operator is diagonal in the total spin. Thus, the sum over excited states in Equation 3.90 will only involve those states which have the same spin as the ground state.<sup>2</sup> To obtain an explicit expression for this second-order contribution to the  $g$ -tensor  $\hat{\mathcal{H}}_{\text{LB}} + \hat{\mathcal{H}}_{\text{SO}}^{\text{eff}}$  must be inserted for  $\hat{\mathcal{H}}_1$  in Equation 3.90. After some rearrangement of the expression and comparison with the electron Zeeman SH matrix element this leads to

$$g_{\mu\nu}^{(\text{OZ/SO})} = -\frac{1}{S} \sum_{b(S_b=S)} \Delta_b^{-1} \left\{ \langle 0SS | \sum_i \hat{l}_{i\mu} | bSS \rangle \langle bSS | \sum_{i,A} \xi(r_{iA}) \hat{l}_{i\nu}^A \hat{s}_{zi} | 0SS \rangle \right. \\ \left. + \langle 0SS | \sum_{i,A} \xi(r_{iA}) \hat{l}_{i\mu}^A \hat{s}_{zi} | bSS \rangle \langle bSS | \sum_i \hat{l}_{i\nu} | 0SS \rangle \right\} \quad (3.108)$$

where  $S$  is the total spin of the ground state. To compute this second-order term one has to know the ‘standard components’ of the excited state multiplets (i.e. the states  $|bSM\rangle$  with  $M = S$ ) and has to evaluate the matrix elements of the angular momentum and the reduced SOC operator between these excited states and the standard components of the ground state multiplet. Moreover, the transition energies from the ground state to the excited states,  $\Delta_b$ , enter in the denominator and it is important to have precise values for these quantities in order to obtain accurate values for the second-order correction. In principle, the sum over excited states is infinite but usually only a few excited states make dominant contributions to the  $g$ -tensor.

In summary, the complete  $g$ -tensor can be calculated from four main contributions

$$g_{\mu\nu} = g_{\mu\nu}^{(\text{SB})} + g_{\mu\nu}^{(\text{RMC})} + g_{\mu\nu}^{(\text{GC})} + g_{\mu\nu}^{(\text{OZ/SO})} \\ = \delta_{\mu\nu} g_e + g_{\mu\nu}^{(\text{RMC})} + g_{\mu\nu}^{(\text{GC})} + g_{\mu\nu}^{(\text{OZ/SO})} \quad (3.109)$$

where the first term is equal to the free electron  $g$ -value. The  $g_{\mu\nu}^{(\text{OZ/SO})}$  term dominates by far over the second and third terms in most cases. Instead of using  $g$ -values  $g_{\mu\nu}$  sometimes  $g$ -shifts  $\Delta g_{\mu\nu}$  are used which are defined as the difference

<sup>2</sup>This is a difference to the ZFS tensor where also excited states of higher and lower multiplicity than the ground state have to be included.

to the free electron  $g$ -value

$$\Delta g_{\mu\nu} = g_{\mu\nu} - \delta_{\mu\nu} g_e. \quad (3.110)$$

Finally, it should be mentioned that the  $g$ -tensors computed as described above are not independent of the choice of a gauge origin since the orbital Zeeman operator includes the angular momentum operator which is measured relative to the chosen origin of the coordinate system. This *gauge dependence* arises from the arbitrariness of the vector potential in a more general context. In an exact treatment a change of gauge is offset by a phase change in the wave function [2, 8]. However, the perturbation treatment with fixed zeroth-order functions lacks the flexibility to accomplish such a phase change. There are several approaches to solve this problem, e.g. the *gauge-including atomic orbital* (GIAO) method or the *individual gauge for localized orbitals* (IGLO) approach. However, since the gauge dependence of the  $g$ -tensor is not as critical as e.g. for NMR chemical shifts, it is often possible to choose a reasonable *common gauge*, such as the center of mass or the center of electronic charge, to obtain results very close to the fully gauge-invariant results. Therefore, this problem will not be discussed any further.

**Hyperfine Couplings** In analogy to the procedure described for the  $g$ -tensor, the elements of the hyperfine coupling tensor can be obtained. In this case matrix elements of the effective Hamiltonian representing terms proportional to the product of the electron spin with the nuclear spin must be found matching the HFC SH matrix elements, e.g. of the  $z$ -component

$$\langle SS, I^{(A)} I | A_{zz}^{(A)} \hat{S}_z \hat{I}_z^{(A)} | SS, I^{(A)} I \rangle = A_{zz}^{(A)} S I^{(A)} \quad (3.111)$$

and for a given nucleus  $A$ . Two BP terms which will contribute to first order are immediately evident from the list of perturbing operators: the Fermi contact term  $\hat{\mathcal{H}}_{\text{SI}}^{(\text{c})}$  and the dipolar hyperfine operator  $\hat{\mathcal{H}}_{\text{SI}}^{(\text{d})}$ .

The isotropic Fermi contact contribution to the HFC of nucleus  $A$  is thus represented by

$$A_{\mu\nu}^{(A;\text{c})} = A_{\text{FC}}^{(A)} = \delta_{\mu\nu} \frac{8\pi}{3} \frac{\alpha}{2} \frac{1}{S} g_e \beta_N g_n^{(A)} \langle 0SS | \sum_i \hat{s}_{zi} \delta(r_{iA}) | 0SS \rangle \quad (3.112)$$

and the anisotropic dipolar HFC contribution is given by

$$A_{\mu\nu}^{(A;\text{d})} = T_{\mu\nu}^{(A)} = \frac{\alpha}{2} \frac{1}{S} g_e \beta_N g_n^{(A)} \langle 0SS | \sum_i \hat{s}_{zi} r_{iA}^{-5} \{ \delta_{\mu\nu} r_{iA}^2 - 3 r_{iA,\mu} r_{iA,\nu} \} | 0SS \rangle. \quad (3.113)$$

The dipolar HFC tensor is symmetric in the indices  $\mu$  and  $\nu$  and has a vanishing trace.

In addition to these two first-order terms one may also include second-order contributions to the HFC tensor by using BP terms which are either proportional to the electron spin or the nuclear spin but not both and are not depending on the magnetic field. Operators that fulfill these requirements are the SOC operator  $\hat{\mathcal{H}}_{\text{SO}}^{\text{eff}}$  and the electron orbital–nucleus dipole operator  $\hat{\mathcal{H}}_{\text{LI}}$ . In analogy to the derivation of the second-order contribution to the  $g$ -tensor an expression of the form

$$\begin{aligned}
 A_{\mu\nu}^{(A;\text{SO})} = & -\frac{\alpha}{2S} g_e \beta_N g_N^{(A)} \\
 & \cdot \sum_{b(S_b=S)} \Delta_b^{-1} \left\{ \left\langle 0SS \left| \sum_i \hat{l}_{i\mu}^A r_{iA}^{-3} \right| bSS \right\rangle \left\langle bSS \left| \sum_{B,i} \xi(r_{iB}) \hat{l}_{i\nu}^B \hat{s}_{zi} \right| 0SS \right\rangle \right. \\
 & \left. + \left\langle 0SS \left| \sum_{B,i} \xi(r_{iB}) \hat{l}_{i\mu}^B \hat{s}_{zi} \right| bSS \right\rangle \left\langle bSS \left| \sum_i \hat{l}_{i\nu}^A r_{iA}^{-3} \right| 0SS \right\rangle \right\}
 \end{aligned} \tag{3.114}$$

may be obtained where the superscript  $(A; \text{SO})$  indicates the SOC contribution to the HFC of nucleus  $A$ . As for the  $g$ -tensor only excited states of the same spin multiplicity as the ground state contribute since  $\hat{\mathcal{H}}_{\text{LI}}$  is diagonal in the total spin. It is important to notice that  $A_{\mu\nu}^{(A;\text{SO})}$  is *not traceless*. Therefore, the trace of the total HFC tensor does in general not simply reduce to the isotropic Fermi contact term. It may be convenient to formally separate the isotropic from the anisotropic contributions of the second-order SOC correction to the HFC, to obtain an isotropic *pseudocontact coupling constant* and an anisotropic traceless *orbital dipolar coupling tensor*.

$$A_{\mu\mu}^{(A;\text{SO})} = A_{\text{PC}}^{(A)} + T_{\mu\mu, \text{orb}}^{(A)} \tag{3.115}$$

The HFC contribution due to SOC ( $A_{\mu\nu}^{(A;\text{SO})}$ ) may often be neglected for organic molecules or HFCs of other light nuclei without too much error. However, for metal nuclei this contribution is usually fairly large and should not be neglected (cf. also Sections 6.7 and 6.8).

Altogether the HFC of a nucleus  $A$  can be expressed as a sum of two first-order and one second-order terms, where the second-order term is only important for heavier elements with large SOC constants.

$$A_{\mu\nu}^{(A)} = \delta_{\mu\nu} A_{\text{FC}}^{(A)} + T_{\mu\nu}^{(A)} + A_{\mu\nu}^{(A;\text{SO})} \tag{3.116}$$

where  $A_{\text{FC}}^{(A)}$  is sometimes abbreviated as  $A_{\text{iso}}^{(A)}$ .

**The Use of Molecular Orbitals and Atomic Basis Functions** For the actual calculation of EPR parameters it may be convenient to express the wave functions involved ( $|\alpha SM\rangle$ ) in terms of molecular orbitals  $\chi_i$  or spin density matrix elements  $P_{pq}^-$  and atomic basis functions  $\varphi_i$ .

Here, this procedure will just be demonstrated exemplary for the gauge correction term to the  $g$ -tensor

$$g_{\mu\nu}^{(\text{GC})} = \frac{1}{S} \left\langle 0SS \left| \sum_{i,A} \xi(r_{iA}) \{ \mathbf{r}_{iA} \mathbf{r}_i - r_{iA,\mu} r_{i,\nu} \} \hat{s}_{zi} \right| 0SS \right\rangle. \quad (3.117)$$

Using the singly-occupied molecular orbitals  $\chi_{oi}$  this may be written as

$$g_{\mu\nu}^{(\text{GC})} = \frac{1}{2S} \sum_{i=1}^m \left\langle \chi_{oi} \left| \sum_A \xi(r_A) \{ \mathbf{r}_A \mathbf{r} - r_{A,\mu} r_\nu \} \right| \chi_{oi} \right\rangle \quad (3.118)$$

and in terms of the ground state spin density and atomic basis functions one obtains

$$g_{\mu\nu}^{(\text{GC})} = \frac{1}{2S} \sum_{pq} P_{pq}^- \left\langle \varphi_p \left| \sum_A \xi(r_A) \{ \mathbf{r}_A \mathbf{r} - r_{A,\mu} r_\nu \} \right| \varphi_q \right\rangle. \quad (3.119)$$

Similar expressions may also be obtained for the other SH parameters.

## 3.7 Calculation of Electric Field Gradients and Quadrupole Couplings

The theory of quadrupole coupling [25], i.e. the interaction of the *nuclear electric quadrupole moment*  $Q_N$  with the electric field of surrounding electrons represented by the *electric field gradient* (EFG) at the nucleus, is not included in the BP treatment as presented above but can be accounted for by adding a *finite nuclear model* [2, 3]. The finite size or internal structure of the nucleus leads to an electric quadrupole moment for nuclei with a nuclear spin  $I > \frac{1}{2}$  (the dipole and octopole moments vanish by symmetry) due to a non-spherical charge distribution within the nucleus.

The matrix elements of the QC tensor are defined as

$$Q_{\mu\nu}^{(A)} = \frac{eQ_N^{(A)}}{2I^{(A)}(2I^{(A)} - 1)\hbar} V_{\mu\nu}^{(A)} \quad (3.120)$$

where  $V_{\mu\nu}^{(A)}$  are the components of the electric field gradient tensor at nucleus  $A$ . Based on the traceless EFG tensor one can define the *QC constant*  $\chi$  and the *asymmetry parameter*  $\eta$  as

$$\chi^{(A)} = \frac{e Q_N^{(A)} V_{zz}^{(A)}}{h} \quad \text{and} \quad \eta = \frac{V_{xx}^{(A)} - V_{yy}^{(A)}}{V_{zz}^{(A)}} \quad (3.121)$$

with  $|V_{zz}| \geq |V_{yy}| \geq |V_{xx}|$ . Note, that frequently a QC constant  $\kappa$  with  $\kappa = \chi(4I(2I-1))^{-1}$  is used. To evaluate the elements of the QC tensor, usually standard nuclear quadrupole moments as tabulated in the literature [26] are employed. The physical quantities that remain to be calculated are the elements of the EFG tensor which are given by

$$V_{\mu\nu}^{(A)} = \left\langle 0SS \left| \sum_i r_{iA}^{-5} \{ \delta_{\mu\nu} r_{iA}^2 - 3 r_{iA,\mu} r_{iA,\nu} \} \right| 0SS \right\rangle. \quad (3.122)$$

The EFG tensor is a *first-order property* and is *spin-independent* and therefore related to the electron rather than the spin density.

### 3.8 Calculation of Exchange Interactions

The *exchange interaction parameter*  $J$  is related to the energy difference between states with different spin multiplicity, e.g. the singlet–triplet splitting in nitroxide biradicals. For details concerning the exchange coupling see also Section 6.1 and Refs. 27 and 28.

Thus, to compute this quantity reliable energies of the different spin states are necessary (or at least reliable energy differences between the states). In *ab initio* treatments (e.g. CI methods) where proper multiconfigurational spin eigenfunctions are available the computation is straightforward, although computationally extremely demanding for larger systems. Therefore, often DFT methods are employed which require much less computational effort and are thus applicable to larger systems. However, the problem of DFT in this context is the fact that it cannot describe the multideterminantal low-spin states (e.g. open shell singlet states). To solve this problem the *broken-symmetry* (BS) formalism [29–31] is employed using approximate methods to extract the exchange coupling constant from DFT calculations for the high-spin state (HS) and the so-called broken symmetry state. A relation derived by Yamaguchi and coworkers [32] states that

$$J \approx - \frac{E_{\text{HS}} - E_{\text{BS}}}{\langle \hat{S}^2 \rangle_{\text{HS}} - \langle \hat{S}^2 \rangle_{\text{BS}}} \quad (3.123)$$

where  $E_{\text{HS}}$  and  $E_{\text{BS}}$  denote the energies of the high-spin and broken symmetry states and  $\langle \hat{S}^2 \rangle_{\text{HS}} - \langle \hat{S}^2 \rangle_{\text{BS}}$  is the difference between the spin-squared expectation values of the two states evaluated with the Kohn–Sham determinant.

### 3.9 Computational Approaches to EPR Parameters

In this section it will be briefly discussed which approaches can be employed to obtain many-electron wave functions for the ground (and excited) states of molecular systems to calculate EPR parameters using the equations introduced in the preceding sections. Two methods that may in principle be used for SH parameter computations are *configuration interaction* (CI) or *density functional theory* (DFT) methods. Both of these methods allow to calculate first- and second-order corrections to the non-relativistic ground state using BP Hamiltonian terms. Finally, the possibility to employ *relativistic methods* to obtain ground state wave functions is discussed.

**Configuration Interaction** All expressions for the SH parameters were expressed in terms of a set of many-electron ground and excited state wave functions. For the calculation of the first-order perturbation expressions solely the knowledge of the ground state is necessary whereas second-order perturbation corrections require the computation of *sum-over-states* (SOS) expressions involving sums over all excited states. Such a set of many-electron wave functions may be obtained using the procedure of CI where wave functions are formulated as an expansion in terms of (ground state, singly, doubly, triply, etc. excited) Slater determinants  $\Phi_i$

$$\Psi_{\text{CI}} = \sum_i c_i \Phi_i. \quad (3.124)$$

To calculate the expansion coefficients, the Born–Oppenheimer Hamiltonian  $\hat{\mathcal{H}}_{\text{BO}}$  has to be transformed into the  $\{\Phi\}$  basis where its matrix elements may be expressed as

$$\mathcal{H}_{\text{BO},ij} = \langle \Phi_i | \hat{\mathcal{H}}_{\text{BO}} | \Phi_j \rangle. \quad (3.125)$$

These matrix elements are difficult to calculate and altogether an enormous number of one- and two-electron integrals has to be considered since accurate CI calculations involve as many as  $10^6 - 10^{10}$  different determinants  $\Phi_i$ .

The advantage of CI methods in the context of EPR parameter calculations is that they may be directly applied to the equations derived thus far without any further approximations. However, it is clear that the infinite expansions involved have to be truncated at some point which is usually not critical since the SH parameters are often dominated by only a limited number of excited states. Despite all advantages of CI approaches, they are in general computationally too demanding to be used for large molecules and alternative methods have to be used. One such method which is commonly employed is DFT.

**Density Functional Theory** The fundamentals of DFT are explained in Sections 4.3 and 4.4. DFT partially includes electron correlation effects and yields much better results than Hartree–Fock theory with about the same computational effort. It can, however, not be directly applied to the sum-over-states expressions for the SH parameters since DFT is essentially a ground state theory and for the second order corrections excited states have to be used. Fortunately, there are methods to circumvent the sums over excited states and compute second-order properties from the ground state wave function alone. One method which is the basis of many modern approaches to second order properties for large molecules will be described in the next paragraphs.

**Linear Response Theory and Coupled-Perturbed SCF Methods** It is possible to expand the total ground state energy  $E_0$  of a system in a Taylor series in the various perturbations  $\lambda_n$ , such as magnetic field as well as electron and nuclear spin.

$$\begin{aligned}
 E_0(\lambda_1, \lambda_2, \dots) = E_0(0, 0, \dots) &+ \sum_n \lambda_n \left. \frac{\partial E_0}{\partial \lambda_n} \right|_{\lambda=0} \\
 &+ \frac{1}{2} \sum_{n \neq m} \lambda_n \lambda_m \left. \frac{\partial^2 E_0}{\partial \lambda_n \partial \lambda_m} \right|_{\lambda=0} + \dots
 \end{aligned}
 \tag{3.126}$$

where *first-order properties* (e.g. electric dipole or quadrupole moments) and *second-order properties* (e.g. polarizabilities, magnetizability (susceptibility) or IR or Raman intensities) are defined as first or second derivatives of the energy with respect to the perturbations, respectively. In the context of EPR parameters, the  $\lambda_n$  may be the magnetic field  $\mathbf{B}$ , the electron spin  $\hat{\mathbf{S}}$  or the nuclear spin  $\hat{\mathbf{I}}$ . Writing down all the first and second derivative expansion terms explicitly with

these perturbations and comparing them with terms from the SH (Equation 3.8), one can e.g. identify the  $g$ - or HFC tensor components as mixed second derivatives

$$g_{uv} = \frac{1}{\beta_e} \frac{\partial^2 E_0(\mathbf{B}, \hat{\mathbf{S}})}{\partial B_u \partial S_v} \Big|_{\mathbf{B}=\hat{\mathbf{S}}=0} \quad \text{and} \quad A_{uv}^{(N)} = \frac{\partial^2 E_0(\hat{\mathbf{I}}^{(N)}, \hat{\mathbf{S}})}{\partial I_u^{(N)} \partial S_v} \Big|_{\hat{\mathbf{I}}^{(N)}=\hat{\mathbf{S}}=0}. \quad (3.127)$$

Thus, the calculation of these and other EPR properties requires the calculation of second energy derivatives with respect to perturbations which may be a difficult task. Again, these perturbations consist of the various terms of the BP Hamiltonian as described above in the framework of effective Hamiltonians or perturbation theory. It can be shown for variational zeroth-order wave functions (e.g. from HF or Kohn–Sham DFT methods) that it is sufficient to calculate the *linear response* of the wave function with respect to one perturbation in order to evaluate the mixed second derivatives. Furthermore, the order in which the two perturbations are treated does not matter (interchange theorem of double-perturbation theory).

From *response theory* one may obtain the following expression for the calculation of mixed second derivatives in terms of the electron /spin density matrix  $P_{\mu\nu}^{\pm}$  and a set of atomic basis functions  $\{\varphi\}$

$$\frac{\partial^2 E_0}{\partial \lambda \partial \kappa} \Big|_{\lambda=\kappa=0} = \sum_{\mu,\nu} \frac{\partial P_{\mu\nu}^{\pm}}{\partial \lambda} \langle \varphi_{\mu} | \hat{h}_{\kappa} | \varphi_{\nu} \rangle + \sum_{\mu,\nu} P_{\mu\nu}^{\pm} \langle \varphi_{\mu} | \hat{h}_{\lambda,\kappa} | \varphi_{\nu} \rangle \quad (3.128)$$

where

$$\hat{h}_{\kappa} = \frac{\partial \hat{h}(\lambda, \kappa)}{\partial \kappa} \Big|_{\lambda=\kappa=0} \quad \text{and} \quad \hat{h}_{\lambda,\kappa} = \frac{\partial^2 \hat{h}(\lambda, \kappa)}{\partial \lambda \partial \kappa} \Big|_{\lambda=\kappa=0} \quad (3.129)$$

are derivatives of the perturbing operator  $\hat{h}(\lambda, \kappa)$  which may contain terms depending on the perturbations  $\lambda$  or  $\kappa$  as well as products of both. The total Hamiltonian is defined as a sum of the zeroth-order (non-relativistic) Born–Oppenheimer Hamiltonian  $\hat{\mathcal{H}}_0$  and the perturbation operator  $\hat{h}(\lambda, \kappa)$

$$\hat{\mathcal{H}} = \hat{\mathcal{H}}_0 + \hat{h}(\lambda, \kappa) = \hat{\mathcal{H}}_0 + (\hat{P}_1 \cdot \lambda + \hat{P}'_1 \cdot \kappa + \dots + \lambda \cdot \hat{P}_2 \cdot \kappa + \dots). \quad (3.130)$$

The first term in Equation 3.128 gives rise to second-order contributions to a property and the second term yields first-order contributions. Terms in  $\hat{h}(\lambda, \kappa)$  involving both  $\lambda$  and  $\kappa$  lead to first-order contributions (since the first derivative of these terms at  $\lambda = \kappa = 0$  vanishes) and terms involving either  $\lambda$  or  $\kappa$  yield second-order contribution (since the second derivative with respect to both perturbations of such terms is zero).

As was already mentioned, for this approach to mixed second energy derivatives it is sufficient to determine the first-order response of the wave function with respect to only one of the two perturbations, here  $\partial P_{\mu\nu}^{\pm}/\partial\lambda$ . To accomplish the computation of the perturbed wavefunction parameters (perturbed MO coefficients) the *coupled-perturbed SCF* (CPSCF) procedure [33, 34] is used. The perturbed first-order orbitals  $\psi_i^{\sigma(1)}$  are expanded as a sum over zeroth-order virtual orbitals  $\psi_a^{\sigma(0)}$  of the same spin  $\sigma$

$$\psi_i^{\sigma(1)}(\mathbf{r}) = \sum_{a \in \sigma} U_{ia}^{\sigma} \psi_a^{\sigma(0)}(\mathbf{r}) \quad (3.131)$$

where the  $U_{ia}^{\sigma}$  are the first-order wave function coefficients describing the mixing between occupied and virtual orbitals. They have to be determined as solutions of the CPSCF equations

$$\begin{pmatrix} \mathbf{M}^{\alpha\alpha} & 0 \\ 0 & \mathbf{M}^{\beta\beta} \end{pmatrix} \begin{pmatrix} \mathbf{U}^{\alpha} \\ \mathbf{U}^{\beta} \end{pmatrix} = - \begin{pmatrix} \mathbf{V}^{\alpha} \\ \mathbf{V}^{\beta} \end{pmatrix} \quad (3.132)$$

with the magnetic Hessian  $\mathbf{M}^{\sigma\sigma'}$  and the matrix elements of the perturbing operator

$$V_{ai}^{\sigma} = \langle \psi_a^{\sigma(0)} | \hat{h}_{\lambda} | \psi_i^{\sigma(0)} \rangle \quad \text{where} \quad \hat{h}_{\lambda} = \left. \frac{\partial \hat{h}(\lambda, \kappa)}{\partial \lambda} \right|_{\lambda=\kappa=0}. \quad (3.133)$$

For the perturbed spin density matrix derivative this formalism leads to

$$\frac{\partial \mathbf{P}^{\sigma}}{\partial \lambda} = \mathbf{c}^{\alpha} \begin{pmatrix} 0 & \mathbf{U}^{\alpha} \\ -\mathbf{U}^{\alpha} & 0 \end{pmatrix} (\mathbf{c}^{\alpha})^T - \mathbf{c}^{\beta} \begin{pmatrix} 0 & \mathbf{U}^{\beta} \\ -\mathbf{U}^{\beta} & 0 \end{pmatrix} (\mathbf{c}^{\beta})^T. \quad (3.134)$$

In the case that the matrix elements of the perturbing operator  $\hat{h}_{\lambda}$  are purely imaginary (e.g. for a magnetic field perturbation using the orbital Zeeman operator for  $\hat{h}(\lambda, \kappa)$  and real zeroth-order orbitals), the coefficients  $U_{ia}^{\sigma}$  are also purely imaginary. Moreover, in the absence of exact exchange contributions (pure density functionals) the magnetic Hessian is diagonal and the coefficients can be written as

$$U_{ia}^{\sigma} = \frac{i \text{Im} \langle \psi_a^{\sigma(0)} | \hat{h}_{\lambda} | \psi_i^{\sigma(0)} \rangle}{\epsilon_a^{\sigma(0)} - \epsilon_i^{\sigma(0)}} \quad (3.135)$$

which is similar to the result that could be obtained from Rayleigh–Schrödinger perturbation theory.

**Computational Procedure and Drawbacks** The actual EPR parameter calculation procedure as employed in this thesis schematically works as follows: First, the non-relativistic ground state SCF wave function for an optimized geometry is computed in the DFT Kohn–Sham framework. In the next step the relativistic effects and effects due to a magnetic field are considered perturbationally using the non-relativistic wave function as zeroth-order wave function. Finally, the SH parameters can be obtained from the perturbed energies depending on what type of perturbation operator has been incorporated.

However, there are several problems involved in this procedure mainly concerning the treatment of SOC. First, there are different approximate methods for the calculation of the matrix elements of the spin–orbit operator, e.g. effective nuclear charges or the AMFI approximation partly neglecting two-electron terms. Furthermore, SOC is included only to leading order in the second-order perturbation expressions which may not be sufficient in some cases. The next paragraph addresses how higher-order as well as scalar relativistic effects can be incorporated in a computational treatment.

**Relativistic Methods** Instead of using perturbation theory, relativistic effects, i.e. the scalar relativistic effects and the spin–orbit coupling, can also be directly incorporated into the electronic structure calculation (e.g. based on DFT). Then, only first order perturbation theory is necessary to calculate all magnetic parameters.

However, the inclusion of relativistic effects is a challenging problem for electronic structure calculations. The Breit–Pauli Hamiltonian introduced here is solely suitable for perturbation calculations and other operators (with regular behaviour in a variational procedure) have to be derived from the Dirac equation.

One popular relativistic method is the ZORA (*zeroth-order regular approximation*) method [35] that has been used for the calculation of EPR parameters. Other approaches are based on the application of the *Douglas–Kroll–Hess* (DKH) transformation [36, 37] of the Dirac equation. Examples for the latter method can e.g. be found in works of Malkin et al. [38] or Neese et al. [39] and references therein.

## References

- [1] Kaupp, M.; Malkin, V. G.; Bühl, M., Eds.; *Calculation of NMR and EPR Parameters*; Wiley-VCH: Weinheim, 2004.
- [2] Harriman, J. E. *Theoretical Foundations of Electron Spin Resonance*; Academic Press: New York, 1978.
- [3] Moss, R. E. *Advanced Molecular Quantum Mechanics*; Chapman and Hall: London, 1973.
- [4] Lushington, G. *Hartree-Fock and Configuration Interaction Calculations of Electronic g-Tensors*, Ph.D. thesis, University of New Brunswick, Canada, 1996.
- [5] Neese, F.; Solomon, E. I. In *Magnetism: Molecules to Materials IV*; Miller, J. S.; Drillon, M., Eds.; Wiley-VCH: 2002.
- [6] McWeeny, R. *J. Chem. Phys.* **1965**, *42*, 1717–1725.
- [7] McWeeny, R. *Spins in Chemistry*; Academic Press: New York, 1970.
- [8] McWeeny, R. *Methods of Molecular Quantum Mechanics*; Academic Press: London, 1992.
- [9] Gordy, W. *Theory and Applications of Electron Spin Resonance*; volume XV of *Techniques of Chemistry* John Wiley & Sons: New York, 1980.
- [10] Weltner, W. *Magnetic Atoms and Molecules*; Dover Publications: New York, 1983.
- [11] Mabbs, F. E.; Collison, D. *Electron Paramagnetic Resonance of d Transition Metal Compounds*; Elsevier Science: Amsterdam, 1992.
- [12] Weil, J. A.; Bolton, J. R.; Wertz, J. E. *Electron Paramagnetic Resonance – Elementary Theory and Practical Applications*; Wiley: New York, 1994.
- [13] Dirac, P. A. M. *The Principles of Quantum Mechanics*; Oxford University Press: Oxford, 1958.
- [14] Abragam, A.; Bleaney, B. *Electron Paramagnetic Resonance of Transition Ions*; Clarendon Press: Oxford, 1970.

- [15] Strange, P. *Relativistic Quantum Mechanics*; Cambridge University Press: Cambridge, 1998.
- [16] Einstein, A. *Ann. Phys.* **1905**, *17*, 891–921.
- [17] Dirac, P. A. M. *Proc. Roy. Soc. A* **1928**, *117*, 610–624.
- [18] Foldy, L. L.; Wouthuysen, S. A. *Phys. Rev.* **1950**, *78*, 29–36.
- [19] Pauli, W. *Z. Phys.* **1927**, *43*, 601–623.
- [20] Lorentz, H. A. *Proc. Acad. Sci. Amsterdam* **1904**, *6*, 809–831.
- [21] Breit, G. *Phys. Rev.* **1929**, *34*, 553–573.
- [22] Breit, G. *Phys. Rev.* **1930**, *36*, 383–397.
- [23] Breit, G. *Phys. Rev.* **1932**, *39*, 616–624.
- [24] Hess, B. A.; Marian, C. M.; Wahlgren, U.; Gropen, O. *Chem. Phys. Lett.* **1996**, *251*, 365–371.
- [25] Lucken, E. A. C. *Nuclear Quadrupole Coupling Constants*; Academic Press: London, New York, 1969.
- [26] Pyykkö, P. *Mol. Phys.* **2001**, *99*, 1617–1629.
- [27] Bencini, A.; Gatteschi, D. *EPR of Exchange Coupled Systems*; Springer: Heidelberg, 1990.
- [28] Kahn, O. *Molecular Magnetism*; VCH: Weinheim, 1. ed.; 1993.
- [29] Illas, F.; de P. R. Moreira, I.; de Graaf, C.; Barone, V. *Theor. Chem. Acc.* **2000**, *104*, 265–272.
- [30] Noodleman, L. *J. Chem. Phys.* **1981**, *74*, 5737–5743.
- [31] Noodleman, L.; Case, D. A. *Adv. Inorg. Chem.* **1992**, *38*, 423–470.
- [32] Yamaguchi, K.; Jensen, F.; Dorigo, A.; Houk, K. N. *Chem. Phys. Lett.* **1988**, *149*, 537–542.
- [33] Stevens, R. M.; Pitzer, R. M.; Lipscomb, W. N. *J. Chem. Phys.* **1963**, *38*, 550–560.

- 
- [34] Häser, M.; Ahlrichs, R.; Baron, H. P.; Weis, P.; Horn, H. *Theor. Chim. Acta* **1992**, *83*, 455–470.
- [35] van Lenthe, E.; Baerends, E. J.; Snijders, J. G. *J. Chem. Phys.* **1993**, *99*, 4597–4610.
- [36] Douglas, M.; Kroll, N. M. *Annals Phys.* **1974**, *82*, 89–155.
- [37] Hess, B. A. *Phys. Rev. A* **1986**, *33*, 3742–3748.
- [38] Malkin, I.; Malkina, O. L.; Malkin, V. G.; Kaupp, M. *J. Chem. Phys.* **2005**, *123*, 244103.
- [39] Neese, F.; Wolf, A.; Fleig, T.; Reiher, M.; Hess, B. A. *J. Chem. Phys.* **2005**, *122*, 204107.

*“...the main object of physical science is not the provision of pictures, but is the formulation of laws governing phenomena and the application of these laws to the discovery of new phenomena. If a picture exists, so much the better; but whether a picture exists or not is of secondary importance. In the case of atomic phenomena no picture can be expected to exist in the usual sense of the word ‘picture,’ by which is meant a model functioning essentially on classical lines.”*

P. A. M. DIRAC, 1902–1984

## Chapter 4

# Computational Methods

The description of computational chemistry in this chapter represents just a brief introduction to this topic. The main goal is to explain the theoretical methods that were used to compute the non-relativistic (zeroth-order) wave functions. Starting from these zeroth-order wave functions the EPR parameters may be calculated employing a perturbative treatment of magnetic field and relativistic effects (see previous chapter). Furthermore, the basis sets and computational chemistry programs which were used in these studies will be introduced. Detailed information concerning computational chemistry can be found in Refs. 1–8 and further references will only be given in special cases.

### 4.1 Hartree–Fock Approximation and Electron Correlation

In Hartree–Fock (HF) theory the non-relativistic time-independent Schrödinger equation is solved by using a simple antisymmetrized product of one-electron functions  $\chi_i(\mathbf{x}_i)$  as an approximation for the complicated exact many-electron wave function  $\Psi_0$ . This product is also called *Slater determinant*  $\Phi_{SD}$

$$\Psi_0 \approx \Phi_{SD} = \frac{1}{\sqrt{N!}} \begin{vmatrix} \chi_1(\mathbf{x}_1) & \chi_2(\mathbf{x}_1) & \cdots & \chi_N(\mathbf{x}_1) \\ \chi_1(\mathbf{x}_2) & \chi_2(\mathbf{x}_2) & \cdots & \chi_N(\mathbf{x}_2) \\ \vdots & \vdots & \ddots & \vdots \\ \chi_1(\mathbf{x}_N) & \chi_2(\mathbf{x}_N) & \cdots & \chi_N(\mathbf{x}_N) \end{vmatrix}. \quad (4.1)$$

The one-electron functions  $\chi_i(\mathbf{x}_i)$  are also called *spin orbitals* and consist of a spatial part  $\phi_i(\mathbf{r})$  and one of the two spin functions  $\alpha(s)$  or  $\beta(s)$

$$\chi(\mathbf{x}) = \phi(\mathbf{r})\sigma(s) \quad \text{with} \quad \sigma = \alpha, \beta. \quad (4.2)$$

With this *ansatz* for the wave function, the next step is to search for the Slater determinant with the lowest energy using the *variational principle*. The expectation value of the Hamilton operator with a Slater determinant can be derived by expanding the determinant and collecting the terms with the corresponding terms of the Hamilton operator (in the Born–Oppenheimer approximation and in atomic units)

$$\begin{aligned} \hat{\mathcal{H}}_{\text{BO}} &= \hat{T}_e + \hat{V}_{Ne} + \hat{V}_{ee} \\ &= - \sum_{i=1}^N \frac{1}{2} \nabla_i^2 - \sum_{A=1}^M \sum_{i=1}^N \frac{Z_A}{r_{iA}} + \sum_{i<j}^N \frac{1}{r_{ij}}. \end{aligned} \quad (4.3)$$

$\nabla_i^2$  is the *Laplace operator* and  $Z_A$  is the nuclear charge of nucleus  $A$ .  $r_{iA}$  are the electron–nucleus and  $r_{ij}$  the electron–electron distances, respectively. The operators represent the kinetic energy of the electrons ( $\hat{T}_e$ ), the attractive electrostatic interaction between nuclei and electrons ( $\hat{V}_{Ne}$ ) and the repulsive electron–electron interaction ( $\hat{V}_{ee}$ ). Thus, one obtains for the HF energy

$$E_{\text{HF}} = \langle \Phi_{\text{SD}} | \hat{\mathcal{H}} | \Phi_{\text{SD}} \rangle = \sum_i^N \left( i | \hat{h} | i \right) + \frac{1}{2} \sum_i^N \sum_j^N (ii | jj) - (ij | ji), \quad (4.4)$$

where

$$\left( i | \hat{h} | i \right) = \int \chi_i^*(\mathbf{x}_1) \left\{ -\frac{1}{2} \nabla^2 - \sum_A^M \frac{Z_A}{r_{1A}} \right\} \chi_i(\mathbf{x}_1) \, d\mathbf{x}_1 \quad (4.5)$$

stands for the contribution from kinetic energy and electron–nuclear attraction and

$$(ii | jj) = \iint |\chi_i(\mathbf{x}_1)|^2 \frac{1}{r_{12}} |\chi_j(\mathbf{x}_2)|^2 \, d\mathbf{x}_1 \, d\mathbf{x}_2 \quad (4.6)$$

$$(ij | ji) = \iint \chi_i(\mathbf{x}_1) \chi_j^*(\mathbf{x}_1) \frac{1}{r_{12}} \chi_j(\mathbf{x}_2) \chi_i^*(\mathbf{x}_2) \, d\mathbf{x}_1 \, d\mathbf{x}_2 \quad (4.7)$$

are the so-called *Coulomb* and *exchange integrals* that describe the electron–electron interaction. To minimize  $E_{\text{HF}}$  the spin orbitals  $\chi_i$  are varied and the *Hartree–Fock equations* are obtained

$$\hat{f} \chi_i = \epsilon_i \chi_i \quad \text{with} \quad i = 1, 2, \dots, N. \quad (4.8)$$

The orbital energies  $\epsilon_i$  are the eigenvalues of the *Fock operator*  $\hat{f}$ . This one-electron operator is defined as

$$\hat{f}_i = -\frac{1}{2}\nabla_i^2 - \sum_A \frac{Z_A}{r_{iA}} + \sum_j \left( \hat{J}_j(\mathbf{x}_1) - \hat{K}_j(\mathbf{x}_1) \right). \quad (4.9)$$

Here, the complicated two-electron operator  $\frac{1}{r_{ij}}$  from the exact Hamiltonian operator is replaced by the one-electron Coulomb and exchange operators  $\hat{J}_j(\mathbf{x}_1)$  and  $\hat{K}_j(\mathbf{x}_1)$  that describe the *Hartree–Fock potential*. This potential represents the averaged repulsive interaction of electron  $i$  with the  $N - 1$  other electrons.

To solve the Hartree–Fock equations 4.8 one usually takes advantage of the *LCAO (linear combination of atomic orbitals) ansatz* describing the spin orbitals  $\chi_i$  as linear combinations of one-electron (atom-centered) basis functions  $\varphi_\mu$

$$\chi_i = \sum_{\mu=1}^L c_{i\mu} \varphi_\mu \quad \text{with } L \geq N. \quad (4.10)$$

Now the coefficients  $c_{i\mu}$  can be varied instead of the spin orbitals themselves and application of the variational principle leads to the *Roothaan–Hall equations* [9–11]

$$\sum_{\nu=1}^L (F_{\mu\nu} - \epsilon_i S_{\mu\nu}) c_{\nu i} = 0 \quad \mu = 1, \dots, L \quad (4.11)$$

with the orbital energies  $\epsilon_i$ , the *overlap integrals*

$$S_{\mu\nu} = \int \varphi_\mu^* \varphi_\nu \, d\tau, \quad (4.12)$$

and the *Fock matrix*

$$F_{\mu\nu} = \int \varphi_\mu^* \left( -\frac{1}{2}\nabla_i^2 - \sum_A \frac{Z_A}{r_{iA}} \right) \varphi_\nu \, d\tau + \sum_{\sigma,\lambda} P_{\sigma\lambda} \left[ (\mu\nu|\lambda\sigma) - \frac{1}{2}(\mu\lambda|\nu\sigma) \right] \quad (4.13)$$

where  $P_{\sigma\lambda}$  represents the *density matrix*

$$P_{\sigma\lambda} = 2 \sum_{i=1}^{\text{occ.}} c_{i\sigma}^* c_{i\lambda}. \quad (4.14)$$

Since the elements of the Fock matrix depend on the LCAO coefficients  $c_{i\mu}$ , the Roothaan–Hall equations have to be solved iteratively using a self-consistent field (SCF) methodology.

It has already been mentioned that Hartree–Fock theory makes the fundamental approximation that each electron moves in the static electric field created by all of the other electrons. Using this averaged repulsion the lowest-energy Slater determinant is computed. However, such a single-determinantal wave function can never be the true wave function of a many-electron system, although it is the exact solution for a system of non-interacting particles moving in an effective potential. Due to this approximation  $E_{\text{HF}}$  is always larger (less negative) than the exact Born–Oppenheimer non-relativistic ground state energy  $E_0$ . The difference between these two energies is called *correlation energy*  $E_C^{\text{HF}}$ .

$$E_C^{\text{HF}} = E_0 - E_{\text{HF}} \quad (4.15)$$

$E_C^{\text{HF}}$  is a measure for the error introduced by the HF method. Since correlation effects play an important role for the description of chemical reactions as well as the calculation of molecular properties (e.g. EPR properties), the question arises how the HF wave function might be improved to obtain a lower energy. One obvious choice for a better wave function is to construct it as a linear combination of multiple determinants

$$\Psi_0 = c_0\Psi_{\text{HF}} + c_1\Psi_1 + c_2\Psi_2 + \dots \quad (4.16)$$

where  $\Psi_{\text{HF}} = \Phi_{\text{SD}}$  and the coefficients  $c$  reflect the weight of each determinant in the expansion and also ensure normalization. Two different aspects of electron correlation can be discussed. In many cases the main error in the HF approximation derives from ignoring the correlated motion of each electron with every other meaning pictorially that the electrons come to close to each other within HF theory. This kind of correlation is called *dynamical correlation* because it refers to the dynamical character of the electron–electron interactions. Empirically, it is observed that for most systems the HF determinant dominates in the linear combination for the total wave function. Even though the correlation energy may be large, it tends to be made up from a sum of small contributions from other determinants.

However, in some instances, one or more of the other determinants may have coefficients of similar magnitude to that of the HF wave function. This kind of electron correlation is called *static (or non-dynamical) correlation*. This emphasizes that the error here is not so much that the HF approximation ignores the correlated electron movement, but rather that the HF ansatz uses single-determinantal wave functions, which is not sufficiently flexible for some systems.

Non-dynamical electron correlation is e.g. important for closed-shell singlet states with near or exact degeneracy in frontier orbitals or open-shell singlet states of two antiferromagnetically coupled paramagnetic  $S = \frac{1}{2}$  centers (cf. also the case of nitroxide biradicals in Section 6.1).

Due to the general importance of electron correlation for quantum chemistry, several methods have been developed that include correlation effects into the wave function. Such approaches are MCSCF (multiconfiguration self-consistent field), CI (configuration interaction) or MRCI (multireference CI) methods, perturbation theory (e.g. Møller–Plesset) as well as CC (coupled cluster) approaches. Furthermore, electron correlation is also (partially) recovered within the DFT (density functional theory) framework. The latter two methods are described in a little more detail in the following sections as they were both employed for EPR parameter calculations in this thesis.

## 4.2 Coupled Cluster Methods

The basic principle of CC theory is that the exact wave function within the basis set approximation (full-CI wave function) can be described as

$$\Psi = e^{\hat{T}} \Psi_{\text{HF}} \quad \text{with} \quad e^{\hat{T}} = 1 + \hat{T} + \frac{\hat{T}^2}{2!} + \frac{\hat{T}^3}{3!} + \dots = \sum_{k=0}^{\infty} \frac{1}{k!} \hat{T}^k. \quad (4.17)$$

The cluster operator  $\hat{T}$  is defined as

$$\hat{T} = \hat{T}_1 + \hat{T}_2 + \hat{T}_3 + \dots + \hat{T}_N \quad (4.18)$$

where  $N$  is the total number of electrons and the various  $\hat{T}_i$  operators generate all possible determinants having  $i$  electron excitations from the reference wave function (in this case  $\Psi_{\text{HF}}$ ). For example,

$$\hat{T}_1 \Psi_{\text{HF}} = \sum_i^{\text{occ.}} \sum_a^{\text{virt.}} t_i^a \Psi_i^a \quad (4.19)$$

$$\hat{T}_2 \Psi_{\text{HF}} = \sum_{i < j}^{\text{occ.}} \sum_{a < b}^{\text{virt.}} t_{ij}^{ab} \Psi_{ij}^{ab} \quad (4.20)$$

with  $\Psi_{ij}^{ab}$  representing a determinant where electrons from the orbitals  $i$  and  $j$  (occupied orbitals of the reference determinant) have been excited to the orbitals

$a$  and  $b$  (virtual orbitals of the reference determinant). The expansion of  $\hat{T}$  ends at  $N$  because no more than  $N$  excitations are possible. Now, the wave function  $\Psi_{\text{CCSD}}$  that may be constructed using the single and double excitation operators only ( $\hat{T} = \hat{T}_1 + \hat{T}_2$ ) can be expressed using the Taylor expansion of the exponential operator in Eq. 4.17

$$\begin{aligned}\Psi_{\text{CCSD}} &= e^{\hat{T}} \Psi_{\text{HF}} \\ &= \left( 1 + (\hat{T}_1 + \hat{T}_2) + \frac{(\hat{T}_1 + \hat{T}_2)^2}{2!} + \frac{(\hat{T}_1 + \hat{T}_2)^3}{3!} + \dots \right) \Psi_{\text{HF}} \\ &= \left( 1 + \hat{T}_1 + (\hat{T}_2 + \frac{1}{2}\hat{T}_1^2) + (\hat{T}_2\hat{T}_1 + \frac{1}{6}\hat{T}_1^3) \right. \\ &\quad \left. + (\frac{1}{2}\hat{T}_2^2 + \frac{1}{2}\hat{T}_2\hat{T}_1^2 + \frac{1}{24}\hat{T}_1^4) + \dots \right) \Psi_{\text{HF}}.\end{aligned}\tag{4.21}$$

The  $1 + \hat{T}_1$  terms generate the reference state and all singly excited states and the first parenthesis generates all doubly excited states, which may be considered as connected ( $\hat{T}_2$ ) or disconnected ( $\hat{T}_1^2$ ). The second parenthesis generates all triply excited states, which are only ‘product’ triples ( $\hat{T}_2\hat{T}_1, \hat{T}_1^3$ ) in the case of CCSD, the third parenthesis generates all quadruply excited states and so on. Thus, the idea in CC methods is to include all corrections of a given type to infinite order. Furthermore, the disconnected higher order terms  $\hat{T}_i^n$  ensure size consistency of CC methods. Note, however, that CC methods are not variational.

Using the CC wave function the corresponding energy can be expressed as

$$E_{\text{CC}} = \langle \Psi_{\text{HF}} | \hat{\mathcal{H}} e^{\hat{T}} | \Psi_{\text{HF}} \rangle.\tag{4.22}$$

Since calculations including all terms of  $\hat{T}$  up to  $\hat{T}_N$  are not tractable computationally, the cluster operator must always be truncated at some excitation level (e.g. at the CCSD level). Therefore, the computed energies will be approximate. How severe the approximation is depends on how many terms are included in  $\hat{T}$ . Including only the  $\hat{T}_1$  operator does not give any improvement over HF, as matrix elements between the HF and singly excited states are zero. The lowest level of approximation is therefore  $\hat{T} = \hat{T}_2$ , referred to as coupled cluster doubles (CCD). Using  $\hat{T} = \hat{T}_1 + \hat{T}_2$  gives the CCSD model which is only slightly more demanding than CCD, and yields a more complete model. Both CCD and CCSD involve a computational effort which scales as  $M^6$  ( $M$  being the number of basis functions) in the limit of a large basis set. The next higher level has  $\hat{T} = \hat{T}_1 + \hat{T}_2 + \hat{T}_3$ , giving the CCSDT model which already scales as  $M^8$ . It can only be used for small

systems, and CCSD is the only generally applicable coupled cluster method. Alternatively, the triples contribution may be evaluated by perturbation theory and added to the CCSD results. Several such hybrid methods exist; the most robust and most commonly used is known by the acronym CCSD(T). It was employed in this work for HFC tensor computations in order to validate DFT methods (cf. Section 6.5).

### 4.3 Density Functional Theory

As has already been mentioned at the end of Section 4.1, *density functional theory* (DFT) methods using approximate exchange–correlation functionals (see below) recover part of the important electron correlation. Since the computational effort of standard DFT methods is comparable to HF methods, DFT methods have become widely used for all types of systems involving more than a few heavy atoms.

The central quantity of DFT is the *electron density*  $\rho(\mathbf{r})$  that can be obtained as the square of the wave function for an  $N$ -electron system integrated over  $N - 1$  spatial electron coordinates and  $N$  spin coordinates. Thus, the electron density is a non-negative function of only three spatial coordinates

$$\rho(\mathbf{r}) = N \int \cdots \int |\Psi(\mathbf{x}_1, \dots, \mathbf{x}_N)|^2 ds_1 d\mathbf{x}_2 \dots d\mathbf{x}_N \quad (4.23)$$

that vanishes at infinity and yields the total number  $N$  of electrons in the system when integrated

$$\rho(\mathbf{r} \rightarrow \infty) = 0, \quad (4.24)$$

$$\int \rho(\mathbf{r}_1) d\mathbf{r}_1 = N. \quad (4.25)$$

At the position of atoms  $\rho(\mathbf{r})$  possesses maxima (cusps). In contrast to the many-electron wave function, the electron density is not solely a complicated mathematical structure but a physical observable that can be experimentally determined (e.g. by X-ray diffraction methods). Furthermore, the wave function depends on  $3N$  ( $4N$  including spin) coordinates whereas the electron density has always three variables independently of the system size.

A rigorous theoretical foundation for DFT was provided by the two *Hohenberg–Kohn theorems* [12] that prove that the ground-state electronic energy is determined completely by the electron density  $\rho(\mathbf{r})$  and that there is a variational

principle analogous to that in wave mechanics when using the electron density as a parameter. Thus, a one-to-one correspondence between  $\rho(\mathbf{r})$  of a system and the Hamilton operator / energy exists or, in the language of DFT, the energy is a unique functional<sup>1</sup> of the electron density,  $E[\rho(\mathbf{r})]$ . However, although it has been proven that the ground-state electron density and the ground-state energy are connected with each other, the problem with DFT is that the exact functional to fulfill this task is not known.

In analogy with the wave mechanics approach, the energy functional may be divided into three parts: kinetic energy,  $T[\rho]$ , attraction between the nuclei and electrons,  $E_{Ne}[\rho]$ , and electron–electron repulsion,  $E_{ee}[\rho]$ . The nuclear–nuclear repulsion is a constant in the Born–Oppenheimer approximation. A comparison with Hartree–Fock theory suggests that the  $E_{ee}[\rho]$  term be split into a Coulomb and an exchange part,  $J[\rho]$  and  $K[\rho]$ , implicitly including electron correlation in all terms. Only for the  $E_{Ne}[\rho]$  and  $J[\rho]$  functionals the mathematical form is known and the classical expressions are

$$E_{Ne}[\rho] = \int \rho(\mathbf{r})V_{Ne} \, d\mathbf{r} = \sum_A^M \int \frac{Z_A\rho(\mathbf{r}_1)}{r_{1A}} \, d\mathbf{r} \quad \text{and} \quad (4.26)$$

$$J[\rho] = \frac{1}{2} \iint \frac{\rho(\mathbf{r}_1)\rho(\mathbf{r}_2)}{r_{12}} \, d\mathbf{r}_1 \, d\mathbf{r}_2 \quad (4.27)$$

where the prefactor  $\frac{1}{2}$  allows the integration to run over all space for both variables. Early attempts at finding functionals for the kinetic and exchange energies employed a non-interacting uniform electron gas. For such a system it can be shown that  $T[\rho]$  and  $K[\rho]$  are given by

$$T_{\text{TF}}[\rho] = \frac{3}{10}(3\pi^2)^{2/3} \int \rho^{5/3}(\mathbf{r}) \, d\mathbf{r} \quad \text{and} \quad (4.28)$$

$$K_{\text{D}}[\rho] = -\frac{3}{4} \left(\frac{3}{\pi}\right)^{1/3} \int \rho^{4/3}(\mathbf{r}) \, d\mathbf{r}. \quad (4.29)$$

The energy functional  $E_{\text{TF}}[\rho] = T_{\text{TF}}[\rho] + E_{Ne}[\rho] + J[\rho]$  is known as *Thomas–Fermi* (TF) theory and when the  $K_{\text{D}}[\rho]$  part is included one obtains the *Thomas–Fermi–Dirac* (TFD) model. However, the assumption of a non-interacting uniform electron gas is no good approximation for atomic or molecular systems. The total

---

<sup>1</sup>A *function* is a prescription for producing a number from a set of variables, whereas a *functional* is a prescription for producing a number from a function, which in turn depends on variables. While a function is denoted with parentheses,  $f(x)$ , a functional is denoted with square brackets,  $F[f(x)]$ .

energies are in error by 15–50%, but the worst feature of the TF and TFD theories is that they do not predict bonding, i.e. molecules do not exist.

A major breakthrough for the use of DFT in computational chemistry was the introduction of orbitals by *Kohn* and *Sham* [13]. They had realized that the main problem in TF models is that the kinetic energy is represented poorly whereas orbital-based approaches (e.g. the HF method) perform much better in this respect. Thus, Kohn and Sham introduced the concept of a *non-interacting reference system* built from a set of one-electron orbitals  $\phi_i$  such that the major part of the kinetic energy can be computed exactly. The remainder is merged with the non-classical contributions to the electron–electron repulsion – which are also unknown, but usually fairly small. By this method, as much information as possible is computed exactly, leaving only a small part of the total energy to be determined by an approximate functional.

To clarify the idea behind *Kohn–Sham* (KS) theory to calculate part of the kinetic energy exactly one can assume a Hamilton operator of the form

$$\hat{\mathcal{H}}_\lambda = \hat{T}_e + \hat{V}_{\text{ext}}(\lambda) + \lambda \hat{V}_{ee} \quad (4.30)$$

with  $0 \leq \lambda \leq 1$ . The  $\hat{V}_{\text{ext}}$  operator is equal to  $\hat{V}_{Ne}$  for  $\lambda = 1$ , for intermediate  $\lambda$  values, however, it is assumed that the external potential  $\hat{V}_{\text{ext}}(\lambda)$  is adjusted so that the *same* density is obtained for both  $\lambda = 1$  (the real system) and  $\lambda = 0$  (the hypothetical system of non-interacting electrons). For  $\lambda = 0$  the exact solution to the Schrödinger equation is given as a Slater determinant composed of molecular orbitals  $\phi_i$  for which the exact kinetic energy functional is given as

$$T_S = \sum_{i=1}^N \langle \phi_i | -\frac{1}{2} \nabla_i^2 | \phi_i \rangle \quad (4.31)$$

where the subscript S indicates that it is the kinetic energy of a Slater determinant. The  $\lambda = 1$  case corresponds to interacting electrons, thus  $T_S$  provides only an approximation to the real kinetic energy which is, however, a substantial improvement over the TF model (Eq. 4.28).

The key to KS theory is thus the calculation of the kinetic energy under the assumption of non-interacting electrons (similar to HF theory) employing Eq. 4.31. In reality the electrons are interacting, and this approach does not provide the total kinetic energy of the real system. However, the difference between the exact kinetic energy and that calculated by assuming non-interacting orbitals is small.

The remaining kinetic energy is included into an exchange–correlation term, and a general DFT energy expression can be written as

$$\begin{aligned}
 E_{\text{DFT}}[\rho] &= T_{\text{S}}[\rho] + E_{N_e}[\rho] + J[\rho] + E_{\text{XC}}[\rho] \\
 &= T_{\text{S}}[\rho] + \int V_{N_e}\rho(\mathbf{r}) \, d\mathbf{r} + \frac{1}{2} \iint \frac{\rho(\mathbf{r}_1)\rho(\mathbf{r}_2)}{r_{12}} \, d\mathbf{r}_1 \, d\mathbf{r}_2 + E_{\text{XC}}[\rho] \\
 &= -\frac{1}{2} \sum_i^N \langle \phi_i | \nabla_i^2 | \phi_i \rangle - \sum_i^N \sum_A^M \int \frac{Z_A}{r_{1A}} |\phi_i(\mathbf{r}_1)|^2 \, d\mathbf{r}_1 \\
 &\quad + \frac{1}{2} \sum_i^N \sum_j^N \iint |\phi_i(\mathbf{r}_1)|^2 \frac{1}{r_{12}} |\phi_j(\mathbf{r}_2)|^2 \, d\mathbf{r}_1 \, d\mathbf{r}_2 + E_{\text{XC}}[\rho].
 \end{aligned} \tag{4.32}$$

Using this equation and the exact energy, a definition of  $E_{\text{XC}}$  can be obtained. It is the part of the exact energy which remains after subtraction of the non-interacting kinetic energy and the  $E_{N_e}$  and  $J$  potential energy terms.

$$E_{\text{XC}}[\rho] = (T[\rho] - T_{\text{S}}[\rho]) + (E_{ee}[\rho] - J[\rho]) \tag{4.33}$$

Thus,  $E_{\text{XC}}$  contains all contributions to the exact total energy that are unknown. The first parenthesis may be considered as the kinetic correlation energy, while the second contains both exchange and potential correlation energy.<sup>2</sup>

Next, the question has to be addressed how the orbitals  $\phi_i$  of the non-interacting reference system can be uniquely determined. In other words, how can the external potential be defined that it really provides a Slater determinant which is characterized by exactly the same density as the real system. To solve this problem, the set of orthogonal orbitals  $\phi_i$  which minimize the energy have to be calculated using the *Lagrange method*, in analogy with the HF method.

$$L[\rho] = E_{\text{DFT}}[\rho] - \sum_{ij}^N \lambda_{ij} [\langle \phi_i | \phi_j \rangle - \delta_{ij}] \tag{4.34}$$

Requiring the variation of  $L$  to vanish leads to a set of equations involving the effective one-electron *Kohn–Sham operator*  $\hat{h}_{\text{KS}}$ , similar to the Fock operator in

---

<sup>2</sup>Furthermore,  $E_{\text{XC}}$  does include a self-interaction correction. It shall also be noted here that the DFT definitions of exchange and correlation energies are not completely equivalent to their wave mechanics counterparts.

wave mechanics.

$$\hat{h}_{\text{KS}}\phi_i = \sum_j^N \lambda_{ij}\phi_j \quad (4.35)$$

$$\hat{h}_{\text{KS}} = -\frac{1}{2}\nabla^2 + V_{\text{eff}}(\mathbf{r}) \quad (4.36)$$

$$V_{\text{eff}}(\mathbf{r}) = V_{Ne}(\mathbf{r}) + \int \frac{\rho(\mathbf{r}_2)}{r_{12}} d\mathbf{r}_2 + V_{\text{XC}}(\mathbf{r}) \quad (4.37)$$

It is possible to apply a unitary transformation which makes the Lagrange multiplier diagonal and produces a set of canonical Kohn–Sham (KS) orbitals. The resulting eigenvalue equations are known as the *KS equations*

$$\hat{h}_{\text{KS}}\phi_i = \epsilon_i\phi_i. \quad (4.38)$$

The unknown KS orbitals may be determined numerically or expanded in a set of basis functions, analogously to the HF method.

Knowledge of the different terms in Eq. 4.37 allows to calculate the effective potential  $V_{\text{eff}}$  and thus via Eq. 4.38 the KS orbitals. The orbitals can be used to obtain the density of the non-interacting system  $\rho_S$  which is identical with the ground-state electron density  $\rho_0$

$$\rho_S(\mathbf{r}) = \sum_i^N \sum_s |\phi_i(\mathbf{r}, s)|^2 = \rho_0(\mathbf{r}) \quad (4.39)$$

and finally with Eq. 4.32 the ground state energy  $E_0[\rho_0]$ . Since  $V_{\text{eff}}$  itself depends on the density and hence on the KS orbitals, the one-electron KS equations 4.38 have to be solved iteratively.

It is convenient to separate the exchange–correlation energy  $E_{\text{XC}}$  into two parts, a pure exchange part  $E_{\text{X}}$  and a correlation part  $E_{\text{C}}$ , although it is not clear that this is a valid assumption. Each of these energies is often written in terms of the energy per particle (energy density),  $\epsilon_{\text{X}}$  and  $\epsilon_{\text{C}}$ .

$$E_{\text{XC}}[\rho] = E_{\text{X}}[\rho] + E_{\text{C}}[\rho] = \int \rho(\mathbf{r})\epsilon_{\text{X}}[\rho(\mathbf{r})] d\mathbf{r} + \int \rho(\mathbf{r})\epsilon_{\text{C}}[\rho(\mathbf{r})] d\mathbf{r} \quad (4.40)$$

The corresponding potential required in Eq. 4.37 is then given as the derivative of the energy with respect to the density

$$V_{\text{XC}}(\mathbf{r}) = \frac{\partial E_{\text{XC}}[\rho]}{\partial \rho(\mathbf{r})} = \epsilon_{\text{XC}}[\rho(\mathbf{r})] + \rho(\mathbf{r}) \frac{\partial \epsilon_{\text{XC}}(\mathbf{r})}{\partial \rho}. \quad (4.41)$$

Although there are many similarities between HF theory and DFT, the crucial difference is that DFT would provide the exact total energy, including electron correlation, if the exact  $E_{\text{XC}}[\rho]$  was known. DFT methods therefore have the potential of including the computationally difficult part in wave mechanics, the correlation energy, at a computational effort similar to that for determining the uncorrelated HF energy. However, this is certainly the case for approximations to  $E_{\text{XC}}[\rho]$  but not necessarily true for the exact  $E_{\text{XC}}[\rho]$ . It may be that this functional is so complicated that the computational effort for solving the KS equations will be similar to that required for solving the Schrödinger equation exactly with a wave mechanics approach.

Since the explicit functional form of the exact  $E_{\text{XC}}[\rho]$  is unknown and since there is little theoretical guidance how to construct approximate functionals or systematically improve them, the major problem in DFT is deriving suitable formulas for the approximate exchange–correlation functional. This issue will be briefly addressed in the next section.

DFT methods may be termed *ab initio* if *ab initio* is taken to mean that the method is based on theory which in principle is able to produce exact results. The only problem is that current methods cannot yield the exact results, even in the limit of a complete basis set, due to the unknown functional form of the exact exchange–correlation energy. Wave mechanics employ the exact Hamilton operator and make approximations for the wave function, while DFT makes approximations in the Hamilton operator, and it is easier to improve on the wave function description than to add corrections to the operator.

Accordingly, the lack of a systematic way of extending a series of calculations to approach the exact result is a major drawback of DFT. Even though a sequence of methods such as VWN, BPW91 and B3PW91 (see next section) yields successively lower errors for a suitable set of reference data, there is no guarantee that the same sequence will provide better and better results for a specific property of a given system. Therefore, the performance of a given method for the calculation of a specific property of a specific system can only be judged by investigating the performance for similar systems where experimental or high quality wave mechanics results are available. This renders validation studies indispensable before applying DFT to new systems or for the computation of new properties (cf. also Chapters 6.7 and 6.8).

## 4.4 Exchange–Correlation Functionals

In this section the schematic structure of approximate exchange–correlation functionals  $E_{\text{XC}}[\rho]$  will be explained.

**Local Density Methods** In the *LDA* (local density approximation) it is assumed that the density locally can be treated as a uniform electron gas, or equivalently that the density attains a constant value everywhere.  $E_{\text{XC}}[\rho]$  is then given by

$$E_{\text{XC}}^{\text{LDA}}[\rho] = \int \rho(\mathbf{r}) \epsilon_{\text{XC}}(\rho(\mathbf{r})) \, \text{d}\mathbf{r} \quad (4.42)$$

where  $\epsilon_{\text{XC}}(\rho(\mathbf{r}))$  is the exchange correlation energy per particle in a electron gas with the density  $\rho(\mathbf{r})$ . In the more general case where the  $\alpha$  and  $\beta$  densities,  $\rho_{\alpha}(\mathbf{r})$  and  $\rho_{\beta}(\mathbf{r})$ , respectively, are not equal one arrives at the *LSDA* (local spin-density approximation)

$$E_{\text{XC}}^{\text{LSDA}}[\rho_{\alpha}, \rho_{\beta}] = \int \rho(\mathbf{r}) \epsilon_{\text{XC}}(\rho_{\alpha}(\mathbf{r}), \rho_{\beta}(\mathbf{r})) \, \text{d}\mathbf{r}. \quad (4.43)$$

The LSDA approximation in general underestimates the exchange energy by about 10%, thereby creating errors which are larger than the whole correlation energy. Electron correlation is furthermore overestimated and thus bond strengths are also overestimated.

In this work, the LSDA functional VWN was used which is a combination of the Slater exchange (similar to the Dirac exchange in Eq. 4.29, except from a different prefactor of 9/8 instead of 3/4) and the VWN correlation functional [14].

**Gradient Corrected Methods** To improve LSDA methods a non-uniform electron gas has to be considered in order to account for the non-homogeneity of the true electron density. A step in this direction is to make the exchange and correlation energies dependent not only on the electron density but also on derivatives of the density. Such methods are known as *GGA methods* (generalized gradient approximation) and the corresponding functionals can be generically written as

$$E_{\text{XC}}^{\text{GGA}}[\rho_{\alpha}, \rho_{\beta}] = \int f(\rho_{\alpha}, \rho_{\beta}, \nabla \rho_{\alpha}, \nabla \rho_{\beta}) \, \text{d}\mathbf{r}. \quad (4.44)$$

Practically,  $E_{\text{XC}}^{\text{GGA}}$  is split into an exchange and a correlation contribution

$$E_{\text{XC}}^{\text{GGA}} = E_{\text{X}}^{\text{GGA}} + E_{\text{C}}^{\text{GGA}} \quad (4.45)$$

and approximations for the two terms are sought individually. Well-known GGA-based exchange–correlation functionals that were employed in this thesis are BP86 and BPW91. They consist of Becke’s B (or B88) exchange functional [15] and either the P86 [16, 17] or PW91 [18, 19] correlation functionals.

**Hybrid Methods** Usually the exchange contributions are significantly larger in absolute numbers than the correlation effects. Thus, an accurate expression for the exchange functional is essential for obtaining meaningful results from DFT. One approach to improve the exchange functionals is to include the exact exchange energy of a Slater determinant (cf. also Section 4.1).

From the Hamiltonian in Eq. 4.30 and the definition of the exchange–correlation energy in Eq. 4.33, an exact connection can be made between the exchange–correlation energy and the corresponding potential connecting the non-interacting reference and the real system. As a result the so-called *adiabatic connection formula* can be derived

$$E_{\text{XC}} = \int_0^1 \langle \Psi_\lambda | V_{\text{XC}}(\lambda) | \Psi_\lambda \rangle d\lambda \quad (4.46)$$

which involves integration over the parameter  $\lambda$  turning on the electron–electron interaction. Both the non-interacting KS reference system ( $\lambda = 0$ ) and the real system ( $\lambda = 1$ ) are connected by Eq. 4.46 through a continuum of partially interacting systems. All of the systems with  $0 \leq \lambda \leq 1$  possess the same electron density.

The integral in Eq. 4.46 can be approximated (taking  $V_{\text{XC}}$  to be linear in  $\lambda$ ) as the average value at the two end-points

$$E_{\text{XC}} \approx \frac{1}{2} \langle \Psi_0 | V_{\text{XC}}(0) | \Psi_0 \rangle + \frac{1}{2} \langle \Psi_1 | V_{\text{XC}}(1) | \Psi_1 \rangle = \frac{1}{2} E_{\text{XC}}^{\lambda=0} + \frac{1}{2} E_{\text{XC}}^{\lambda=1}. \quad (4.47)$$

In the  $\lambda = 0$  limit there is no correlation energy, only exchange energy. Furthermore, since the exact wave function in this case is a single Slater determinant composed of KS orbitals, the exchange energy is exactly that given by Hartree–Fock theory and can easily be computed. Thus,  $E_{\text{XC}}^{\lambda=0}$  is often called  $E_{\text{X}}^{\text{HF}}$ . The last term in Eq. 4.47, however, is still unknown. It may be approximated using the LSDA result or, since GGA methods give substantial improvement over LDA, a generalized version may be defined by writing the exchange energy as a suitable combination of LSDA, exact exchange and a gradient correction term. Similarly, the correlation energy may be described as the LSDA formula plus a gradient correction term.

Models which include exact (Hartree–Fock) exchange are often termed *hybrid density functional methods*, the names ACM (adiabatic connection model) and B3 (Becke 3 parameter functional) are examples of such hybrid methods:

$$E_{\text{XC}}^{\text{B3}} = (1 - a) E_{\text{X}}^{\text{LSDA}} + a E_{\text{X}}^{\text{HF}} + b \Delta E_{\text{X}}^{\text{B88}} + E_{\text{C}}^{\text{LSDA}} + c \Delta E_{\text{C}}^{\text{GGA}}. \quad (4.48)$$

The  $a$ ,  $b$  and  $c$  parameters are determined by fitting experimental data. Two types of such three-parameter functionals were used in this work, namely the B3LYP [20–22] and the B3PW91 [18–21] methods. B3PW91 is expressed as

$$E_{\text{XC}}^{\text{B3PW91}} = (1 - a) E_{\text{X}}^{\text{LSDA}} + a E_{\text{X}}^{\text{HF}} + b \Delta E_{\text{X}}^{\text{B88}} + E_{\text{C}}^{\text{LSDA}} + c \Delta E_{\text{C}}^{\text{PW91}}. \quad (4.49)$$

and the parameters have values of  $a = 0.20$ ,  $b = 0.72$  und  $c = 0.81$  (B3LYP uses the same values). Both B3-type functionals incorporate 20% HF exchange. Another functional that was used in this thesis is the PBE0 (or PBE1PBE) functional [23] that uses no empirically optimized parameter and possesses 25% exact exchange. Furthermore, the BHPW91 method [20] with 50% HF exchange was used.

In addition to these standard functionals also user-defined BPW91- $a$ HF functionals of the type

$$\begin{aligned} E_{\text{XC}}^{\text{BPW91-}a\text{HF}} &= a E_{\text{X}}^{\text{HF}} + (1 - a) (E_{\text{X}}^{\text{LSDA}} + \Delta E_{\text{X}}^{\text{B88}}) + E_{\text{C}}^{\text{LSDA}} + \Delta E_{\text{C}}^{\text{PW91}} \\ &= a E_{\text{X}}^{\text{HF}} + (1 - a) E_{\text{X}}^{\text{B88}} + E_{\text{C}}^{\text{PW91}} \end{aligned} \quad (4.50)$$

were employed with different amounts of HF exchange from 30% up to 70% to investigate the influence of the exact exchange admixture on EPR properties. For further details cf. manuscripts in Chapter 6 and references therein.

## 4.5 Basis Sets

One of the approximations inherent in *ab initio* methods is the introduction of a basis set. Expanding an unknown function, such as a molecular orbital, in a set of known functions is not an approximation, if the basis is complete. However, a complete basis means that an infinite number of functions must be used, which is not feasible in actual calculations. An unknown MO can be thought of as a function in the infinite coordinate system spanned by the complete basis set. When a finite basis is used, only the components of the MO along those coordinate

axes corresponding to the selected basis can be represented. The smaller the basis, the poorer the representation. The type of basis functions used also influence the accuracy. The better a single basis function is able to reproduce the unknown function, the fewer basis functions are necessary for achieving a given level of accuracy. Since the computational effort of *ab initio* methods scales formally as at least  $M^4$  ( $M$  is the number of basis functions), it is of great importance to make the basis set as small as possible without losing accuracy.

One type of basis functions that is very common in electronic structure calculations are the *Gaussian-type orbitals* (GTOs) where the atom-centered functions are chosen to have the form of a Gaussian function ( $e^{-r^2}$ ).<sup>3</sup> One major advantage of the GTOs is that the calculation of three- and four-center two-electron integrals can be performed analytically. The general functional form of a normalized GTO in atom-centered Cartesian coordinates is

$$\varphi(x, y, z; \alpha, i, j, k) = \left(\frac{2\alpha}{\pi}\right)^{3/4} \left[\frac{(8\alpha)^{i+j+k} i! j! k!}{(2i)!(2j)!(2k)!}\right]^{1/2} x^i y^j z^k e^{-\alpha(x^2+y^2+z^2)} \quad (4.51)$$

where  $\alpha$  is an exponent controlling the width of the GTO and  $i$ ,  $j$  and  $k$  are non-negative integers that determine the nature of the orbital in a Cartesian sense. In particular, when all three of these indices are zero, the GTO has spherical symmetry and is called an s-type GTO. When exactly one of the indices is one, the function has axial symmetry about a single Cartesian axis and is called a p-type GTO ( $p_x$ ,  $p_y$  or  $p_z$  if  $i$ ,  $j$  or  $k$  is one, respectively). When the sum of the indices is equal to two, the orbital is called a d-type GTO.

However, although GTOs are convenient from a computational point of view they have some undesirable features. First of all, they are not able to correctly reproduce the shape of the radial part of the orbitals since GTOs are smooth and differentiable at the nucleus while true hydrogenic orbitals have a cusp at  $r=0$ . Furthermore, the decay of GTOs is not exponential as found for all hydrogenic AOs and they do not exhibit radial nodal behavior. No choice of variables in Eq. 4.51 permits to mimic a 2s orbital with a node. Therefore, it is necessary to combine several GTOs in a linear combination to construct functions that

---

<sup>3</sup>Also other functional forms are used for basis sets, e.g. *Slater-type orbitals* (STOs) with an exponential dependence on the distance between the nucleus and the electron mirroring the exact orbitals for the hydrogen atom or *plane waves* to describe periodic systems, but they will not be discussed here.

reproduce all the desired features as accurately as possible, i.e.

$$\varphi_{\text{CGTO}}(x, y, z; \{\alpha\}, i, j, k) = \sum_{a=1}^L c_a \varphi_{\text{PGTO}}(x, y, z; \alpha_a, i, j, k) \quad (4.52)$$

where  $L$  is the number of Gaussians used in the linear combination. The coefficients  $c_a$  are chosen to optimize the shape of the basis function sum and ensure normalization. When a basis function is defined as a linear combination of Gaussians with fixed coefficients, it is called *contracted* GTO (CGTO) and the individual Gaussians from which it is constructed are referred to as *primitive* GTOs (PGTOs). Contraction, i.e. the use of linear combinations of primitives with constant coefficients as basis functions, is especially useful for orbitals describing the inner (core) electrons, since they require a relatively large number of functions for representing the wave function cusp near the nucleus, and furthermore are largely independent of the environment. Contracting a basis set will always increase the energy, since it is a restriction of the number of variational parameters (coefficients), and makes the basis set less flexible, but will also reduce the computational cost significantly. The decision is thus how much loss in accuracy is acceptable compared to the gain in computational efficiency.

The *degree of contraction* is the number of PGTOs entering the CGTO, typically varying between 1 and 10. The specification of a basis set in terms of primitive and contracted functions is given by the notation (10s4p1d/4s1p) / [3s2p1d/2s1p]. The basis in parentheses is the number of primitives for heavy atoms before the slash and hydrogen after. The basis in the square brackets is the number of contracted functions. See also below for an example of an atomic basis set for molybdenum.

Having decided on the how to construct each basis function (as a single primitive or a contraction), another important factor is the number of functions to be used. The smallest number of functions possible is a *minimum basis set*. Only enough functions are employed to contain all the electrons of the neutral atom(s). The next improvement in the basis sets is a doubling of all basis functions, producing a double- $\zeta$  (double zeta, DZ) basis. The next step up in basis set size is a triple- $\zeta$  (TZ) basis. Such a basis contains three times as many functions as the minimum basis, i.e. six s-functions and three sets of p-functions (each consisting of  $p_x$ ,  $p_y$  and  $p_z$ ) for the elements from Li to Ne.

In this thesis several different basis sets were used which are listed with a short description in the following. For structure optimizations and EPR property

calculations various *split-valence*<sup>4</sup> basis sets of Pople et al. [24–26] were employed: 3-21G, 3-21G(d), 6-31G(d), 6-31+G(d), 6-31+G(d,p), 6-311G(d), 6-311+G(d), 6-311G(d,p), 6-311G(df,pd) and 6-311+G(df,pd). Those are of valence-double- or valence-triple- $\zeta$  quality (two or three numbers after hyphen) partially including additional polarization (indicated by letters in parentheses) or diffuse (indicated by + -sign) functions. The first number indicates the number of primitives used in contracted core functions and the numbers after the hyphen indicate the numbers of primitives used in the valence functions.

For some of the structure optimizations the all-electron TZVP (triple zeta valence polarized) basis of Ahlrichs and coworkers [27] was used. In case of molybdenum a TZVP valence basis set (5s3p3d) was employed together with an energy-adjusted small-core effective core potential [28] for the geometry optimizations.

For the computation of EPR parameters usually more flexible basis sets are necessary, thus specifically designed basis sets were used. Those were the EPR-II or EPR-III basis sets of Barone and coworkers [29, 30] and the IGLO-II or IGLO-III basis sets of Kutzelnigg and coworkers [31]. Since the EPR and IGLO basis sets are not available for transition metals, alternatives had to be found for manganese and molybdenum. For manganese the 9s7p4d basis of Munzarová et al. [32] was chosen and for molybdenum a 12s6p5d basis was developed in this work [33]. The latter basis was derived from the TZVP basis of Ahlrichs and May [34] by partial decontraction to yield a (19s14p9d) / [12s6p5d] {811111111111/641111/51111} contraction scheme. The nomenclature of the contraction scheme description is as follows: In parentheses the total number and type of primitives is given whereas the numbers and letters in square brackets indicate the contracted functions. In curly brackets a detailed description of the contractions can be found, e.g. the d-function part consists of altogether five contracted functions (five numbers in ‘51111’) where four of them consist of only one primitive and the fifth one is a contraction of five primitives.

For further details cf. manuscripts in Chapter 6 and references therein.

---

<sup>4</sup>For this type of basis set only the number of valence basis functions is increased, e.g. doubled for a valence-double- $\zeta$  basis, while core orbitals are always represented by a single (contracted) basis function.

## 4.6 Computational Chemistry Program Packages

The quantum chemical calculations in this thesis were conducted using a number of different quantum chemistry program packages. *Structure optimizations* were performed with Gaussian 98 [35], Gaussian 03 [36], Q-Chem [37] and Turbomole [38]. For *single-point SCF calculations* and/or *EPR property computations* Gaussian 98/03 (single-point SCF, broken symmetry DFT, quadrupole coupling (electric field gradient) and hyperfine coupling tensors), ACES II (CCSD(T) HFC tensors) [39] and MAG-ReSpect (HFC tensors including spin-orbit corrections, *g*-tensors) [40] were employed. For further details cf. manuscripts in Chapter 6 and references therein.

## References

- [1] Cramer, C. J. *Essentials of Computational Chemistry: Theories and Models*; Wiley: Chichester, 2002.
- [2] Parr, R. G.; Yang, W. *Density-Functional Theory of Atoms and Molecules*; Oxford University Press: New York, 1989.
- [3] Szabo, A.; Ostlund, N. S. *Modern Quantum Chemistry: Introduction to Advanced Electronic Structure Theory*; MacMillan Publishing Co.: New York, 1982.
- [4] Hehre, W. J.; Radom, L.; Schleyer, P. v. R.; Pople, J. A. *Ab Initio Molecular Orbital Theory*; J. Wiley: New York, 1986.
- [5] Jensen, F. *Introduction to Computational Chemistry*; John Wiley & Sons: Chichester, 1999.
- [6] Koch, W.; Holthausen, M. C. *A Chemist's Guide to Density Functional Theory: An Introduction*; VCH-Wiley: Weinheim, 2000.
- [7] Helgaker, T.; Jørgensen, P.; Olsen, J. *Molecular Electronic-Structure Theory*; John Wiley & Sons: Chichester, 2000.
- [8] Leach, A. R. *Molecular Modelling. Principles and Applications.*; Prentice Hall: Englewood Cliffs, NJ, 2001.

- [9] Roothaan, C. C. J. *Rev. Mod. Phys.* **1951**, *23*, 69–89.
- [10] Roothaan, C. C. J. *Rev. Mod. Phys.* **1960**, *32*, 179–185.
- [11] Hall, G. G. *Proc. Roy. Soc. (London) A* **1951**, *205*, 541–552.
- [12] Hohenberg, P.; Kohn, W. *Phys. Rev.* **1964**, *136*, B864–B871.
- [13] Kohn, W.; Sham, L. J. *Phys. Rev.* **1965**, *140*, A1133–A1138.
- [14] Vosko, S. H.; Wilk, L.; Nusair, M. *Can. J. Phys.* **1980**, *58*, 1200–1211.
- [15] Becke, A. D. *Phys. Rev. A* **1988**, *38*, 3098–3100.
- [16] Perdew, J. P.; Wang, Y. *Phys. Rev. B* **1986**, *33*, 8822–8824.
- [17] Perdew, J. P.; Wang, Y. *Phys. Rev. B* **1986**, *34*, 7406.
- [18] Perdew, J. P. *Physica B* **1991**, *172*, 1–6.
- [19] Perdew, J. P.; Wang, Y. *Phys. Rev. B* **1992**, *45*, 13244–13249.
- [20] Becke, A. D. *J. Chem. Phys.* **1993**, *98*, 1372–1377.
- [21] Becke, A. D. *J. Chem. Phys.* **1993**, *98*, 5648–5652.
- [22] Stephens, P. J.; Devlin, F. J.; Chabalowski, C. F.; Frisch, M. J. *J. Phys. Chem.* **1994**, *98*, 11623–11627.
- [23] Perdew, J. P.; Burke, K.; Ernzerhof, M. *Phys. Rev. Lett.* **1996**, *77*, 3865–3868.
- [24] Hariharan, P. C.; Pople, J. A. *Theor. Chim. Acta* **1973**, *28*, 213–222.
- [25] Krishnam, R.; Binkley, J. S.; Seeger, R.; Pople, J. A. *J. Chem. Phys.* **1980**, *72*, 650–654.
- [26] Clark, T.; Chandrasekhar, J.; Spitznagel, G. W.; v. R. Schleyer, P. J. *Comp. Chem.* **1983**, *4*, 294–301.
- [27] Schäfer, A.; Huber, C.; Ahlrichs, R. *J. Chem. Phys.* **1994**, *100*, 5829–5835.
- [28] Andrae, D.; Häussermann, U.; Dolg, M.; Stoll, H.; Preuss, H. *Theor. Chim. Acta* **1990**, *77*, 123–141.

- [29] Barone, V. In *Recent Advances in Density Functional Methods*; Chong, D. P., Ed.; World Scientific Publ.: Singapur, 1995.
- [30] Rega, N.; Cossi, M.; Barone, V. *J. Chem. Phys.* **1996**, *105*, 11060–11067.
- [31] Kutzelnigg, W.; Fleischer, U.; Schindler, M. In *NMR Basic Principles and Progress*, Vol. 23; Diehl, P.; Fluck, E.; Günther, H.; Kosfeld, R.; Seelig, J., Eds.; Springer Verlag: Berlin/Heidelberg, 1991.
- [32] Munzarová, M.; Kaupp, M. *J. Phys. Chem. A* **1999**, *103*, 9966–9983.
- [33] Fritscher, J.; Hrobárik, P.; Kaupp, M. *J. Phys. Chem. B* **2007**, *Computational Studies of EPR Parameters for Paramagnetic Molybdenum Complexes. I. Method Validation on Small and Medium-Sized Systems*, accepted.
- [34] Ahlrichs, R.; May, K. *Phys. Chem. Chem. Phys.* **2000**, *2*, 943–945.
- [35] Frisch, M. J.; Trucks, G. W.; Schlegel, H. B.; Scuseria, G. E.; Robb, M. A.; Cheeseman, J. R.; Zakrzewski, V. G.; Montgomery, J. A., Jr.; Stratmann, R. E.; Burant, J. C.; Dapprich, S.; Millam, J. M.; Daniels, A. D.; Kudin, K. N.; Strain, M. C.; Farkas, O.; Tomasi, J.; Barone, V.; Cossi, M.; Cammi, R.; Mennucci, B.; Pomelli, C.; Adamo, C.; Clifford, S.; Ochterski, J.; Petersson, G. A.; Ayala, P. Y.; Cui, Q.; Morokuma, K.; Salvador, P.; Dannenberg, J. J.; Malick, D. K.; Rabuck, A. D.; Raghavachari, K.; Foresman, J. B.; Cioslowski, J.; Ortiz, J. V.; Baboul, A. G.; Stefanov, B. B.; Liu, G.; Liashenko, A.; Piskorz, P.; Komaromi, I.; Gomperts, R.; Martin, R. L.; Fox, D. J.; Keith, T.; Al-Laham, M. A.; Peng, C. Y.; Nanayakkara, A.; Challacombe, M.; Gill, P. M. W.; Johnson, B. G.; Chen, W.; Wong, M. W.;res, J. L.; Gonzalez, C.; Head-Gordon, M.; Replogle, E. S.; Pople, J. A., Gaussian 98 (Revision A.11); Gaussian, Inc., Pittsburgh PA, 2001.
- [36] Gaussian 03, Revision C.02, M. J. Frisch; G. W. Trucks; H. B. Schlegel; G. E. Scuseria; M. A. Robb; J. R. Cheeseman; Montgomery, Jr., J. A.; T. Vreven; K. N. Kudin; J. C. Burant; J. M. Millam; S. S. Iyengar; J. Tomasi; V. Barone; B. Mennucci; M. Cossi; G. Scalmani; N. Rega; G. A. Petersson; H. Nakatsuji; M. Hada; M. Ehara; K. Toyota; R. Fukuda; J. Hasegawa; M. Ishida; T. Nakajima; Y. Honda; O. Kitao; H. Nakai; M. Klene; X. Li; J. E. Knox; H. P. Hratchian; J. B. Cross; V. Bakken; C. Adamo; J. Jaramillo; R. Gomperts; R. E. Stratmann; O. Yazyev; A. J. Austin; R. Cammi; C. Pomelli;

- J. W. Ochterski; P. Y. Ayala; K. Morokuma; G. A. Voth; P. Salvador; J. J. Dannenberg; V. G. Zakrzewski; S. Dapprich; A. D. Daniels; M. C. Strain; O. Farkas; D. K. Malick; A. D. Rabuck; K. Raghavachari; J. B. Foresman; J. V. Ortiz; Q. Cui; A. G. Baboul; S. Clifford; J. Cioslowski; B. B. Stefanov; G. Liu; A. Liashenko; P. Piskorz; I. Komaromi; R. L. Martin; D. J. Fox; T. Keith; M. A. Al-Laham; C. Y. Peng; A. Nanayakkara; M. Challacombe; P. M. W. Gill; B. Johnson; W. Chen; M. W. Wong; C. Gonzalez; J. A. Pople, Gaussian, Inc., Wallingford, CT, 2004.
- [37] *Q-Chem 2.0: A high-performance ab initio electronic structure program*, J. Kong, C. A. White, A. I. Krylov, C. D. Sherrill, R. D. Adamson, T. R. Furlani, M. S. Lee, A. M. Lee, S. R. Gwaltney, T. R. Adams, C. Ochsenfeld, A. T. B. Gilbert, G. S. Kedziora, V. A. Rassolov, D. R. Maurice, N. Nair, Y. Shao, N. A. Besley, P. E. Maslen, J. P. Dombroski, H. Daschel, W. Zhang, P. P. Korambath, J. Baker, E. F. C. Byrd, T. Van Voorhis, M. Oumi, S. Hirata, C.-P. Hsu, N. Ishikawa, J. Florian, A. Warshel, B. G. Johnson, P. M. W. Gill, M. Head-Gordon, and J. A. Pople, *J. Comput. Chem.* **2000**, *21*, 1532–1548.
- [38] Ahlrichs, R.; Bär, M.; Baron, H.-P.; Bauernschmitt, R.; Böcker, S.; Deglmann, P.; Ehrig, M.; Eichkorn, K.; Elliott, S.; Furche, F.; Haase, F.; Häser, M.; Horn, H.; Hättig, C.; Huber, C.; Huniar, U.; Kattannek, M.; Köhn, A.; Kölmel, C.; Kollwitz, M.; May, K.; Ochsenfeld, C.; Öhm, H.; Schäfer, A.; Schneider, U.; Sierka, M.; Treutler, O.; Unterreiner, B.; Arnim, M. von; Weigend, F.; Weis, P.; Weiss, H., *Turbomole*, version 5.6, Quantum Chemistry Group, University of Karlsruhe: Karlsruhe, Germany, 2002.
- [39] ACES II is a program product of the Quantum Theory Project, University of Florida. Authors: Stanton, J. F.; Gauss, J.; Watts, J. D.; Nooijen, M.; Oliphant, N.; Perera, S. A.; Szalay, P.; Lauderdale, W. J.; Kucharski, S. A.; Gwaltney, S. R.; Beck, S.; Balkova, A.; Bernholdt, D. E.; Baeck, K. K.; Rozyczko, P.; Sekino, H.; Huber, C.; Pittner, J.; Bartlett, R. J. Integral packages included are VMOL (Almlöf, J.; Taylor, P. R.), VPROPS (Taylor, P. R.), and ABACUS (Helgaker, T.; Jensen, H. J. A.; Jørgensen, P.; Olsen, J.; Taylor, P. R.).
- [40] Malkin, V. G.; Malkina, O. L.; Reviakine, R.; Arbuznikov, A. V.; Kaupp,

---

M.; Schimmelpfennig, B.; Malkin, I.; Helgaker, T.; Ruud, K., *MAG-ReSpect*,  
Version 1.2, 2004.



*“Today, the situation has been reached where, in many cases, the computational chemist can substitute the computing machine for the test tube. Not that the computational approach to the study of chemistry should be regarded as a rival to the traditional experimental techniques. Often the two approaches are complementary, one approach providing data which are not available from the other, and vice versa.”*

S. WILSON, 1986

## Chapter 5

# Summary of Results and Discussion

In this chapter the results of the different research projects [1–8] which are presented in detail in Chapter 6 will be summarized and discussed.<sup>1</sup> However, the main focus in this chapter is set on the quantum chemical parts of the projects and the experimental results (if available) are usually mentioned without in-depth explanation of the experimental methodologies.

For the sake of clarity a classification of the studies into two main categories will be used – depending whether a project deals with *transition metal systems* or *systems involving organic radicals*. Within these sections, investigations of *small molecules* or *model systems* (e.g. nitroxides, imidazole–semiquinone complexes or Mo<sup>V</sup> complexes) will be presented first, followed by direct applications to *biological systems*.

---

<sup>1</sup>The contributions of the author of this Ph.D. thesis to the different publications shall be clarified in the following. In almost all cases the computational work contained was performed by the author of this thesis independently. Furthermore, he was always involved in the interpretation of the theoretical results in the context of the experimental (EPR) data. In case of the work presented in Section 6.5 [7] the CCSD(T) calculations were performed by S. Kacprzak and M. Kaupp. The studies in Sections 6.7 [1] and 6.8 [3] were carried out in close collaboration with M. Kaupp. Here, P. Hrobárik was instructed by the author of this thesis and performed many of the computations under his supervision. All publications where the author of this thesis is first author were to large parts written by himself. In all other cases those parts of the manuscript dealing with computational methods or results were written by himself.

## 5.1 Organic Radicals in Model Systems

### 5.1.1 Theoretical Investigation of the Exchange Coupling Mechanisms for a Nitroxide Biradical

A theoretical investigation of the magnetic properties of the novel nitroxide biradical BITPAN (1,8-bis(3-ethynyl-2,2,5,5-tetramethyl-3-pyrroline-1-oxyl)-naphthalene, **2<sup>••</sup>**, Figure 5.1) was conducted to gain deeper insight into the electron spin–spin exchange coupling between unpaired electrons localized on different centers (cf. Section 6.1 and Ref. 2).

This interaction is the basis for all bulk and molecular magnetic phenomena like ferro- or antiferromagnetism and its correlation with structural parameters is a long-standing research topic [9]. It is known that the exchange coupling constant  $J$  (cf. also Chapter 3) decreases exponentially with the electron–electron distance [10], that it depends on the relative orientation of the magnetic orbitals [11] and that the geometry and nature of the bridge connecting the paramagnetic centers is of great importance [12, 13]. However, all the acquired knowledge does not yet allow an unequivocal understanding of the exchange interaction. This may to some part be due to the fact that the experimentally observable exchange coupling constant  $J$  is the result of various interaction pathways [12]. It was shown that quantum chemical calculations can be used to separate the different through-space and through-bond contributions from each other thus facilitating a deeper understanding of the mechanisms driving the magnetic interaction [14].

In Ref. 2 the synthesis and crystal structure of BITPAN (**2<sup>••</sup>**, Figure 5.1) as well as its magnetic properties obtained from magnetic susceptibility (SQUID) and EPR measurements and broken symmetry (BS) DFT calculations are presented. The discussion in this section focusses mainly on the latter issue including a theoretical separation of through-bond and through-space mechanisms contributing to the total exchange interaction. The experimental parts have already been presented and discussed in the author’s diploma thesis [15].

**Computation of the Exchange Coupling** For the evaluation of the exchange coupling  $2J$  ( $\hat{\mathcal{H}}_J = -2J\hat{\mathbf{S}}_A \cdot \hat{\mathbf{S}}_B$ ) within the broken symmetry formalism the energies of the broken symmetry ( $E_{\text{BS}}$ ) and triplet ( $E_{\text{T}}$ ) states have to be calculated (see also Chapter 3) since [16]

$$2J = 2(E_{\text{BS}} - E_{\text{T}}), \quad (5.1)$$

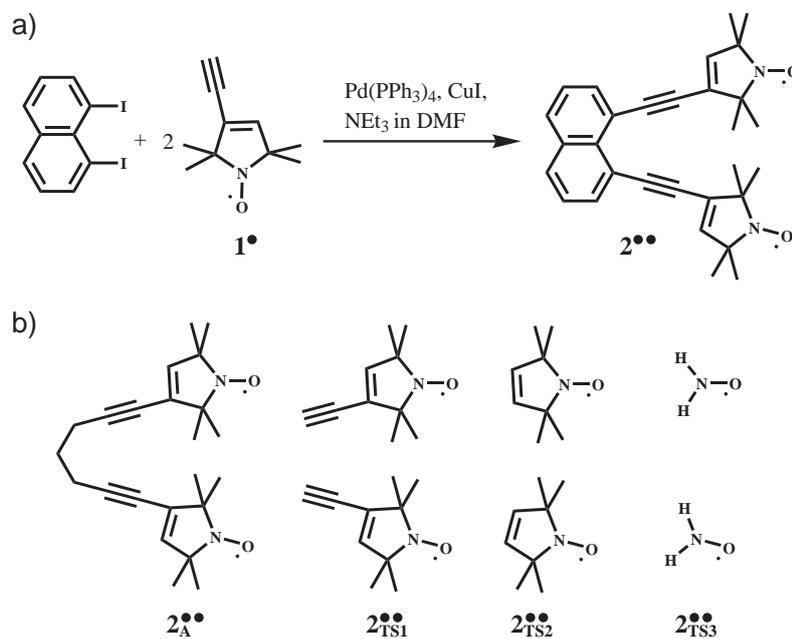


**Figure 5.1** a) Reaction scheme for the synthesis of BITPAN ( $2^{\bullet\bullet}$ ). b) Structures of model systems used in the theoretical evaluation of the exchange mechanism for BITPAN ( $2^{\bullet\bullet}$ ).

where  $2J$  corresponds to the singlet–triplet splitting. Table 5.1 displays the results of unrestricted single-point calculations of the exchange interaction for BITPAN ( $2^{\bullet\bullet}$ ) using the B3LYP functional together with various different basis sets. For all computations the geometry was taken from the crystal structure analysis. The data in Table 5.1 reveal that even a semi-quantitative agreement between theory and experiment can only be achieved with large triple- $\zeta$  quality basis sets including polarization functions. It is possible to nearly quantitatively predict  $2J$  for BITPAN using the large 6-311G(df,pd) basis set. The negative value of  $2J = -6.3$  K (experimentally  $-3.5$  or  $-4.1$  K) indicates an antiferromagnetic exchange coupling corresponding to a singlet ground state. The localized singly-occupied magnetic orbitals of BITPAN are visualized in Figure 5.2a demonstrating an almost perpendicular arrangement of the orbitals located at the different nitroxide units.

**Study of the Exchange Coupling Mechanisms** After the successful computation of  $2J$  for BITPAN further efforts were made to unravel the mechanisms of the exchange interaction. For this purpose calculations on four model systems

**Table 5.1** Singlet-triplet separation  $2J$  computed for BITPAN ( $\mathbf{2}^{\bullet\bullet}$ ) and various model systems (cf. Figure 5.1) using unrestricted B3LYP broken symmetry (BS) DFT methods and comparison with experimental data from Ref. 2

System	Method	$2J$ [K]	$\langle \hat{S}^2 \rangle_{\text{BS}}$	$\langle \hat{S}^2 \rangle_{\text{T}}$
$\mathbf{2}^{\bullet\bullet}$	6-31G(d)	-265.2	1.0074	2.0074
	6-31+G(d)	-1.3 <sup>a</sup>	1.0090	2.0090
	6-31+G(d,p)	-3852.4	1.0090	2.0090
	6-311G(d)	-37.9	1.0082	2.0082
	6-311G(d,p)	-18.9	1.0082	2.0082
	6-311+G(d)	-12.6	1.0090	2.0090
	6-311G(df,pd)	-6.3	1.0084	2.0084
	SQUID	-3.5		
	EPR	-4.1		
$\mathbf{2}^{\bullet\bullet}_{\text{A}}$	6-311G(df,pd)	-88.4	1.0083	2.0084
$\mathbf{2}^{\bullet\bullet}_{\text{TS1}}$	6-311G(df,pd)	-138.9	1.0082	2.0084
$\mathbf{2}^{\bullet\bullet}_{\text{TS2}}$	6-311G(df,pd)	0.0	1.0084	2.0084
$\mathbf{2}^{\bullet\bullet}_{\text{TS3}}$	6-311G(df,pd)	0.0	1.0072	2.0072

<sup>a</sup> Energy difference below  $10^{-5} E_{\text{h}}$ .

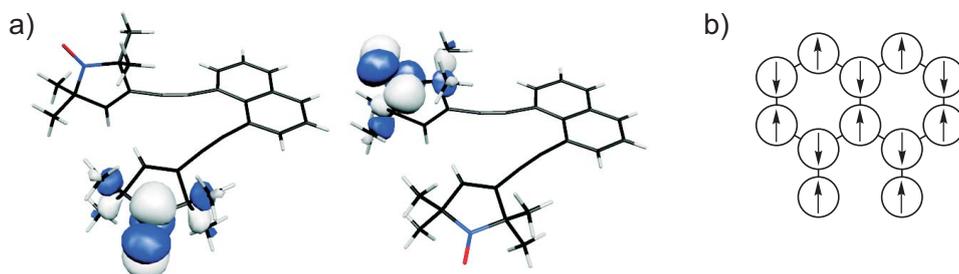


**Figure 5.2** a) Singly-occupied magnetic orbitals of BITPAN ( $\mathbf{2}^{\bullet\bullet}$ ). b) Spin polarization pattern for 1,8-substituted naphthalene bridges mediating ferromagnetic exchange coupling via the  $\pi$ -network.

$\mathbf{2}^{\bullet\bullet}_{\text{A}}$ ,  $\mathbf{2}^{\bullet\bullet}_{\text{TS1}}$ ,  $\mathbf{2}^{\bullet\bullet}_{\text{TS2}}$  and  $\mathbf{2}^{\bullet\bullet}_{\text{TS3}}$  (Figure 5.1b) were performed. In these models the distance and relative orientation of the two nitroxide moieties were taken from the crystal structure of BITPAN ( $\mathbf{2}^{\bullet\bullet}$ ). Then the aromatic naphthalene ring system was replaced by an alkyl chain ( $\mathbf{2}^{\bullet\bullet}_{\text{A}}$ ) or completely deleted ( $\mathbf{2}^{\bullet\bullet}_{\text{TS1}}$ ). Furthermore, the two acetylene units were omitted in  $\mathbf{2}^{\bullet\bullet}_{\text{TS2}}$  and  $\mathbf{2}^{\bullet\bullet}_{\text{TS3}}$  simply consists of two  $\text{H}_2\text{NO}$  molecules. Table 5.1 shows that for  $\mathbf{2}^{\bullet\bullet}_{\text{A}}$  and  $\mathbf{2}^{\bullet\bullet}_{\text{TS1}}$   $2J$  becomes more negative compared to BITPAN, i.e. the omission of the  $\pi$ -system or of the whole

bridge both lead to a much stronger antiferromagnetic interaction of  $-88.4$  K and  $-138.9$  K, respectively.  $\mathbf{2}_{\text{TS2}}^{\bullet\bullet}$  and  $\mathbf{2}_{\text{TS3}}^{\bullet\bullet}$  show no magnetic interaction as is expected for two nitroxide radicals separated by a distance of  $\sim 7-8$  Å and interacting only through space [10].

The result of the computation on the model system where the naphthalene unit is deleted ( $\mathbf{2}_{\text{TS1}}^{\bullet\bullet}$ ) should reveal those contributions to  $J$  that are only due to intramolecular through-space interactions. The value of  $2J = -138.9$  K shows that the total exchange coupling through space is strongly antiferromagnetic. Considering that for  $\mathbf{2}_{\text{TS2}}^{\bullet\bullet}$  and  $\mathbf{2}_{\text{TS3}}^{\bullet\bullet}$ , which represent through-space interactions between the two five-membered nitroxide rings or the N–O groups themselves, no magnetic interaction was found, it can be concluded that the strong antiferromagnetic interaction of  $-138.9$  K is solely due to a through-space coupling via the two acetylene units. The small distance of  $2.89$  Å between the triple bonds is close enough to allow through-space interactions of these  $\pi$ -orbitals. The model system  $\mathbf{2}_{\text{A}}^{\bullet\bullet}$  with the alkyl chain as linking bridge instead of naphthalene should include through-space coupling and additionally through-bond interactions via the alkyl linker. The exchange coupling of  $2J = -88.4$  K for  $\mathbf{2}_{\text{A}}^{\bullet\bullet}$  is less negative compared to  $\mathbf{2}_{\text{TS1}}^{\bullet\bullet}$ . What is interesting about  $\mathbf{2}_{\text{A}}^{\bullet\bullet}$  is the fact that including all interaction pathways except the one through the  $\pi$ -system of the naphthalene bridge, it is not possible to model the small antiferromagnetic exchange interaction found experimentally and theoretically for BITPAN ( $\mathbf{2}^{\bullet\bullet}$ ). Therefore, it becomes obvious that the naphthalene unit mediates a ferromagnetic through-bond interaction of the same order of magnitude as the antiferromagnetic through-space coupling. This ferromagnetic coupling through the  $\pi$ -system can be explained by the 1,8-substitution pattern which resembles the *meta*-benzene substitution. Such a *meta* substitution is known to evoke ferromagnetic interactions [17] which can be rationalized using a simple spin polarization picture of the  $\pi$ -system (Figure 5.2b). The surprisingly strong antiferromagnetic and ferromagnetic exchange couplings calculated can be understood by assuming an effective coupling of the magnetic N–O  $\pi$ -orbitals to the  $\pi$ -system of the bridge (consisting of the pyrroline ring double bonds, the acetylene linkers and the naphthalene unit) via a superexchange mechanism [18]. This is supported by the close distance of  $2.2$  Å between the nitrogen of the N–O unit and the center of the double bond of the pyrroline ring. The sum of the ferromagnetic through-bond interaction and the antiferromagnetic short-circuit through-space interaction via the acetylene groups ( $2J = -138.9$  K) finally leads to the observed small antiferromagnetic

exchange coupling for BITPAN (**2<sup>••</sup>**).

In conclusion, it was shown that BS DFT methods are capable of predicting exchange interactions in good agreement with experimental values for nitroxide biradicals provided that suitable computational methods are used. However, the potential and advantage of the theoretical methods lies in the possibility of separating different contributions to the overall exchange coupling constant thus gaining deeper insight into the physical processes leading to the molecular magnetic properties. The BS DFT methods are also applicable to metal complexes [19, 20] or clusters [21]. This may especially be helpful when studying biological systems with exchange coupled paramagnetic centers / metal clusters or when trying to design and modify molecular magnets and other magnetic materials.

### 5.1.2 Spin Density Distributions and Hyperfine Couplings for Aromatic Nitroxides

Novel aromatic nitroxides were synthesized and their structural and magnetic properties characterized with EPR spectroscopy and DFT calculations to investigate whether they might be promising candidates as DNA-intercalating spin probes (cf. also Section 6.2 and Ref. 5).

Spin labeling of DNA [22, 23] or RNA [24] with nitroxides is used to gain insight into the structure [25] and mobility [26] of these biopolymers. Nevertheless, spin labeling on the periphery of DNA or RNA may yield less insight if motions or electronic properties of bases within oligonucleotides, e.g. spin-exchange coupling through DNA bases, are studied. One way to overcome this problem would be to use nitroxides that intercalate between two base pairs. These intercalating nitroxides need to be stable in liquid solution and to possess extended planar and heterocyclic  $\pi$ -systems. They should also be polarizable and polar or charged, as the well-known diamagnetic intercalators ethidium [27] or acridine [28]. Furthermore, they ought to intercalate with the N–O group between the bases or the spin density should be delocalized into the intercalating part of the nitroxide. Aromatic nitroxides [29, 30] may be a class of substances, which could match these criteria. However, they are rare and mostly characterized as unstable [29, 30]. Therefore, syntheses of novel aromatic nitroxides (**3<sup>•</sup>**, **4<sup>•</sup>** and **5<sup>•</sup>** in Figure 5.3) were developed [5] and the properties of these aromatic nitroxides were studied using EPR spectroscopy [5] and DFT calculations. The main goal of the theoretical investigation was to get more insight into their molecular and

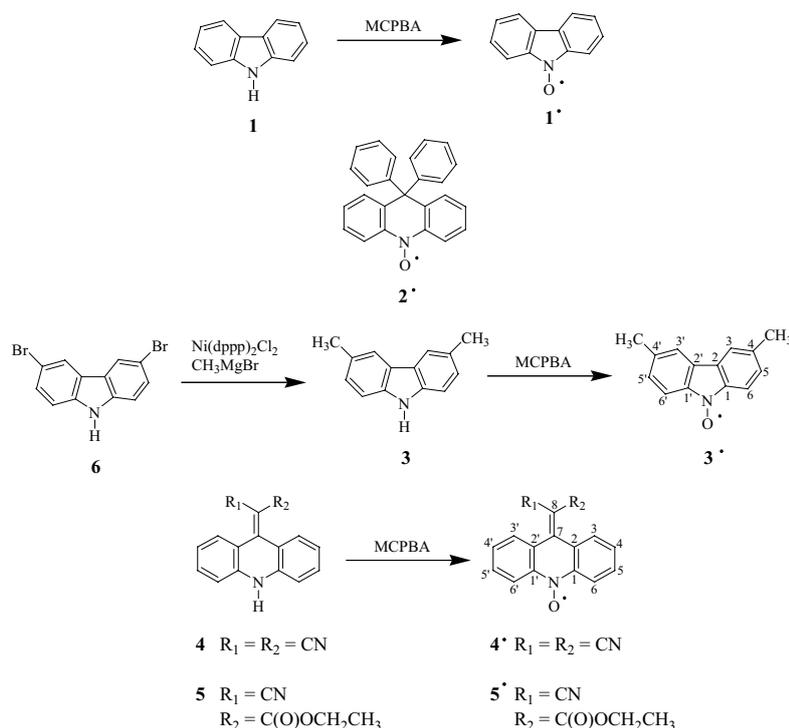


**Figure 5.3** Structures of aromatic nitroxides **1<sup>•</sup>**–**5<sup>•</sup>** and reaction schemes.

electronic structure as well as to assign the experimental hyperfine couplings.

Figure 5.3 depicts the structures of the carbazole-based aromatic nitroxides **1<sup>•</sup>** and **3<sup>•</sup>** as well as the acridane-based nitroxides **2<sup>•</sup>**, **4<sup>•</sup>** and **5<sup>•</sup>** together with reaction pathways to synthesize the radical species. Measurements of the room temperature EPR signal intensity as a function of time for diluted solutions of the aromatic nitroxides [5] (**1<sup>•</sup>**–**5<sup>•</sup>**) revealed that the stability of **1<sup>•</sup>** and **3<sup>•</sup>** is too low to use them as DNA intercalators whereas **2<sup>•</sup>**, **4<sup>•</sup>** and **5<sup>•</sup>** are suitable candidates from a stability point of view. The X-band EPR spectra for all nitroxides were also simulated in Ref. 5 and  $g_{\text{iso}}$ -values as well as isotropic  $^1\text{H}$  and  $^{14}\text{N}$  hyperfine coupling constants (see Chapter 3 for an explanation of EPR parameters) were obtained from best fits of the simulations to the experimental spectra. The detection of  $^1\text{H}$  HFCs from ring protons together with the fact that the  $^{14}\text{N}$  HFC constants are considerably reduced compared to alkyl nitroxides [29, 30] ( $\sim 7\text{--}9$  G vs.  $\sim 14\text{--}15$  G) indicate a delocalization of spin density from the N–O groups into the ring systems, leaving only roughly 50% of the spin density on the N–O

nitrogen.

DFT-based geometry optimizations (PBE0/6-31G(d)) of all five nitroxides revealed that the carbazole nitroxides **1**<sup>•</sup> and **3**<sup>•</sup> are planar whereas the three acridane nitroxides **2**<sup>•</sup>, **4**<sup>•</sup> and **5**<sup>•</sup> possess a ring system structure that deviates from planarity by roughly 20° due to steric interaction of the 3 and 3' hydrogens with the phenyl, nitrile or ester substituents.

In contrast to the localized singly occupied molecular orbitals (SOMOs) of alkyl nitroxides [2, 31] the SOMOs of all five aromatic nitroxides are extended over the whole  $\pi$ -system and even onto the substituents in the case of **3**<sup>•</sup>, **4**<sup>•</sup> and **5**<sup>•</sup> as shown for **3**<sup>•</sup> and **5**<sup>•</sup> in Figure 5.4a and c. The positive spin density distribution (Figure 5.4b and d) follows the shape of the SOMOs. Due to spin polarization, negative spin density is induced at those carbon atoms of the rings for which the SOMOs possess a node [32]. The spin density on the ring hydrogens is also caused by spin polarization, as indicated by the opposite sign of the spin density at the corresponding carbon atom (Figure 5.4b and d). On the other hand, the spin density at the hydrogens of the methyl groups of **3**<sup>•</sup> is transferred by hyperconjugation, leading to the same sign for the spin density as for the methyl substituted ring carbon atoms. Finally, it should be mentioned that the total atomic spin density of about +0.50 on the oxygen of the N–O group observed for the aromatic nitroxides is comparable to those found in alkyl nitroxides, whereas the spin density on the nitrogen (+0.25) is diminished by 50%.

With these spin density distributions, isotropic <sup>14</sup>N and <sup>1</sup>H hyperfine coupling constants were calculated that are in very good agreement with the experimentally obtained ones, allowing a reliable assignment of the experimental hyperfine couplings to the respective nuclei. Yet, the calculated isotropic <sup>14</sup>N hyperfine coupling constants of the N–O group are slightly smaller than the experimental ones, as commonly found in DFT calculations for nitroxides [33].

Additionally, the dipole moments and average polarizabilities of compounds **1**<sup>•</sup>–**5**<sup>•</sup> were calculated. A comparison of the dipole moments showed that they are increasing from 2.7 to 5.6 D in the order **1**<sup>•</sup>, **2**<sup>•</sup>, **3**<sup>•</sup>, **5**<sup>•</sup> and **4**<sup>•</sup>, which is attributed to the increasing number and strength of electron-withdrawing groups. The dipolar vectors point from the nitriles to the N–O group for **4**<sup>•</sup> and **5**<sup>•</sup> and along the O–N bond axis from the oxygen to the nitrogen for **1**<sup>•</sup>, **2**<sup>•</sup> and **3**<sup>•</sup>. Hobza and coworkers have shown that the intercalation between base pairs is mostly driven by dispersion forces caused by the polarizability [34]. The average calculated polarizabilities for the aromatic nitroxides are relatively large with

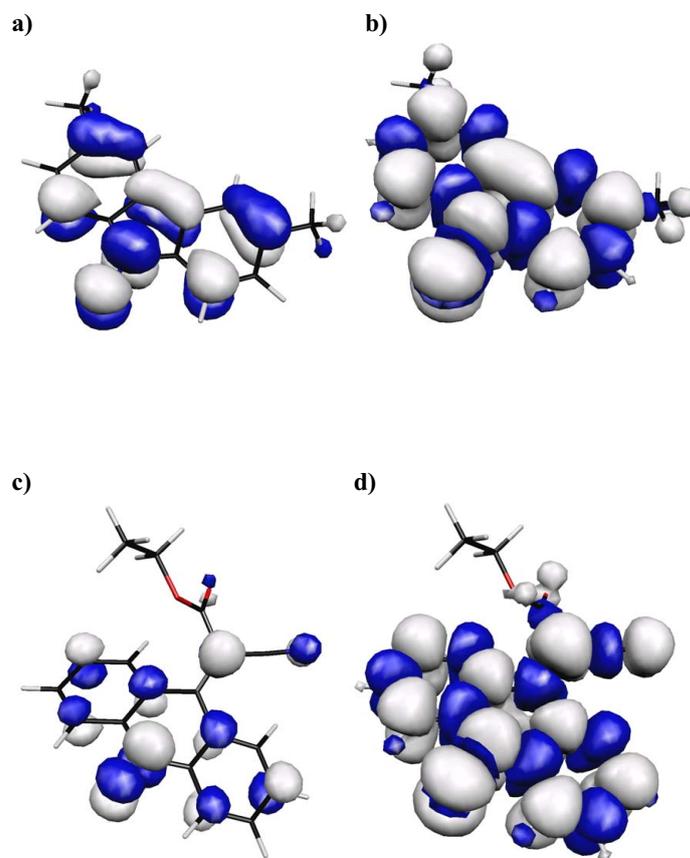


**Figure 5.4** Singly occupied molecular orbitals (SOMOs; a and c) and spin density distributions (b and d) of the aromatic nitroxides **3•** and **5•**, respectively, showing the delocalization of the unpaired electron due to the heterocyclic  $\pi$ -system. Computations were performed on the unrestricted PBE0/6-31G(d) level of theory. Positive amplitudes or spin densities are shown in light gray and negative ones in blue.

values up to 260 B<sup>3</sup>. A comparison of the large dipole moments of 5.6, 4.4 and 3.0 D as well as the large polarizabilities of 204, 222 and 260 B<sup>3</sup> calculated for **4•**, **5•** and **2•**, respectively, with the ones of ethidium (2.3 D, 236 B<sup>3</sup>) and daunomycin (18.6 D, 297 B<sup>3</sup>) [34], both well-known and strong DNA intercalators, makes all three aromatic nitroxides promising candidates as DNA intercalators.

In summary, it could be shown by EPR spectroscopy in combination with DFT calculations that among the five different aromatic nitroxides under study the compounds **2•**, **4•** and **5•** are the most promising potential DNA intercalators.

This is due to their high stability in solution, their (almost) planar molecular structure and because of the delocalisation of spin density into the  $\pi$ -system and their large dipole moments as well as polarizabilities.

### 5.1.3 Influence of Hydrogen Bond Geometry on Quadrupole Coupling Parameters of Imidazole Complexes

In order to systematically elucidate the influence of hydrogen bond geometry on  $^{14}\text{N}$  quadrupole coupling (QC) parameters of diamagnetic imidazole–water as well as paramagnetic imidazole–semiquinone complexes a theoretical study based on DFT was carried out (cf. Section 6.4 and Ref. 4).

Various magnetic resonance spectroscopic techniques such as electron nuclear double resonance (ENDOR), electron spin echo envelope modulation (ESEEM), nuclear quadrupole resonance (NQR) or nuclear magnetic resonance (NMR) can provide nuclear QC tensors that contain valuable information about the electrostatic environment and bonding situation of the interacting nuclei [35–37]. It has been shown in the past that DFT methods are capable of predicting QC parameters (QC constants  $\chi$  and asymmetry parameters  $\eta$ ; cf. also Chapter 3) of different types of nuclei and molecules [6, 38–46] thereby demonstrating the reliability of theoretical predictions.

Hydrogen bonding plays a crucial role in structural and functional aspects of many biologically relevant systems [47]. Since hydrogen bonding interactions may strongly influence the observed QC parameters of involved nuclei, a deeper understanding of the dependence of these parameters on the geometry of the hydrogen bond is of great importance. Even though it is usually difficult to investigate systematic structure–property relationships experimentally, theoretical approaches can contribute substantially in this context. Imidazole–water and imidazole–semiquinone complexes were chosen as model systems in this work due to the widespread biological importance of imidazole (histidine side chain) as a common ligand of metal ions or clusters [48–54] as well as of quinone cofactors [53, 54]. Thus, results of this study might be directly applicable to current problems in structure determination, e.g. of quinone binding sites.

**Imidazole–Water Complexes** The effects of a variation of the hydrogen bond length ( $r(\text{O–N})$ ) as well as of in- ( $\alpha$ ) and out-of-plane ( $\beta$ ) distortions (Figure 5.5) on the QC parameters are visualized in Figure 5.6 for the imidazole–water sys-

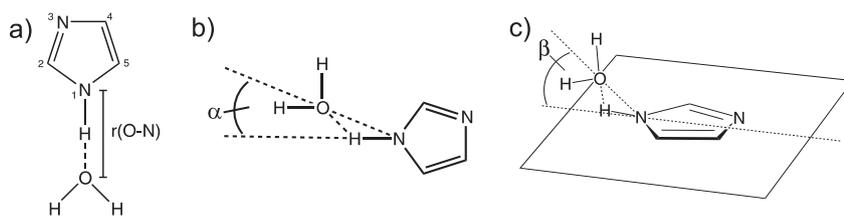


**Figure 5.5** Definition of the atom numbering scheme and geometric variables for the imidazole–water complexes: a) shows the hydrogen bond length  $r(\text{O-N})$ , b) the in-plane hydrogen bond angle  $\alpha$  and c) the out-of-plane hydrogen bond angle  $\beta$ .

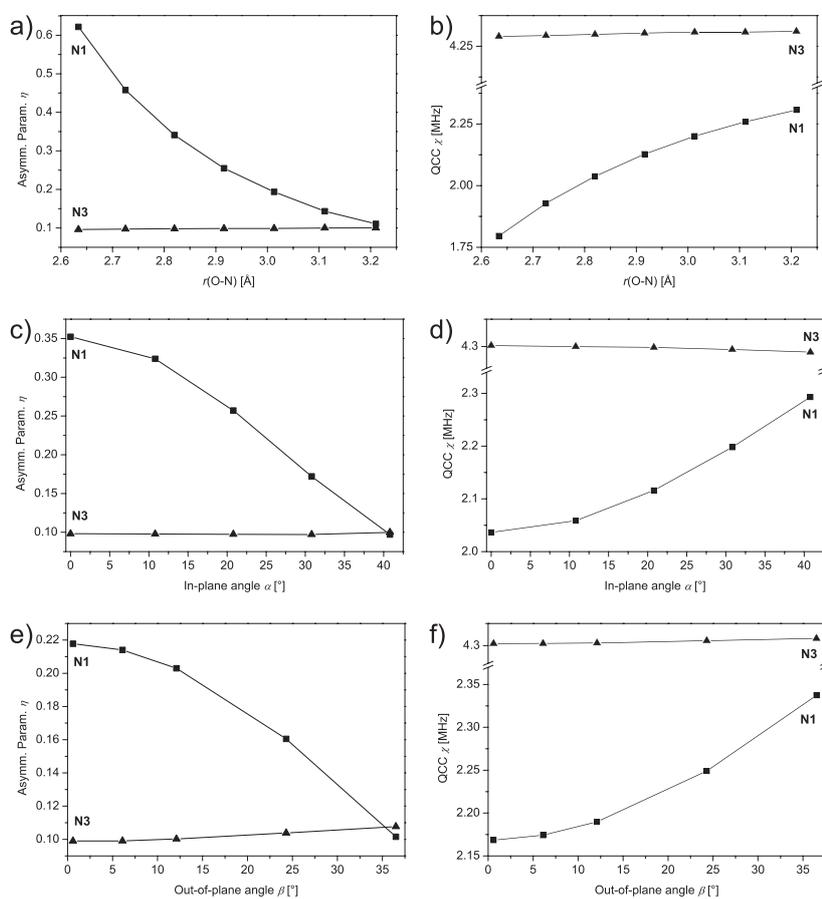


**Figure 5.6** Influence of the hydrogen bond length  $r(\text{O-N})$  (a, b), the in-plane hydrogen bond angle  $\alpha$  (c, d) and the out-of-plane hydrogen bond angle  $\beta$  (e, f) on the asymmetry parameters  $\eta$  as well as the QCCs  $\chi$  of the nitrogen atoms of charge neutral imidazole–water complexes as calculated on the B3PW91/6-311+G(df,pd) level of theory.

tem. A significant effect of hydrogen bond length variation was found for the QC parameters of the amino nitrogen N1 whereas the effect on the N3 coupling parameters is negligibly small. The asymmetry parameter  $\eta$  of N1 decreases and the QCC increases when elongating the hydrogen bond, i.e. the electric field gradient (EFG) tensor becomes more axially-symmetric and the  $V_{zz}$  component increases. Very similar observations could be made for in- or out-of-plane distortions of the hydrogen bond. In both cases a trend towards axial symmetry of the EFG tensor as well as an enlargement of the  $V_{zz}$  component was found for N1. Thus, the deformation or weakening of the hydrogen bond by variation of any of these three geometric parameters leads to an electronic situation around the amino nitrogen which is increasingly symmetric. Comparison with QC parameters of an isolated imidazole molecule revealed that the value of  $\chi$  for the hydrogen bonded nitrogen N1 is always lower than that for free imidazole, whereas the value of  $\eta$  approaches the value for free imidazole when  $r$ ,  $\alpha$  or  $\beta$  are increased. Based on these findings it should be possible to identify imidazoles which are involved in hydrogen bonding by simply comparing the amino nitrogen QC parameters with those of unbound imidazole: the QCC values will be lower and the asymmetry parameter values will be higher for typical hydrogen bond geometries. Especially the asymmetry parameter  $\eta$  also seems to be a sensitive indicator for the hydrogen bond length.

**Imidazole–Semiquinone Complexes** Having identified the QC parameters as sensitive probes to detect hydrogen bonding interactions and to gain valuable information about the hydrogen bond geometry, a wider applicability of these trends was verified for paramagnetic methylimidazole–benzosemiquinone complexes. Such complexes are supposed to be good models for quinone binding pockets in biological systems containing histidines as ligands, e.g. in bacterial reaction centres (bRCs) [53] or photosystem II (PSII) [54]. It was found for the amino nitrogen QC parameters that the QCC  $\chi$  is always smaller and the asymmetry parameter  $\eta$  is always larger than for a free methylimidazole molecule. Thus, again it is possible to identify hydrogen bonding to the amino nitrogen just by comparison with the non-bonded species. The largest effect on  $\eta$  as well as on  $\chi$  of the amino nitrogen was found for an alteration of the bond length. A shortening of this variable lead to a huge increase of the asymmetry parameter and a decrease of the QCC. Any distortions of the bonding geometry by introducing in- or out-of-plane angles resulted in a much smaller increase of the QCC

and a much smaller decrease of the asymmetry parameter. Analysis of these trends made it possible to map specific  $(\chi, \eta)$  values onto specific hydrogen bond characteristics, e.g. allowing predictions of hydrogen bond lengths based on QC parameters of the amino nitrogen.

**Transfer to Biological Systems** To finally test whether the results of this systematic study are transferable to quinone binding pockets in biological systems, available experimental QC and hydrogen bond geometry data for histidine residues involved in binding of semiquinone anion radicals in bRCs [55] and PSII [56, 57] was analyzed and compared with some of the theoretical results. In this comparison solely the hydrogen bond length was considered since this parameter has by far the strongest influence on the QC parameters. Based on the experimental  $\chi$  and  $\eta$  values and employing the structure–property correlations found in this study, O–N distances of 2.50–2.75 Å were predicted theoretically. Taking into account experimental uncertainties these predictions agree well with distances obtained from experimental hyperfine coupling constants for both biological systems. Thus, this application to biological systems clearly demonstrates a more general validity of the trends found for the model systems and emphasizes the predictive power of the computational methods.

The systematic insight into the sensitivity of quadrupole interaction parameters towards changes in the hydrogen bonding geometry provided by this work may be used as an aid to interpret experimental  $^{14}\text{N}$  quadrupole coupling data involving imidazole derivatives or histidines and to relate them to geometric features of hydrogen bonds.

## 5.2 Organic Radicals in Biological Systems

### 5.2.1 Structure of the Nitrogen-Centered Radical Formed During Inactivation of RNR by $\text{N}_3\text{UDP}$

EPR spectroscopic studies on the interaction of 2'-azido-2'-deoxy-3'- $^{17}\text{O}$ -uridine-5'-diphosphate (3'- $^{17}\text{O}$ - $\text{N}_3\text{UDP}$ , **5**, Figure 5.7) with ribonucleotide reductase (RNR) in conjunction with DFT calculations were conducted to elucidate the structure of the nitrogen-centered radical ( $\text{N}^\bullet$ ) generated during the inactivation of RNR by  $\text{N}_3\text{UDP}$  (cf. also Section 6.5 and Ref. 7). The results provide direct ev-

idence for the trapping of a 3'-ketonucleotide (**2** or **3**, Figure 5.7) in the reduction process catalyzed by RNR.

RNRs catalyze an essential step in DNA replication and repair, conversion of nucleotides to deoxynucleotides, by providing the monomeric precursors required for these processes [58–60]. The class I RNRs are proposed to be composed of a 1:1 mixture of two homodimeric subunits: R1 and R2 [61, 62]. R1 is the business end of the RNR containing the active site with three cysteines essential for catalysis [63–68] and allosteric sites that govern substrate specificity and turnover rate [69–72]. R2 contains the radical initiator, the diiron tyrosyl radical ( $Y^\bullet$ ) cofactor [73]. This  $Y^\bullet$  is proposed to generate a thiyl radical ( $S^\bullet$ ) in the active site on R1 that then initiates nucleotide reduction. The mechanism of nucleotide reduction has been studied for more than two decades using biochemical, chemical, and structural probes.

It was recently shown that the rate-determining step in *Escherichia coli* RNR is a physical step prior to generation of the putative  $S^\bullet$  on C439 [74]. This has precluded detection of intermediates in the reduction process with the normal substrate. Perturbation of the system using mechanism-based inhibitors and site-directed mutants of R1 and R2 has provided the bulk of the insight into the reduction mechanism by inference.

2'-Azido-2'-deoxynucleoside-5'-diphosphates,  $N_3NDPs$ , have been studied in detail since their discovery as potent mechanism-based inhibitors of RNRs by the Eckstein and Thelander groups in 1976 [77]. These early studies revealed that incubation of RNRs with  $N_3NDPs$  resulted in loss of the  $Y^\bullet$ . Subsequent studies revealed that this loss was accompanied by formation of a new nitrogen-centered radical ( $N^\bullet$ ) and provided the first evidence for the involvement of nucleotide radicals in the reduction process [78, 79]. Despite the wealth of knowledge about the interaction of this inhibitor with RNR, the structure of the  $N^\bullet$  has remained an issue [76, 80, 81]. Two options (structures **6** and **7**, Figure 5.7) have been considered based on isotopic labeling experiments using 1'-, 2'-, 3'-, 4'- $^2H$ ,  $^{13}C$ , and  $^{15}N$  labeled  $N_3UDP$  and analysis of the resulting  $N^\bullet$  by EPR and ESEEM spectroscopies at 9 and 140 GHz [76, 81].

The availability of 3'- $^{17}O$ - $N_3UDP$  [82] allowed further EPR studies to distinguish between the two structural models (**6**, CNS, and **7**, ONS, Figure 5.7) that were originally proposed [76] for the long-sought  $N^\bullet$ . The new X-band (9 GHz) and 140 GHz EPR spectra [7] exhibited considerable hyperfine broadening due to the interaction of the unpaired electron with the  $^{17}O$  nuclear magnetic mo-

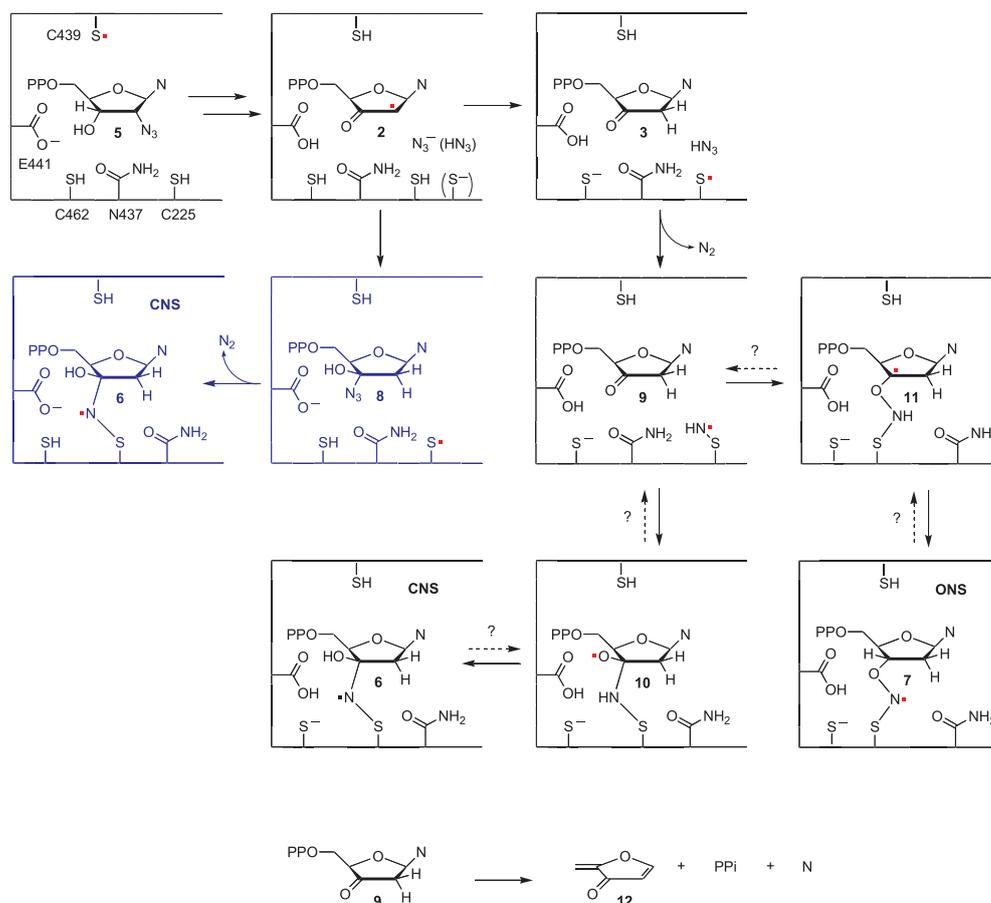
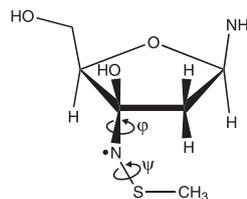


**Figure 5.7** Two previously proposed structures for  $N^\bullet$  (**6** and **7**) and pathways for their generation. The blue pathway is proposed based on theoretical studies [75], while the black pathways were proposed by van der Donk, Stubbe and coworkers [76]. The major differences involve the timing of  $N_2$  release and the role of E441.

ment. It was possible to quantify this HFC and simulations yielded a  $^{17}\text{O}$  HFC tensor with  $|A_{xx}| = 8.5$  G,  $|A_{yy}| = 1.5$  G and  $|A_{zz}| = 1.0$  G. However, there is no information in the literature on hyperfine couplings of  $\text{R-}^{17}\text{O-N}^\bullet\text{-S-R-}$  or  $\text{H-}^{17}\text{O-C-N}^\bullet\text{-S-R-}$  type radicals. Thus, it was not feasible to distinguish between **6** and **7** solely based on direct comparison of the observed  $^{17}\text{O}$  hyperfine tensor with literature data.

To interpret the EPR data and get more insight into the structure of the unusual  $N^\bullet$  radical and into the mechanism of the  $^{17}\text{O}$  hyperfine coupling, DFT calculations were employed. To make the calculations tractable, models of  $N^\bullet$  were generated in which the 5'-diphosphate group was removed and the nucle-

**Figure 5.8** Structure of the CNS model of the N<sup>•</sup> radical including the definitions of the dihedral side chain angles  $\varphi$  and  $\psi$ .



obase was replaced by an NH<sub>2</sub> group (cf. Figure 5.8 for CNS model). Finally, the C225 in the active site of R1 was represented by -S-CH<sub>3</sub>. These models were structurally optimized without constraints (BP86/TZVP) to obtain the equilibrium geometries.

**Ab Initio Validation** Before calculating the EPR parameters of these model compounds, the DFT method was validated by *ab initio* CCSD(T) calculations on smaller substructures of the ONS and CNS radical models.<sup>2</sup> A comparison of the HFC tensors obtained at CCSD(T) and DFT levels (Table 5.2) reveals that DFT calculations (B3PW91) employing the IGLO-II basis sets [83] yield satisfying spin densities and HFC constants for the systems under study, even though the Fermi contact contributions ( $A_{\text{iso}}$ ; cf. Chapter 3 for a description of EPR parameters) may be underestimated. Thus, this computational model was used for all further calculations on the larger model structures.

**Identification of N<sup>•</sup> Using DFT Methods** After method validation, the EPR parameters for the larger freely optimized model systems ONS and CNS were computed (see Figure 5.8 for CNS structure). For both types of radicals the <sup>14</sup>N HFC tensors were in good agreement with experiment. However, a comparison of the <sup>17</sup>O HFC tensors allowed to rule out ONS-type structures as candidates for N<sup>•</sup>. The direct bonding of the oxygen nucleus to the N<sup>•</sup> gives rise to a <sup>17</sup>O HFC tensor much larger than the one calculated for the CNS structure and the one observed experimentally. This preliminary calculation with free structure optimization gave <sup>17</sup>O HFC constants for the CNS model that are smaller than the values found experimentally for N<sup>•</sup>, but suggested that this structure should be considered for further refinement.

To find a better model for N<sup>•</sup>, focus was turned to CNS-type structures in which the orientation of the N-S-CH<sub>3</sub> side chain relative to the sugar ring was

<sup>2</sup>The CCSD(T) computations of the HFC tensors were conducted by S. Kacprzak and M. Kaupp (Würzburg).

**Table 5.2** Comparison of isotropic ( $A_{\text{iso}}$ ) and dipolar ( $T_{ii}$ ) hyperfine coupling constants obtained by UB3PW91/IGLO-II and IGLO-III and by *ab initio* CCSD(T)/IGLO-III calculations for small model substructures of ONS- and CNS-type radical structures (all coupling constants in G)

	HO-N <sup>•</sup> -SH (ONS)			HO-CH <sub>2</sub> -N <sup>•</sup> -SH (CNS)		
	B3PW91	B3PW91	CCSD(T)	B3PW91	B3PW91	CCSD(T)
	IGLO-II	IGLO-III	IGLO-III	IGLO-II	IGLO-III	IGLO-III
<sup>14</sup> N $A_{\text{iso}}$	+9.43	+10.91	+14.56	+8.19	+9.16	+9.05
$T_{11}$	-13.80	-14.05	-13.77	-11.41	-11.50	-10.30
$T_{22}$	-12.90	-13.15	-12.94	-11.16	-11.27	-9.93
$T_{33}$	+26.70	+27.20	+26.70	+22.57	+22.77	+20.23
<sup>17</sup> O $A_{\text{iso}}$	-6.05	-6.35	-7.98	-3.46	-3.86	-5.87
$T_{11}$	-20.34	-19.97	-17.90	-6.03	-5.96	-5.55
$T_{22}$	+10.87	+10.65	+9.84	+3.16	+3.11	+2.55
$T_{33}$	+9.47	+9.32	+8.07	+2.87	+2.85	+3.00

altered. For these computations, the dihedral angle  $\varphi$  (cf. Figure 5.8) was set to a specific value and kept fixed during the structure optimizations, while all other degrees of freedom were allowed to fully relax. Furthermore, a different sugar ring conformation corresponding to a shorter N-H1' distance was tested in calculations with two fixed constraints (angle  $\varphi$  and  $r(\text{N-H1}')$ ). Freezing of the side chain orientation or N-H1' distance was done to mimic structural constraints imposed on the sugar conformation by the protein surroundings, in particular the positioning of the C225 side chain on the  $\alpha$  face of the sugar ring [84].

From calculations on many different conformers of the CNS model it was possible to obtain a CNS-type structure (Figure 5.9) exhibiting a <sup>17</sup>O HFC tensor with  $A_{xx} = -8.80$  G,  $A_{yy} = +0.88$  G and  $A_{zz} = +1.11$  G. The EPR properties of this model are in good agreement with all available experimental data (not just <sup>17</sup>O HFCs) thus providing strong support for the N<sup>•</sup> structure being best represented by **6** with a conformation as depicted in Figure 5.9. Furthermore, the energy difference between this model (CNS<sub>140</sub><sup>\*</sup>, Figure 5.9) and the CNS equilibrium structure amounts to only 2.5 kcal/mol, a value reasonably small to represent structural influences of the protein surroundings on the geometry of N<sup>•</sup>.

During these studies a critical dependence of the <sup>17</sup>O HFC on the conformation of the side chain connecting the protein to the plane of the sugar ring determined by C1', C3', and C4' could be observed. A rotation of this side chain

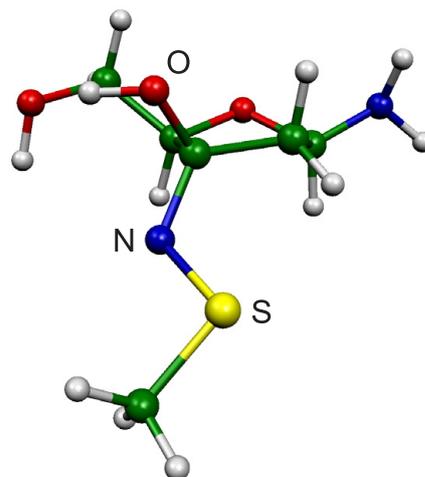


**Figure 5.9** Structure of the  $\text{N}^\bullet$  radical with the  $\text{CNS}_{140}^*$  conformation as obtained from the quantum chemical calculations ( $\varphi = 140^\circ$  and  $r(\text{N}-\text{H}1') = 3.33 \text{ \AA}$ ).

into a position in which the  $\text{S}-\text{CH}_3$  points below and almost perpendicular to the sugar ring plane ( $\text{CNS}_{140}^*$  model, Figure 5.9) leads to a  $^{17}\text{O}$  HFC tensor in good agreement with the experimental data. These results have now allowed us to qualitatively rationalize the mechanism of the  $^{17}\text{O}$  HFC and the substantial value of roughly  $-3 \text{ G}$  for  $A_{\text{iso}}(^{17}\text{O})$ . Since the main portion of spin density in  $\text{N}^\bullet$  is localized in the  $p_z$ -orbitals of the nitrogen and sulfur, rotation of the side chain can produce overlap between the nitrogen  $p_z$ -orbital and the  $p_z$ -orbital of the 3'-oxygen for some specific conformations, inducing spin density at the  $^{17}\text{O}$  nucleus. The situation is best illustrated in Figure 5.10, where the calculated spin density distribution is displayed for two different side chain conformations.

In summary, sophisticated chemical, biochemical, spectroscopical and computational methods were combined to elucidate the structure of the nitrogen-centered radical that is generated upon incubation of RNR with the stoichiometric inhibitor  $\text{N}_3\text{UDP}$ . It was possible to interpret the EPR data with the help of DFT calculations for a number of possible model structures thus correlating the experimental findings with molecular structure parameters. Identification of the structure of the nitrogen-centered radical that had been subject to debate for more than 20 years has furthermore for the first time provided evidence for the trapping of a 3'-ketonucleotide in the reduction process catalyzed by RNR. Thus, the structural information obtained with the help of DFT calculations also lead to valuable insights into the catalytic mechanism of RNR. Since the first reaction steps of reduction and inhibition are similar to the normal reduction reaction for mechanism-based inhibitors as  $\text{N}_3\text{NDPs}$ , such an approach is also mechanistically informative about the normal NDP reduction.

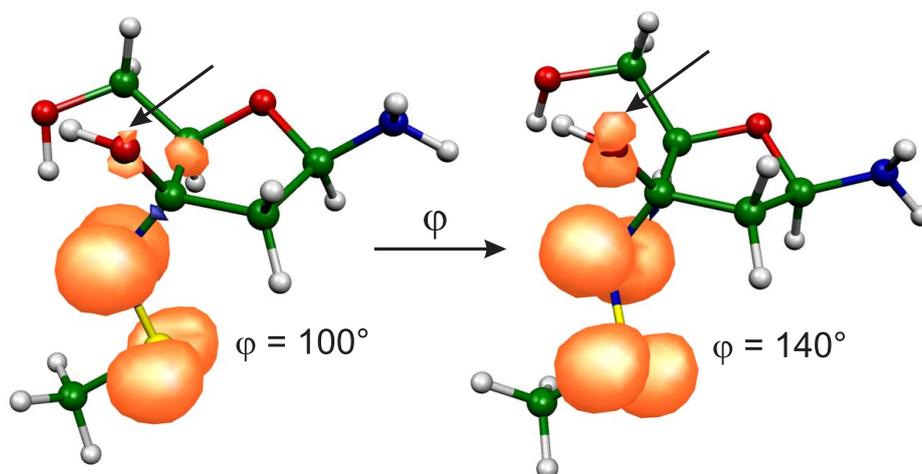


**Figure 5.10** Plot of the spin density distribution for two different  $\varphi$ -conformers ( $\text{CNS}_{100}$  and  $\text{CNS}_{140}^*$ ) of the CNS-type model structure (isodensity cutoff value  $\pm 0.0045$  a.u.). Rotation of the side chain about the N–C3' bond leads to a better overlap between the nitrogen  $p_z$ -orbital and the  $p_z$ -orbital of the 3'-oxygen for the  $\varphi=140^\circ$  conformer, enabling a more efficient transfer of spin density from the nitrogen to the 3'-oxygen. Thus, one observes a larger 3'-oxygen spin density for the  $\text{CNS}_{140}^*$  model. The arrows indicate the different spin densities at the 3'-oxygen for the two structures.

## 5.3 Transition Metals in Model Complexes

### 5.3.1 Computational Studies of $g$ -Tensors and Molybdenum Hyperfine Couplings for Paramagnetic Molybdenum Complexes

DFT methods were employed to calculate electronic  $g$ -tensors and molybdenum HFC tensors (see Chapter 3 for an explanation of EPR parameters) of different paramagnetic molybdenum species in order to test the capabilities of standard DFT methods to predict EPR parameters for the 4d transition metal molybdenum (cf. also Sections 6.7 and 6.8 as well as Refs. 1 and 3). The first part [1] of this project deals with small and medium-sized systems such as the Mo atom, MoN as well as several  $\text{Mo}^{\text{V}}$  complexes whereas the second part [3] extends the studies to larger  $\text{Mo}^{\text{V}}$  model complexes relevant to molybdenum enzymes. For the application of DFT methods to ‘new’ or more complicated systems (e.g. heavier transition metals) *validation studies* are of great importance to discover the performance of different exchange–correlation functionals and basis sets and find

out about systematic errors of the various computational models.<sup>3</sup>

A number of *molybdenum-containing enzymes*, like e.g. sulfite oxidase, nitrate reductase, xanthine oxidase, xanthine dehydrogenase, dimethylsulfoxide (DMSO) reductase or polysulfide reductase, play an important role in biological two-electron redox processes [85–88]. Since these catalytic reactions directly involve the molybdenum ion, it is of great importance for a deeper understanding of the reaction mechanism to study the structure of the catalytically active molybdenum binding site [88]. Due to the occurrence of paramagnetic Mo<sup>V</sup> species during the catalytic cycles of these enzymes, electron paramagnetic resonance (EPR) spectroscopy can be a valuable tool to reveal details about the molybdenum coordination sphere [85, 88–92].

The parameters that can be extracted from EPR spectra, like electronic *g*-tensors, hyperfine coupling (HFC) tensors or nuclear quadrupole coupling (QC) tensors, contain indirect information about the electronic and molecular structure of the metal binding site. However, it is often difficult or even impossible to relate these spin Hamiltonian EPR parameters to structural information. It may even be hard to find a unique solution for the simulation of the EPR spectra using the spin Hamiltonian concept. Thus, models or theories are needed that are able to provide the link between molecular structure and EPR parameters.

For the study of molybdoenzymes (as well as for other biological systems) it has been made use of paramagnetic model complexes that have been designed and synthesized to mimick the structure of molybdenum binding sites in the enzymes. Comparison of the EPR properties of these model compounds of well-known structure with EPR data from the corresponding biological systems allowed structural insight into the catalytic site of the enzyme in a number of cases [87]. The larger Mo<sup>V</sup> model complexes that are subject of this work (cf. Figures 5.12 and 5.14) have also been used to investigate molybdenum binding sites in molybdoenzymes, like e.g. sulfite oxidase or xanthine oxidase [93–100]. However, the development of suitable paramagnetic model systems may be very difficult or impossible in many cases and even if potentially suitable complexes are available the analysis and interpretation of their EPR spectra will often not be straightforward.

In some specific cases ligand field theory, semiempirical McConnell relations or

---

<sup>3</sup>See also Section 4.3 concerning problems of DFT methods to systematically approach exact results for different properties with the same series of computational methods.

the point-dipole approximation are suitable for the interpretation of EPR parameters. In general, these approaches fail for systems that possess a complicated electronic structure or that are not yet calibrated for the use of semiempirical theories [7].

At that stage quantum chemical DFT-based calculations come into play and turn out to be very useful for correlating experimental EPR data with molecular structure. Such computations may help to find species and geometries with calculated EPR properties similar to those found experimentally thus revealing the type and structure of the system under study. Quantum chemical methods may also aid in the primary analysis of EPR spectra by providing precise starting parameters for spectral simulations based on spin Hamiltonians.

Before dealing with molybdenum binding sites in biological systems and drawing extensive conclusions about their structure based on computational results, a critical validation of the available DFT methods and basis sets for treating such types of model systems containing the 4d transition metal molybdenum is necessary in order to avoid misinterpretation.

Until now only very few computational studies of  $g$ - and molybdenum HFC tensors of  $\text{Mo}^{\text{V}}$  compounds have been performed [94, 99, 101–110]. Only the two most recent theoretical studies [99, 110] employ modern DFT methods for the computation of the EPR properties of two larger  $\text{Mo}^{\text{V}}$  complexes modeling the active site of molybdenum enzymes:  $\text{MoOCIL}^1$  and  $[\text{MoO}(\text{SPh})_4]^-$ . However, although very promising results were obtained in these works, until now no systematic validation of modern DFT methods for the computation of  $g$ - and HFC tensors of  $\text{Mo}^{\text{V}}$  species has been performed.

Therefore, in this work such a validation of DFT methods was carried out together with an in-depth analysis of the physical origin of the EPR parameters. Electronic  $g$ -tensors and molybdenum HFC tensors were calculated with a recently developed methodology [103, 111, 112] using unrestricted Kohn–Sham DFT together with hybrid functionals. The results of the computations were then compared with experimental values from literature.

**Molybdenum Basis-Set Studies** Due to the lack of molybdenum basis sets specifically tailored for the calculation of EPR parameters, calculations on the Mo atom, the MoN molecule and the two well-studied small  $\text{Mo}^{\text{V}}$  complexes  $[\text{MoOCl}_4]^-$  and  $[\text{MoOF}_5]^{2-}$  were used to construct a suitable basis set for molybdenum which is accurate but sufficiently efficient computationally to be applied

to large systems. From the results of these  $g$ - and HFC tensor calculations using various uncontracted TZVP-based [113] molybdenum basis sets together with the B3PW91 functional and the AMFI approximation [114, 115] for the matrix elements of the SO operator it could be deduced that the influence of basis set size on the  $g$ -values and the dipolar HFC constant  $T_{\text{dip}}$  is rather small. In contrast, the isotropic HFC constant  $A_{\text{iso}}$  is substantially influenced by basis set contractions if the s-function part is contracted from 12s to 9s. Thus, the 12s6p5d basis was identified as the smallest basis set that still yields EPR parameters close to the ‘basis-set limit’ values and was therefore used as a standard molybdenum basis for all further EPR parameter calculations.

**Dependence on Functional:  $[\text{MoOCl}_4]^-$  and  $[\text{MoOF}_5]^{2-}$**  The second task of the molybdenum study was to find generally applicable exchange–correlation functionals providing accurate EPR parameters for  $\text{Mo}^{\text{V}}$  complexes. Results of initial calculations for the  $C_{4v}$  symmetrical model complex  $[\text{MoOCl}_4]^-$  revealing the dependence of the  $g$ - and HFC values on the choice of the density functional are shown in Figure 5.11. These data showed that the negative perpendicular  $g$ -shift component  $\Delta g_{\perp}$  reaches the experimental value at an exact-exchange admixture of 30–40%. However, even at 70% HF exchange admixture, the negative  $\Delta g_{\parallel}$ -values cannot be reproduced. This points to a systematic error of the one-component second-order perturbation approach used (see also below).

Closer analysis of the different contributions to the  $g$ -tensor showed that the dominant contributions to  $\Delta g_{\perp}$  arise from d–d couplings of the SOMO (essentially Mo-4 $d_{xy}$ ) to  $d_{xz}$ - and  $d_{yz}$ -based virtual MOs, and  $\Delta g_{\parallel}$  is dominated by a negative contribution due to coupling of the SOMO to a  $d_{x^2-y^2}$ -based virtual MO and a positive contribution from a double–SOMO excitation from a Mo–Cl- $\sigma$  bonding orbital to the  $\beta$  component of the SOMO. Furthermore, it was possible to quantify the role of ligand SO effects on the  $g$ -values. Such an atomic analysis showed that oxygen SO contributions are negligible and that the  $\Delta g_{\perp}$ -shift is totally dominated by metal SO coupling. In contrast,  $\Delta g_{\parallel}$  would be much more negative with metal SO coupling alone and is rendered more positive by sizeable chlorine SO contributions. Thus, for the  $g$ -tensor analysis not only ligand-field transitions but also effects of ‘charge-transfer-type’ couplings as well as the role of metal–ligand covalency and ligand spin–orbit coupling have to be considered.

To check whether the insufficiently negative  $\Delta g_{\parallel}$ -components for  $[\text{MoOCl}_4]^-$  (and  $[\text{MoOF}_5]^{2-}$ ) are due to the neglect of higher-order SO contributions in the

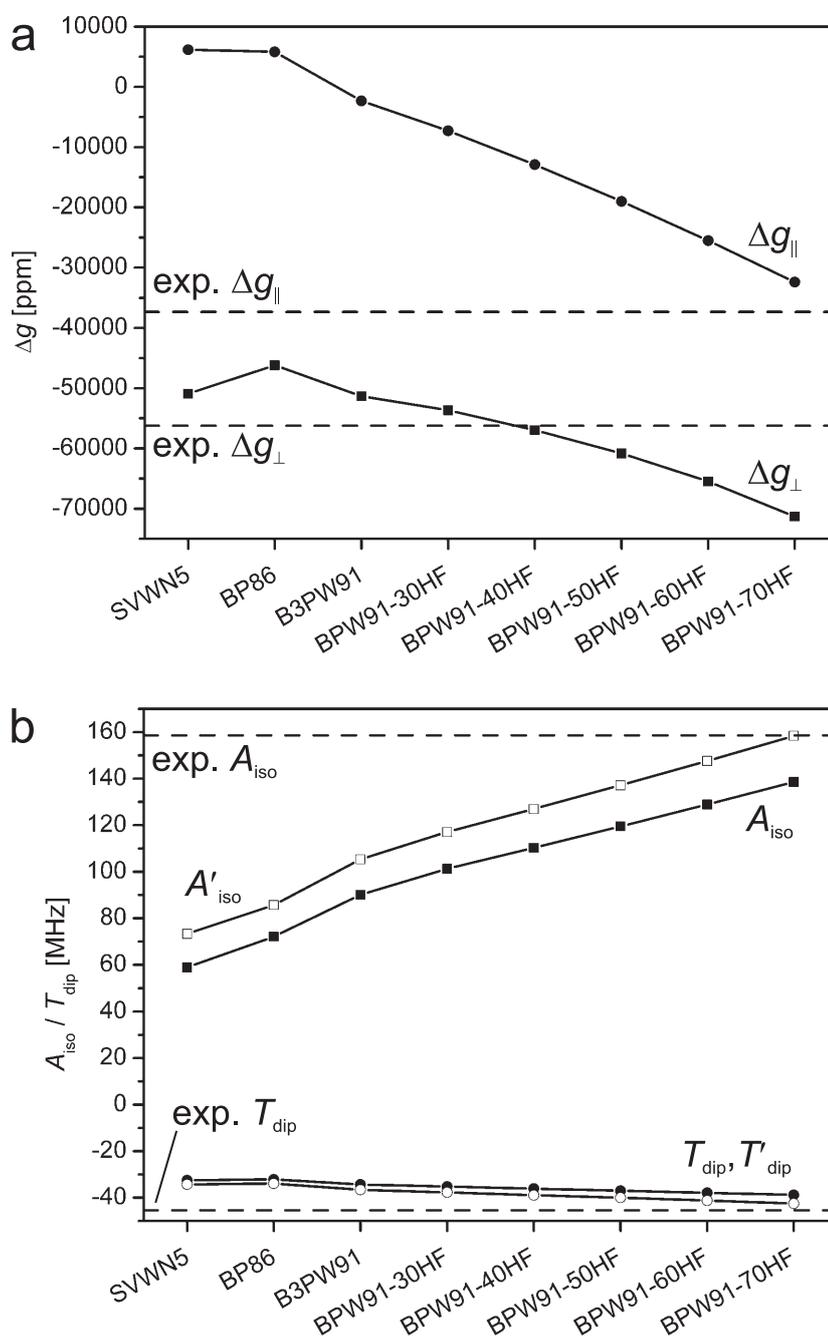


**Figure 5.11** Dependence of a)  $\Delta g_{\perp}$  (squares) and  $\Delta g_{\parallel}$  (circles) and b)  $^{95}\text{Mo}$   $A_{\text{iso}}$  (squares) and  $T_{\text{dip}}$  (circles) – both with (open symbols) and without (closed symbols) SO-HFC corrections – on the choice of the density functional for  $[\text{MoOCl}_4]^-$  ( $^2B_2$ ). The calculations were performed using the 12s6p5d basis set for molybdenum and IGLO-II basis sets for all other atoms. The dashed lines indicate the experimental values [116].

second-order perturbational treatment of the  $g$ -tensor, a relativistic non-collinear two-component DKH approach including spin polarization [117] was applied. While changes in  $\Delta g_{\perp}$  compared to the one-component results are moderate, the more negative two-component  $\Delta g_{\parallel}$ -values are notable and lie appreciably closer to the experimental values than the one-component results. Thus, it becomes obvious that the  $\Delta g_{\parallel}$ -components depend on higher-order SO contributions and are insufficiently described by the standard second-order perturbation approaches.

Turning to the  $^{95}\text{Mo}$  HFC tensors it could be noted that large HF exchange admixtures are required to approach the experimental values. Interestingly this holds for both isotropic and anisotropic contributions. However, already around 40% HF exchange, where good  $g$ -tensors may be obtained, the agreement with experimental hyperfine tensors is acceptable. Furthermore, it can be clearly seen from Figure 5.11 that an inclusion of SO corrections is absolutely necessary to approach the experimental values. The SO corrections can by no means be neglected for  $\text{Mo}^{\text{V}}$  complexes and are on the order of 12–15% for  $[\text{MoOCl}_4]^-$  and  $[\text{MoOF}_5]^{2-}$ .

**EPR Parameters of  $\text{MoOLCl}_2$  and  $\text{MoSLCl}_2$**  Next, the validation study was extended to larger  $\text{Mo}^{\text{V}}$  complexes providing a more challenging test of the methodology due to their lower symmetry. The latter point renders the orientations of the  $g$ - and HFC tensors non-trivial. The first group of complexes to be studied were  $\text{MoOLCl}_2$  and  $\text{MoSLCl}_2$  ( $\text{L} = \text{tris}(3,5\text{-dimethylpyrazolyl})\text{hydroborate}$ ) which are schematically depicted in Figure 5.12. Since very reliable single-crystal EPR studies are available [93] for these two compounds, the performance of DFT methods for the prediction of relative as well as absolute tensor orientations could be evaluated. Therefore, these two complexes served as ‘reference’ systems before dealing with other complexes.

Analysing the results of the  $g$ -tensor computations for the structurally optimized (BP86/TZVP) complexes where a number of different exchange–correlation functionals were employed, a similar behaviour as for the smaller models could be seen: Hybrid functionals with about 30–40% HF exchange admixture provide good agreement with experiment for the ‘perpendicular’ components ( $\Delta g_{22}$  and  $\Delta g_{33}$ ) but insufficiently negative ‘parallel’  $\Delta g_{11}$ -values. As explained above, the latter point is due to the neglect of higher-order spin–orbit contributions in the perturbational treatment.

For the HFC tensors good agreement with experimental couplings was also

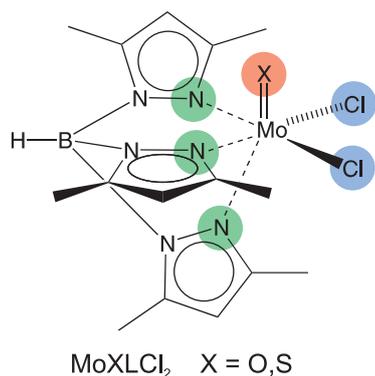


**Figure 5.12** Schematic structure of the two larger  $\text{Mo}^{\text{V}}$  complexes  $\text{MoOLCl}_2$  and  $\text{MoSLCl}_2$  with  $\text{L} = \text{tris}(3,5\text{-dimethylpyrazolyl})\text{hydroborate}$ .

found at 30–40% exact exchange admixture. Thus, this ratio seems to provide a reasonable description of core-shell spin polarization. It should be noted here, that the  $\text{MoSLCl}_2$  system is the only  $\text{Mo}^{\text{V}}$  complex in the whole study where spin contamination was observed upon increasing the HF exchange admixture beyond 20%. This renders the choice of an ideal functional more difficult for this particular complex and probably B3PW91 calculations would appear the most reliable approach in this case.

Again, an inspection of the SO contributions to the HFC tensors indicated that they are about 15–25% for the isotropic HFC constants and around 10% for the anisotropic part. In both cases the HFC values tend to move closer to the experimental data emphasizing that SO corrections should always be included in accurate calculations.

Another aspect that was investigated is the orientation of the  $g$ - and HFC tensors – either with respect to each other or in an absolute sense with respect to the molecular frame. Figure 5.13a visualizes the computed tensor orientations for  $\text{MoOLCl}_2$ . The  $A_{11}$  axis points along the Mo–O bond, the  $A_{33}$  axis lies between the two chlorine atoms and the  $A_{22}$  axis between a chlorine and an equatorial nitrogen atom. The  $g_{22}$  axis is almost collinear with  $A_{22}$  and  $g_{11}$  and  $g_{33}$  are simply rotated clockwise around the  $g_{22}/A_{22}$  axis with respect to the principal axes of the HFC tensor. Comparison of the computed angles between the axes of the  $g$ - and HFC tensor principal axis systems with those obtained from single-crystal EPR experiments showed a very satisfying agreement for both complexes. In general, the influence of the density functional is rather small and SO corrections do not alter the relative tensor orientations much in both cases. The BPW91-30HF and BPW91-40HF functionals (including SO corrections to the HFC tensor) yield smallest deviations from experiment which amount to below 5% for the large

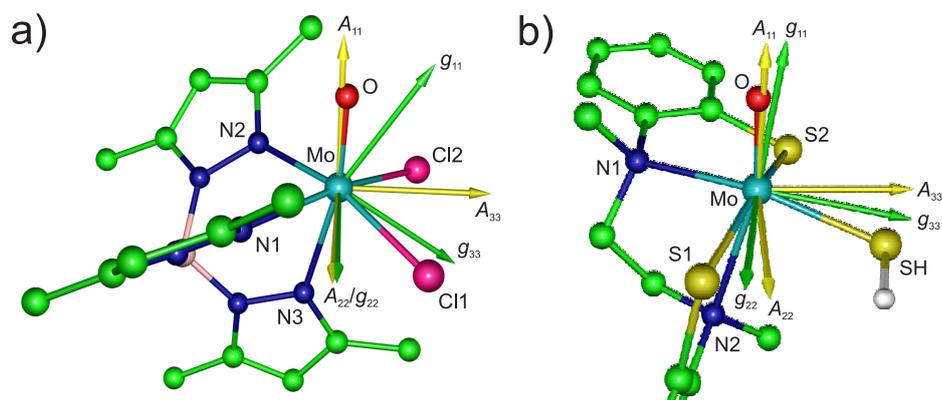


**Figure 5.13** Computed orientations of the  $g$ - (green) and HFC (yellow, including SO corrections to the tensor orientation) tensors in the molecular frame for a) MoOLCl<sub>2</sub> and b) MoOSHL<sup>1</sup> (BPW91-40HF results). Principal axis systems are taken to be right-handed coordinate systems. For the sake of clarity hydrogen atoms (except for SH group) and parts of the lower phenyl ring of MoOSHL<sup>1</sup> are omitted.

$g_{11}$ – $A_{11}$  and  $g_{33}$ – $A_{33}$  angles.

The orientation of  $g$ - and molybdenum HFC tensors in the molecular frame was also reproduced very well by the calculations, with the same influence of functional and SO corrections as discussed for the relative tensor orientations. Deviations from experiment were usually smaller than 5° for the angles between the principal tensor axes and the Mo–X (X = O/S, Cl1, Cl2, N1, N2, N3) bonds.

These results support thus the predictive power of appropriate DFT methods for the relative and absolute tensor orientations.

**EPR Parameters of Larger Mo<sup>V</sup> Model Complexes** In this paragraph mainly results from the second part [3] (Chapter 6.8) of the molybdenum studies will be summarized. Since these data essentially support the trends and conclusions found in the first part [1] (Chapter 6.7) and discussed above, the presentation will be kept rather concise and only specific aspects will be described explicitly. Further details can be found in Chapter 6.8.

The second part of the study focussed on larger Mo<sup>V</sup> compounds which have been designed and synthesized to mimic molybdenum sites in molybdoenzymes such as sulfite oxidase or xanthine oxidase. The structures of these model complexes are schematically depicted in Figure 5.14. Their geometries were also optimized at the DFT level (BP86/TZVP) and for the EPR property calcula-

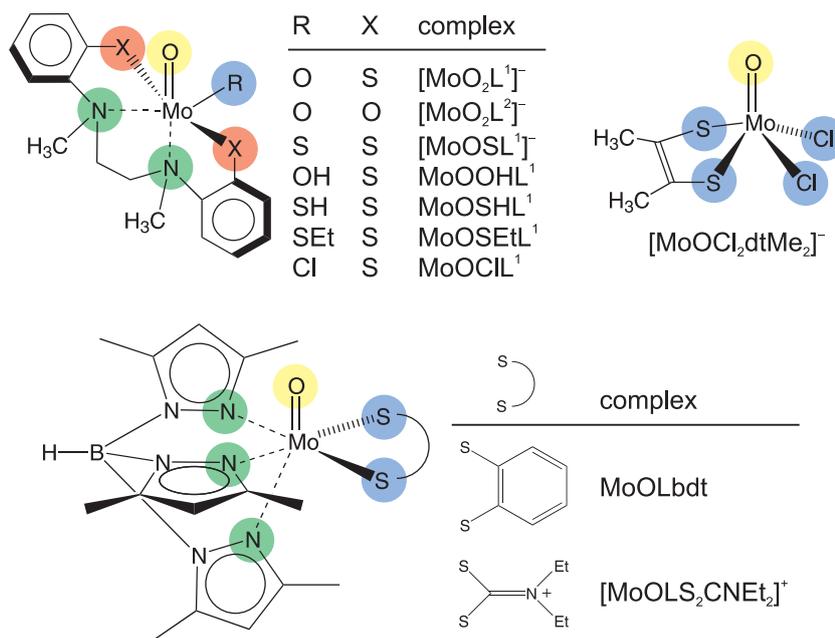


**Figure 5.14** Schematic structures of larger  $\text{Mo}^{\text{V}}$  model complexes studied in this work. *Abbreviations:*  $\text{dtMe}_2$  = 1,2-dimethyl-ethene-1,2-dithiolate (dimethyldithiolene ligand),  $\text{bdt}$  = 1,2-benzenedithiolate,  $\text{L}^1\text{H}_2$  = N,N'-bis(2-mercaptophenyl)-N,N'-dimethyl-1,2-diaminoethane,  $\text{L}^2\text{H}_2$  = N,N'-bis(2-hydroxyphenyl)-N,N'-dimethyl-1,2-diaminoethane and  $\text{L}$  = tris(3,5-dimethylpyrazolyl)hydroborate.

tions the molybdenum 12s6p5d basis as well as IGLO-II basis sets [83] for all other atoms were used.

The overall performance of EPR parameter calculations for the larger  $\text{Mo}^{\text{V}}$  model complexes will be summarized at the end of this section in combination with the results for the small and medium-sized compounds. In the following only some special aspects will be touched.

Among the complexes under study there is a group of compounds with two terminal oxo/sulfido ligands ( $[\text{MoO}_2\text{L}^1]^-$ ,  $[\text{MoO}_2\text{L}^2]^-$  and  $[\text{MoOSL}^1]^-$ ) which represent a very special type of electronic structure leading to very low  $g_{33}$ -values (as low as e.g. 1.754) and thus large  $g$ -anisotropies. A closer analysis of the major MO contributions to the  $g$ -tensor of these complexes indicated that the negative  $\Delta g_{33}$ -components are dominated by SOMO–virtual couplings, with one particular excitation being dominating (cf. Figure 5.15 for an example). The important difference to the other complexes with only one terminal oxo ligand is that the

spin density is more metal-centered and less delocalized onto the ligands. Moreover, the presence of low-lying excited states with appreciable metal character also plays a role in this context.

Another interesting feature of the dioxo complexes is the character of the SOMO. In complexes with only one strong  $\pi$ -donor oxo ligand X, the SOMO is essentially orthogonal to the Mo–X vector. However, the presence of two strong  $\pi$ -donor oxo ligands requires the SOMO to lie in the bisector plane of the O–Mo–O angle which is also reflected in a different orientation of the  $g$ - and HFC tensors ( $g_{11}$ - and  $A_{11}$ -components are pointing between the two oxo ligands) compared to the other Mo<sup>V</sup> complexes ( $A_{11}$  lies along Mo–O bond and usually  $g_{11}$  is also roughly pointing along this bond).

The  $\Delta g_{11}$ -component for the dioxo and oxo-sulfido complexes obtains positive contributions from couplings between Mo–ligand bonding MOs and the SOMO, especially for [MoOSL<sup>1</sup>]<sup>–</sup> due to the larger covalency of the Mo–S bond (see Figure 5.15). Thus, for the description of the  $\Delta g_{11}$ -component, effects of metal–ligand covalency, ‘charge-transfer-type’ excitations as well as ligand SO coupling have to be considered.

Notably, all three complexes exhibit unusually large SO corrections to the HFC tensor which may be attributed to the same reasons that are responsible for the large  $g$ -anisotropies.

The complexes MoOOHL<sup>1</sup>, MoOSHL<sup>1</sup> and MoOSetL<sup>1</sup> possess an oxygen- or sulfur-containing ligand (OH, SH, SEt) which has some rotational freedom, i.e. there may be different conformers with respect to the orientation of the hydrogen atoms or the ethyl chain. To test the sensitivity of the EPR parameters upon structural changes of such type, for MoOOHL<sup>1</sup> the results of the energy-minimized conformer (dihedral angle  $\angle(\text{H–O–Mo–O})$  of 80.5°) were compared with those from a geometry with a different OH orientation ( $\angle(\text{H–O–Mo–O}) = 175.0^\circ$ ). For the altered geometry one obtains a slightly increased  $A_{\text{iso}}$  constant (5%), slightly decreased  $T_{ii}$  values (roughly 5%) and smaller  $g$ -values than for the equilibrium structure. The most pronounced effect of the altered OH orientation is found for  $g_{33}$  (about 23000 ppm) which is the component of the  $g$ -tensor pointing towards the OH ligand. The second largest change is obtained for  $g_{22}$  (about 15000 ppm), the other  $g$ -tensor component in the equatorial plane of the molybdenum coordination sphere. Moreover, the tensor orientation is also influenced by the structural changes. However, the altogether agreement with experimental data is better for the equilibrium structure.

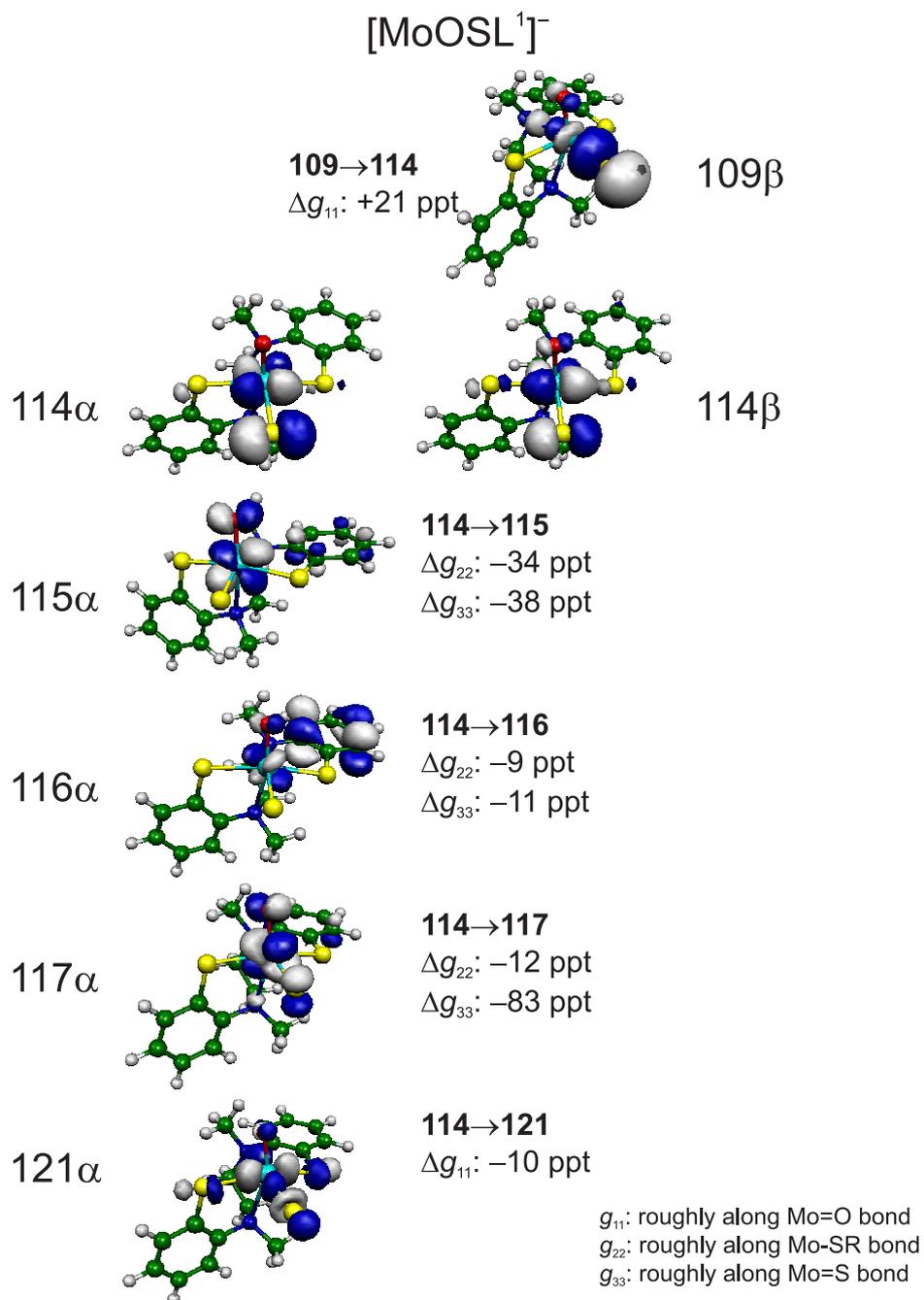


**Figure 5.15** MO scheme and  $g$ -tensor MO analysis for  $[\text{MoOSL}^1]^-$ . Isosurface plots of selected MOs ( $\pm 0.05$  a.u.) as calculated with the BP86 functional are shown together with main  $g$ -shift contributions from excitations involving these orbitals. Positive amplitudes are shown in gray, negative amplitudes in blue.

In Figure 5.13b the  $g$ - and HFC tensor orientation within the molecular frame is depicted exemplarily for MoOSHL<sup>1</sup> showing that the different local symmetry around the molybdenum – compared to MoOLCl<sub>2</sub> in Figure 5.13a – leads to a different orientation of the tensor principal axis systems.

It should be noted that a general problem for the validation of computed molybdenum HFC constants and HFC tensor orientations is the difficulty of finding precise and reliable experimental data. The reason for this is on the one hand side the low natural abundance of molybdenum nuclei with a nuclear spin  $I > 0$  (<sup>95</sup>Mo: 15.9%, <sup>97</sup>Mo: 9.6%; both with  $I = 5/2$ ) and on the other side spectral overlap for CW EPR spectra taken at S- or X-band microwave frequencies (roughly 3 and 9 GHz). Therefore, in some of the cases where the agreement between theory and experiment was not satisfying for the HFC tensors (MoOLbdt, [MoOLS<sub>2</sub>CNEt<sub>2</sub>]<sup>+</sup> and [MoOCl<sub>2</sub>dtMe<sub>2</sub>]<sup>-</sup>), new simulations of EPR spectra using the computed HFC values as starting parameters were performed. It could be shown that these new simulations are very similar to simulations using the HFC values from literature. Thus, both sets of parameters are ‘equally’ suitable to reproduce the experimental EPR spectrum and no unique solution of the simulation problem exists. In other words, the disagreement between the calculations and the values taken from literature is most likely not due to problems of the computational method but rather due to erroneous simulations of the experimental data to extract HFC values and tensor orientations. The agreement of the calculated HFC tensors with the ‘new’ experimental data (from own simulations) is very satisfying. Thus, DFT computations may also aid in the simulation of EPR spectra.

Additionally, also for the larger Mo<sup>V</sup> complexes detailed analyses of the shape of the SOMOs and spin density distributions as well as the influence of exact-exchange admixtures on both were carried out leading to a deeper insight into physical mechanisms governing e.g. HFC in such compounds. Moreover, analyses of MO contributions and atomic SO contributions to the  $g$ -tensor were performed for a number of the larger complexes leading to in-depth understanding of differences and similarities between the different Mo<sup>V</sup> model complexes. Such an analysis of the different  $g$ -tensor contributions originating from couplings between different MOs is depicted exemplarily in Figure 5.15 for [MoOSL<sup>1</sup>]<sup>-</sup>. However, the results of these analyses will not be discussed any further here. Details can be found in Chapters 6.7 and 6.8.

**General Performance of the Computational Model** Considering a compromise between computational accuracy and computing time these studies on paramagnetic molybdenum complexes suggest to use hybrid DFT methods with about 30–40% exact-exchange admixture in a one-component perturbational unrestricted DFT treatment together with the developed 12s6p5d basis set for molybdenum and IGLO-II basis sets for all ligand atoms to compute the  $g$ - and molybdenum HFC tensors of large  $\text{Mo}^{\text{V}}$  complexes. The inclusion of SO corrections to the molybdenum HFC constants is very important for accurate calculations and the qualitative influence of higher-order SO effects on the  $g$ -tensor should always be kept in mind when discussing  $g$ -shifts (since an explicit computation in a two-component framework may not be feasible in most cases).

It is in principle possible to achieve good agreement of computed HFC tensors with experimental data employing the abovementioned methods. Usually isotropic HFC constants are underestimated by roughly 5% and anisotropic HFC constants are under- or overestimated by roughly 4–16% at the BPW91-40HF level including SO corrections to the HFC tensor. Isotropic SO correction terms amount to 14–17% of the first-order Fermi contact term and the size of the anisotropic orbital HFC correction term is 5–16% for around 40% exact-exchange admixture. Notably, there are also cases (e.g.  $[\text{MoO}_2\text{L}^1]^-$  and  $[\text{MoOSL}^1]^-$ ) where the SO corrections are even larger (around 25% for the isotropic HFC constants and up to 59% for the anisotropic couplings).

Comparison of the calculated (using around 30% HF exchange) and experimental  $g$ -tensors revealed that generally two of the computed components ( $g_{22}$  and  $g_{33}$ ) are in good or at least fair agreement with the experiment whereas the  $g$ -shift for the third component ( $g_{11}$ ) is considerably underestimated, i.e. insufficiently small / negative. This deviation could be attributed to higher-order relativistic effects.

Furthermore, it was also shown that computations may also provide relative and absolute tensor orientations in good agreement with experimental data – properties that are not straightforward to obtain experimentally. The orientation of the HFC tensor was in general not much affected by SO corrections for the systems under study except for the case of  $[\text{MoOSL}^1]^-$ .

### **Implications for Future Computational Studies of Molybdoenzymes**

This validation study may help to differentiate between (systematic) errors caused by the computational method and deviations from experimental values due to a

different / wrong molecular structure. Thus, in the future, DFT-based calculations may be employed to correlate experimental findings with structural information by selecting species with a specific constitution and conformation which possess computed EPR parameters in accordance with experimental EPR parameters (within the limits of inherent inaccuracies of the computational methods).

However, the deviations from experiment as well as the variance of the computed EPR parameters might not allow a distinction of very tiny conformational changes as is possible for organic radicals [4, 7, 118, 119] but in many cases not even the number or nature of molybdenum ligands in various intermediate states of the catalytic cycle of molybdenum enzymes are known [85–88, 120]. It seems very probable that one may indeed discriminate between such types of structural differences. Hence, in the future, the DFT methods used and validated in this work can and will be applied to systems of biological relevance where experimental data is available but the structure of the molybdenum binding site is not yet fully resolved (e.g. the  $\text{Mo}^{\text{V}}$  state of polysulfide reductase [120]).

## 5.4 Transition Metals in Biological Systems

### 5.4.1 Structural Characterization of a $\text{Mn}^{2+}$ Binding Site in the Hammerhead Ribozyme

EPR spectroscopic and quantum chemical calculations were employed to study the structure of a single high-affinity  $\text{Mn}^{2+}$  binding site in the hammerhead ribozyme (Figure 5.16) and to determine whether the binding site in frozen solution is identical to the A9–G10.1 site found to be occupied by  $\text{Mn}^{2+}$  in crystals (cf. also Section 6.3 and Ref. 6).

Metal ions are important for the structure and function of RNA [121–123]. While monovalent ions can promote the folding of RNA into its secondary structure, divalent metal ions such as  $\text{Mg}^{2+}$  are usually required for its folding into a biologically active tertiary structure. In addition to their structural roles, divalent metal ions have also been implicated as Lewis acid or base cofactors in the catalysis of chemical reactions by RNA [124, 125]. Substantial knowledge about RNA–metal ion interactions has come from the study of ribozymes. A major driving force for extensive structure–function investigations on ribozymes, in addition to study of how RNA catalyzes reactions, is the fact that the catalytic activity

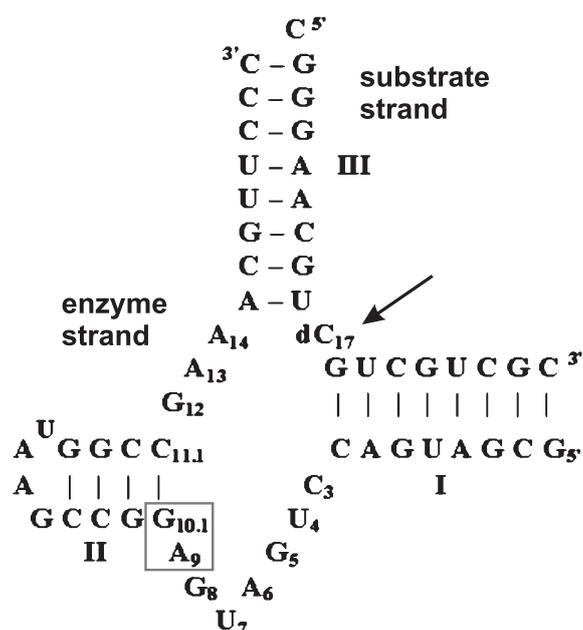


**Figure 5.16** Secondary structure of the hammerhead ribozyme. The cleavage site is indicated by the arrow. The position of the  $Mn^{2+}$  binding site as found in the crystal structure [126] is marked by the box.

can be used to monitor reaction conditions and chemical modifications. This fact has enabled chemical and biochemical experiments to probe the functional role of metal ions in RNA.

EPR spectroscopy can be used for the direct determination of metal ion coordination to RNA through the replacement of  $Mg^{2+}$  with the paramagnetic  $Mn^{2+}$  ion. This approach has been used by DeRose and coworkers to study metal ion binding to the hammerhead ribozyme in solution [127–130]. They deduced from their electron spin echo envelope modulation (ESEEM) and electron nuclear double resonance (ENDOR) studies that a nitrogen and a phosphorous nucleus are located in the coordination sphere of the  $Mn^{2+}$  ion and they speculated that this metal ion binding site may be situated between nucleotides A9 and G10.1 as found by X-ray crystallography [126] (cf. Figure 5.17).

Continuous wave (CW) EPR titration experiments have been used to show that the hammerhead ribozyme possesses a single high-affinity binding site with a  $K_d$ -value of  $4.3 \mu M$  at a salt concentration of 1 M NaCl [6]. Furthermore, a combination of ESEEM and HYSCORE (hyperfine sublevel correlation) experi-

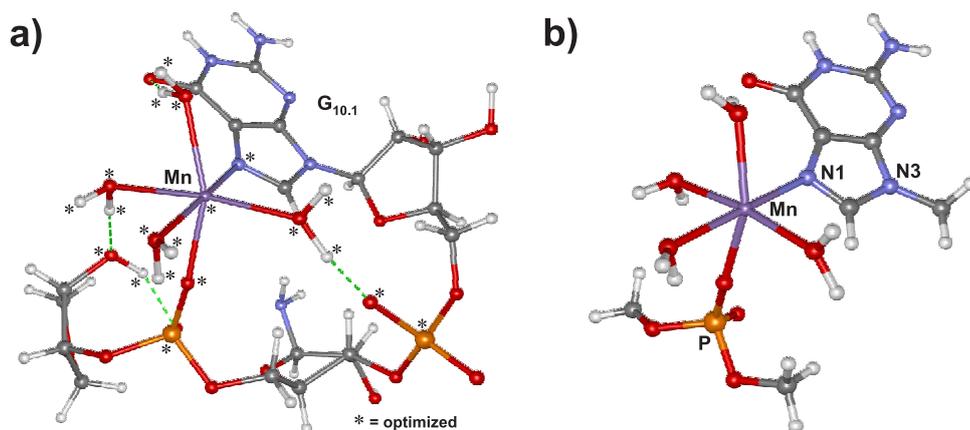


**Figure 5.17** a) Partially geometry-optimized (UHF/3-21G) large model of the  $\text{Mn}^{2+}$  binding site based on the crystal structure [126]. Water ligands were added to the open coordination sites of the  $\text{Mn}^{2+}$  ion and hydrogen atoms were included to saturate valences where necessary. Optimized atoms are marked by an asterisk; all other atoms were kept fixed. b) Reduced structure of the geometry-optimized model of the  $\text{Mn}^{2+}$  binding site, as used for the EPR parameter calculations.

ments revealed that the paramagnetic  $\text{Mn}^{2+}$  ion in this binding site is coupled to a single nitrogen atom with a quadrupole coupling constant  $\kappa$  of 0.7 MHz, an asymmetry parameter  $\eta$  of 0.4, and an isotropic hyperfine coupling constant of  $A_{\text{iso}}(^{14}\text{N})=2.3$  MHz. Since all of these EPR parameters are sensitive to the arrangement of the  $\text{Mn}^{2+}$  ligand sphere they can be used to determine the structure of the binding site.

To investigate whether the structure of the binding site in frozen solution (as studied by EPR) is the same as the structure of the A9–G10.1 binding site from the crystal structure [126] DFT calculations of EPR parameters (hyperfine and quadrupole couplings; see Chapter 3 for a description of EPR parameters) were performed for binding site models based on the structure of the  $\text{Mn}^{2+}$  site in the crystal (Figure 5.17). The results from these computations were then compared with the experimental data.

For the computation of EPR properties for the model in Figure 5.17b several density functionals were compared. The results of the calculations reveal a strong influence of the choice of functional on the isotropic manganese hyperfine coupling constant. On going from BP86 to BHPW91, the coupling varies by over 60%. This large effect is due to the increasing admixture of exact Hartree–Fock

exchange which leads to an increase of spin polarization effects and thus to an increase of negative spin density at the manganese nucleus and a larger negative isotropic hyperfine coupling constant. Such polarization mechanisms are especially important for paramagnetic transition metal centers in which the unpaired electrons are mainly located in d-type orbitals, as in high-spin  $\text{Mn}^{\text{II}}$  [131, 132]. The BHPW91 functional containing 50% exact exchange therefore yields a value for the isotropic manganese hyperfine coupling constant  $A_{\text{iso}}(^{55}\text{Mn})$  that comes closest to experimentally determined values for  $\text{Mn}^{\text{II}}$  complexes. In contrast to the  $A_{\text{iso}}(^{55}\text{Mn})$  hyperfine coupling, the  $^{14}\text{N}$  hyperfine and quadrupole parameters are less strongly altered by the different functionals and lie within the experimental error ranges for all methods used.

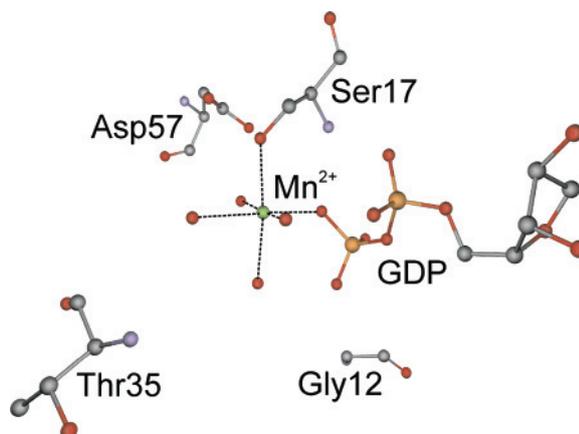
Computations with the BHPW91 density functional in combination with a 9s7p4d basis set [131] for manganese and the IGLO-II basis sets [83] for all other atoms yielded values of  $\kappa(^{14}\text{N})=+0.80$  MHz,  $\eta=0.324$ , and  $A_{\text{iso}}(^{14}\text{N})=+2.7$  MHz, in excellent agreement with the experimentally obtained EPR parameters. Since these parameters are very sensitive to geometrical changes, the results suggest that the binding site found in the crystal and in frozen solution are the same. Thus, a combined use of advanced EPR spectroscopic and DFT computational methods allowed to solve the structural problem posed at the beginning of this project.

### 5.4.2 Structural Characterization of the Metal Binding Site in Ras

High-frequency electron nuclear double resonance (ENDOR) spectroscopy was employed to gain structural information about the metal binding site of Ras. In this context quantum chemical calculations of EPR parameters were used to aid in the interpretation of the experimental data (cf. Section 6.6 and Ref. 8).

The human Ras (rat sarcoma) protein plays a central role as molecular switch in cellular signal transduction, regulating important processes such as differentiation, proliferation, and apoptosis of cells [133]. Specific oncogenic mutations in Ras proteins can be found in up to 30% of all human tumors [134]. Ras binds  $\text{Mg}^{2+} \cdot \text{GDP}$  and  $\text{Mg}^{2+} \cdot \text{GTP}$  with nanomolar to picomolar affinity in the active center if an excess of  $\text{Mg}^{2+}$  is present. With GTP bound, Ras interacts with effectors such as Raf-kinase or PI(3)-kinase and activates the corresponding signaling pathway. The signal is switched off when GTP is hydrolyzed to GDP either by

**Figure 5.18** Structure of the metal-GDP complex of Ras. The coordination of  $\text{Mn}^{2+} \cdot \text{GDP}$  in Ras is depicted from the X-ray structure of Ref. 136.



the intrinsic GTPase activity of Ras or by GTPase activating proteins (GAPs). The oncogenic variants contain point mutations, which block the GTPase activity in the presence and absence of GAP. This leads to the accumulation of Ras in the active form and thus contributes to tumor formation. Since the bound nucleotides control the activation state of the protein, a detailed knowledge of their interaction with the surroundings is of central importance.

Substitution of the diamagnetic  $\text{Mg}^{2+}$  ion with a paramagnetic  $\text{Mn}^{2+}$  ion allows to apply EPR spectroscopy to study the local structure of the metal binding site (cf. Figure 5.18). High-field EPR spectroscopy of the GDP complexes in solution displayed differences in the ligand sphere of the wild-type complex as compared to its oncogenic mutant Ras(G12V) [135]. Only three water ligands were found in the former with respect to four in the G12V mutant. For the first time, spectroscopic results showed a difference in the ligand sphere of the catalytic center between the wild-type and the oncogenic mutant of the protein-nucleotide complex in its inactive state. These differences were not detected in previous X-ray structures in the crystalline state. The question about the nature of the ligand that would replace one water molecule in the Ras(wt)·GDP complex is the starting point of this investigation. Two types of ligands would be the most likely candidates: an amino acid from the protein environment or a free phosphate ion.

High-frequency 94 GHz ENDOR spectroscopy in conjunction with selective isotope labeling was used to search for this “missing” ligand [8]. The  $^{31}\text{P}$  and  $^{13}\text{C}$  ENDOR spectra of the Ras(wt)·GDP complex and its oncogenic mutant Ras(G12V) did not show differences within the signal-to-noise and the ENDOR

**Table 5.3** Hyperfine tensor components for Ras•nucleotide complexes obtained from ENDOR studies and DFT calculations<sup>a</sup>

nucleus	nucleotide		$A_{11}$	$A_{22}$	$A_{33}$	$A_{\text{iso}}$	$T_{\perp}$
<sup>13</sup> C(Ser17)	GDP	exp.	-0.19	-0.19	+1.76	+0.46	-0.65
		calc.	+0.07	+0.19	+1.63	+0.62	-0.49
<sup>13</sup> C(Thr35)	GppNHp	exp.	-0.07	-0.07	+1.72	+0.62	-0.55
		calc.	-0.03	+0.13	+1.91	+0.67	-0.63
<sup>13</sup> C(Ser17)	GppNHp	exp.	+0.52	+0.52	+2.02	+1.02	-0.50
		calc.	+0.27	+0.42	+2.10	+0.93	-0.59

<sup>a</sup> All hyperfine values are given in MHz. For the experimental HFC constants, the sign of the largest tensor component was taken from the DFT calculations.

line width in frozen solution. Additional comparison with spectra of the non-hydrolyzable GTP analogue GppNHp did not give evidence that any of the proposed candidates is ligated to the Ras(wt)•GDP complex.

However, the interpretation and simulation of the experimental <sup>13</sup>C ENDOR spectra of Ras•GDP and Ras•GppNHp was not straightforward. Therefore, DFT computations of EPR parameters were performed for two structural models of the Mn<sup>2+</sup> binding site based on the crystal structures of the GDP [136] and GppNHp [137] complexes. The models consist of the Mn<sup>2+</sup> ion, the directly bound water molecules, the di- or triphosphate chain of the GDP or GTP (GppNHp), the Ser17 residue and in the case of the GppNHp complex also the directly ligated Thr35 residue. For these structures, DFT-based (BP86/3-21G(d)) partial optimizations of the H atom positions were performed. For the computation of the <sup>13</sup>C hyperfine coupling tensors (see also Chapter 3 for an explanation of HFC parameters), the B3PW91 hybrid functional was chosen together with a 9s7p4d basis set [131] for manganese and the IGLO-II basis sets [83] for all other atoms. The computed HFC values (Table 5.3) were used as starting parameters in the spectral simulation procedure enabling simulated spectra to be in very good agreement with the experimental ones (by only slightly varying the starting values). An important information that can easily be obtained from calculations but is not easily accessible experimentally are the signs of the HFC constants. Hence, the signs of the HFC constants were taken from the computations to fully determine the experimental HFC tensor. Since the couplings obtained from the DFT computations and the simulations of the EPR data are in very good agreement (Table 5.3), it

was furthermore possible to assign the different experimental HFCs to the specific  $^{13}\text{C}$  nuclei of the ligating amino acid residue(s) Ser17 as well as Ser17 and Thr35 for the GDP and GppNHp complexes, respectively.

The results of this study emphasize that DFT calculations of EPR parameters may be a valuable tool to interpret complicated experimental spectra and aid in the simulation of these data thus leading to a correlation of EPR spectra with molecular structure.

## References

- [1] Fritscher, J.; Hrobárik, P.; Kaupp, M. *J. Phys. Chem. B* **2007**, *Computational Studies of EPR Parameters for Paramagnetic Molybdenum Complexes. I. Method Validation on Small and Medium-Sized Systems*, accepted.
- [2] Fritscher, J.; Beyer, M.; Schiemann, O. *Chem. Phys. Lett.* **2002**, *364*, 393–401.
- [3] Fritscher, J.; Hrobárik, P.; Kaupp, M. *Inorg. Chem.* **2007**, *Computational Studies of EPR Parameters for Paramagnetic Molybdenum Complexes. II. Larger  $\text{Mo}^{\text{V}}$  Systems Relevant to Molybdenum Enzymes*, submitted.
- [4] Fritscher, J. *Phys. Chem. Chem. Phys.* **2004**, *6*, 4950–4956.
- [5] Beyer, M.; Fritscher, J.; Feresin, E.; Schiemann, O. *J. Org. Chem.* **2003**, *68*, 2209–2215.
- [6] Schiemann, O.; Fritscher, J.; Kisseleva, N.; Sigurdsson, S. T.; Prisner, T. F. *ChemBioChem* **2003**, *4*, 1057–1065.
- [7] Fritscher, J.; Artin, E.; Wnuk, S.; Bar, G.; Robblee, J. H.; Kacprzak, S.; Kaupp, M.; Griffin, R. G.; Bennati, M.; Stubbe, J. *J. Am. Chem. Soc.* **2005**, *127*, 7729–7738.
- [8] Bennati, M.; Hertel, M. M.; Fritscher, J.; Prisner, T. F.; Weiden, N.; Hofweber, R.; Spörner, M.; Horn, G.; Kalbitzer, H.-R. *Biochemistry* **2006**, *45*, 42–50.

- [9] Gatteschi, D.; Kahn, O.; Miller, J. S.; Palacio, F., Eds.; *Magnetic Molecular Materials*; NATO ASI Series Kluwer: Dordrecht, 1991.
- [10] Yamaguchi, K.; Okumura, M.; Maki, J.; Noro, T.; Namimoto, H.; Nakano, M.; Fueno, T.; Nakasuji, K. *Chem. Phys. Lett.* **1992**, *190*, 353–360.
- [11] Barone, V.; Bencini, A.; di Matteo, A. *J. Am. Chem. Soc.* **1997**, *119*, 10831–10837.
- [12] Kahn, O. *Molecular Magnetism*; VCH: Weinheim, 1. ed.; 1993.
- [13] Elschenbroich, C.; Schiemann, O.; Burghaus, O.; Harms, K. *J. Am. Chem. Soc.* **1997**, *119*, 7452–7457.
- [14] Barone, V.; di Matteo, A.; Mele, F.; de P. R. Moreira, I.; Illas, F. *Chem. Phys. Lett.* **1999**, *302*, 240–248.
- [15] Fritscher, J. *EPR-spektroskopische und quantentheoretische Untersuchungen an Nitroxid-Spinlabeln*, Diploma thesis, Johann Wolfgang Goethe-Universität Frankfurt am Main, 2000.
- [16] Noodleman, L. *J. Chem. Phys.* **1981**, *74*, 5737–5743.
- [17] Mitani, M.; Mori, H.; Takano, Y.; Yamaki, D.; Yoshioka, Y.; Yamaguchi, K. *J. Chem. Phys.* **2000**, *113*, 4035–4051.
- [18] McConnell, H. M. *J. Chem. Phys.* **1961**, *35*, 508–515.
- [19] Sinnecker, S.; Neese, F.; Noodleman, L.; Lubitz, W. *J. Am. Chem. Soc.* **2004**, *126*, 2613–2622.
- [20] Schöneboom, J. C.; Neese, F.; Thiel, W. *J. Am. Chem. Soc.* **2005**, *127*, 5840–5853.
- [21] Noodleman, L.; Case, D. A. *Adv. Inorg. Chem.* **1992**, *38*, 423–470.
- [22] Berliner, L. J., Ed.; *Biological Magnetic Resonance*; volume 14 Plenum Press: New York, 1998.
- [23] Strube, T.; Schiemann, O.; MacMillan, F.; Prisner, T. F.; Engels, J. W. *Nucleosides Nucleotides Nucleic Acids* **2001**, *20*, 1271–1274.

- [24] Edwards, T. E.; Okonogi, T. M.; Robinson, B. H.; Sigurdsson, S. T. *J. Am. Chem. Soc.* **2001**, *123*, 1527–1528.
- [25] Rabenstein, M. D.; Shin, Y.-K. *Proc. Natl. Acad. Sci. USA* **1995**, *92*, 8239–8243.
- [26] Edwards, T. E.; Okonogi, T. M.; Sigurdsson, S. T. *Chem. Biol.* **2002**, *9*, 699–706.
- [27] Wan, C.; Fiebig, T.; Kelley, S. O.; Treadway, C. R.; Barton, J. K.; Zewail, A. H. *Proc. Natl. Acad. Sci. USA* **1999**, *96*, 6014–6019.
- [28] Davis, W. B.; Hess, S.; Naydenova, I.; Haselsberger, R.; Ogrodnik, A.; Newton, M. D.; Michel-Beyerle, M.-E. *J. Am. Chem. Soc.* **2002**, *124*, 2422–2423.
- [29] Volodarsky, L. B.; Reznikov, V. A.; Ovcharenko, V. I. *Synthetic Chemistry of Stable Nitroxides*; CRC Press: Boca Raton, New York, 1994.
- [30] Kochi, J. K. *Free Radicals, Vols. 1 and 2*; Wiley Interscience: New York, 1973.
- [31] Improta, R.; Scalmani, G.; Barone, V. *Chem. Phys. Lett.* **2001**, *336*, 349–356.
- [32] Weil, J. A.; Bolton, J. R.; Wertz, J. E. *Electron Paramagnetic Resonance – Elementary Theory and Practical Applications*; Wiley: New York, 1994.
- [33] Barone, V. In *Recent Advances in Density Functional Methods*; Chong, D. P., Ed.; World Scientific Publ.: Singapur, 1995.
- [34] Řeha, D.; Kabeláč, M.; Ryjáček, F.; Šponer, J.; Šponer, J. E.; Elstner, M.; Suhai, S.; Hobza, P. *J. Am. Chem. Soc.* **2002**, *124*, 3366–3376.
- [35] Schweiger, A.; Jeschke, G. *Principles of Pulse Electron Paramagnetic Resonance*; Oxford University Press: Oxford, 2001.
- [36] Abragam, A. *The Principles of Nuclear Magnetism*; Oxford University Press: Oxford, New York, 1961.
- [37] Lucken, E. A. C. *Nuclear Quadrupole Coupling Constants*; Academic Press: London, New York, 1969.

- [38] Salzmann, R.; Kaupp, M.; McMahon, M. T.; Oldfield, E. *J. Am. Chem. Soc.* **1998**, *120*, 4771–4783.
- [39] Torrent, M.; Musaev, D. G.; Morokuma, K.; Ke, S.-C.; Warncke, K. J. *J. Phys. Chem. B* **1999**, *103*, 8618–8627.
- [40] Bailey, W. C. *Chem. Phys.* **2000**, *252*, 57–66.
- [41] Torrent, M.; Mansour, D.; Day, E. P.; Morokuma, K. *J. Phys. Chem. A* **2001**, *105*, 4546–4557.
- [42] Sicilia, E.; de Luca, G.; Chiodo, S.; Russo, N.; Calaminici, P.; Köster, A. M.; Jug, K. *Mol. Phys.* **2001**, *99*, 1039–1051.
- [43] Latosińska, J. N. *Int. J. Quant. Chem.* **2003**, *91*, 284–296.
- [44] Zhang, Y.; Gossman, W.; Oldfield, E. *J. Am. Chem. Soc.* **2003**, *125*, 16387–16396.
- [45] Gambarelli, S.; Mouesca, J.-M. *Inorg. Chem.* **2004**, *43*, 1441–1451.
- [46] Sinnecker, S.; Reijerse, E.; Neese, F.; Lubitz, W. *J. Am. Chem. Soc.* **2004**, *126*, 3280–3290.
- [47] Jeffrey, G. A.; Saenger, W. *Hydrogen Bonding in Biological Structures*; Springer-Verlag: Berlin, New York, 1991.
- [48] Nordlund, P.; Sjöberg, B.-M.; Eklund, H. *Nature* **1990**, *345*, 593–598.
- [49] Houseman, A. L. P.; Doan, P. E.; Goodin, D. B.; Hoffman, B. M. *Biochemistry* **1993**, *32*, 4430–4443.
- [50] Ito, N.; Phillips, S. E. V.; Yadav, K. D. S.; Knowles, P. F. *J. Mol. Biol.* **1994**, *238*, 794–814.
- [51] Iwata, S.; Saynovits, M.; Link, T. A.; Michel, H. *Structure* **1996**, *4*, 567–579.
- [52] Deacon, A.; Gleichmann, T.; Kalb (Gilboa), A. J.; Price, H.; Raftery, J.; Bradbrook, G.; Yarov, J.; Helliwell, J. R. *J. Chem. Soc., Faraday Trans.* **1997**, *93*, 4305–4312.

- [53] Stowell, M. H. B.; McPhillips, T. M.; Rees, D. C.; Soltis, S. M.; Abresch, E.; Feher, G. *Science* **1997**, *276*, 812–816.
- [54] Ferreira, K. N.; Iverson, T. M.; Maghlaoui, K.; Barber, J.; Iwata, S. *Science* **2004**, *303*, 1831–1838.
- [55] Lubitz, W.; Feher, G. *Appl. Magn. Reson.* **1999**, *17*, 1–48.
- [56] Astashkin, A. V.; Kawamori, A.; Kodera, Y.; Kuroiwa, S.; Akabori, K. *J. Chem. Phys.* **1995**, *102*, 5583–5588.
- [57] Deligiannakis, Y.; Hanley, J.; Rutherford, A. W. *J. Am. Chem. Soc.* **1999**, *121*, 7653–7664.
- [58] Licht, S.; Stubbe, J. In *Comprehensive Natural Products Chemistry*, Vol. 5; Barton, S. D.; Nakanishi, K.; Meth-Cohn, O.; Poulter, C. D., Eds.; Elsevier Science: New York, 1999.
- [59] Eklund, H.; Uhlin, U.; Farnegardh, M.; Logan, D. T.; Nordlund, P. *Prog. Biophys. Mol. Biol.* **2001**, *77*, 177–268.
- [60] Zhou, B. B. S.; Elledge, S. J. *Nature* **2000**, *408*, 433–439.
- [61] Thelander, L. *J. Biol. Chem.* **1973**, *248*, 4591–4601.
- [62] Brown, N. C.; Reichard, P. *J. Mol. Biol.* **1969**, *46*, 25–38.
- [63] Lin, A. N.; Ashley, G. W.; Stubbe, J. *Biochemistry* **1987**, *26*, 6905–6909.
- [64] Aberg, A.; Hahne, S.; Karlsson, M.; Larsson, A.; Ormo, M.; Ahgren, A.; Sjoberg, B. M. *J. Biol. Chem.* **1989**, *264*, 12249–12252.
- [65] Mao, S. S.; Johnston, M. I.; Bollinger, J. M.; Stubbe, J. *Proc. Natl. Acad. Sci. U.S.A.* **1989**, *86*, 1485–1489.
- [66] Mao, S. S.; Holler, T. P.; Bollinger, J. M., J.; Yu, G. X.; Johnston, M. I.; Stubbe, J. *Biochemistry* **1992**, *31*, 9744–9751.
- [67] Mao, S. S.; Holler, T. P.; Yu, G. X.; Bollinger, J. M., J.; Booker, S.; Johnston, M. I.; Stubbe, J. *Biochemistry* **1992**, *31*, 9733–9743.
- [68] Mao, S. S.; Yu, G. X.; Chalfoun, D.; Stubbe, J. *Biochemistry* **1992**, *31*, 9752–9759.

- [69] Brown, N. C.; Reichard, P. *J. Mol. Biol.* **1969**, *46*, 39–55.
- [70] Thelander, L.; Reichard, P. *Annu. Rev. Biochem.* **1979**, *48*, 133–158.
- [71] Kashlan, O. B.; Scott, C. P.; Lear, J. D.; Cooperman, B. S. *Biochemistry* **2002**, *41*, 462–474.
- [72] Kashlan, O. B.; Cooperman, B. S. *Biochemistry* **2003**, *42*, 1696–1706.
- [73] Sjöberg, B. M.; Reichard, P.; Graslund, A.; Ehrenberg, A. *J. Biol. Chem.* **1978**, *253*, 6863–6865.
- [74] Ge, J.; Yu, G.; Ator, M. A.; Stubbe, J. *Biochemistry* **2003**, *42*, 10071–10083.
- [75] Pereira, S.; Fernandes, P.; Ramos, M. J. *J. Comput. Chem.* **2004**, *25*, 227–237.
- [76] van der Donk, W. A.; Stubbe, J.; Gerfen, G. J.; Bellew, B. F.; Griffin, R. G. *J. Am. Chem. Soc.* **1995**, *117*, 8908–8916.
- [77] Thelander, L.; Larsson, B. *J. Biol. Chem.* **1976**, *251*, 1398–1405.
- [78] Sjöberg, B. M.; Graslund, A.; Eckstein, F. *J. Biol. Chem.* **1983**, *258*, 8060–8067.
- [79] Ator, M.; Salowe, S. P.; Stubbe, J.; Emptage, M. H.; Robins, M. J. *J. Am. Chem. Soc.* **1984**, *106*, 1886–1887.
- [80] Salowe, S. P.; Ator, M. A.; Stubbe, J. *Biochemistry* **1987**, *26*, 3408–3416.
- [81] Salowe, S. P.; Bollinger, J. M., Jr.; Ator, M.; Stubbe, J.; McCracken, J.; Peisach, J.; Samano, M. C.; Robins, M. J. *Biochemistry* **1993**, *32*, 12749–12760.
- [82] Wnuk, S. F.; Chowdhury, S. M.; Garcia, P. I.; Robins, M. J. *J. Org. Chem.* **2002**, *67*, 1816–1819.
- [83] Kutzelnigg, W.; Fleischer, U.; Schindler, M. In *NMR Basic Principles and Progress*, Vol. 23; Diehl, P.; Fluck, E.; Günther, H.; Kosfeld, R.; Seelig, J., Eds.; Springer Verlag: Berlin/Heidelberg, 1991.

- [84] Uhlin, U.; Eklund, H. *Nature* **1994**, *370*, 533–539.
- [85] Hille, R. *Chem. Rev.* **1996**, *96*, 2757–2816.
- [86] Hille, R. *Trends Biochem. Sci.* **2002**, *27*, 360–367.
- [87] Enemark, J. H.; Cooney, J. J. A.; Wang, J.-J.; Holm, R. H. *Chem. Rev.* **2004**, *104*, 1175–1200.
- [88] Sigel, A.; Sigel, H., Eds.; *Molybdenum and Tungsten: Their Roles in Biological Processes*; volume 39 of *Metal Ions in Biological Systems* Marcel Dekker: New York, 2002.
- [89] Mabbs, F. E.; Collison, D. *Electron Paramagnetic Resonance of d Transition Metal Compounds*; Elsevier Science: Amsterdam, 1992.
- [90] Bray, R. C. *Quart. Rev. Biophys.* **1988**, *21*, 299–329.
- [91] Astashkin, A. V.; Feng, C.; Raitsimring, A. M.; Enemark, J. H. *J. Am. Chem. Soc.* **2005**, *127*, 502–503.
- [92] Astashkin, A. V.; Hood, B. L.; Feng, C.; Hille, R.; Mendel, R. R.; Raitsimring, A. M.; Enemark, J. H. *Biochemistry* **2005**, *44*, 13274–13281.
- [93] Collison, D.; Eardley, D. R.; Mabbs, F. E.; Rigby, K.; Bruck, M. A.; Enemark, John H., W. P. A. *J. Chem. Soc., Dalton Trans.* **1994**, 1003–1011.
- [94] Peng, G.; Nichols, J.; McCullough Jr., E. A.; Spence, J. T. *Inorg. Chem.* **1994**, *33*, 2857–2864.
- [95] Wilson, G. L.; Greenwood, R. J.; Pilbrow, J. R.; Spence, J. T.; Wedd, A. G. *J. Am. Chem. Soc.* **1991**, *113*, 6803–6812.
- [96] Mader, M. L.; Carducci, M. D.; Enemark, J. H. *Inorg. Chem.* **2000**, *39*, 525–531.
- [97] Dhawan, I. K.; Enemark, J. H. *Inorg. Chem.* **1996**, *35*, 4873–4882.
- [98] Barnard, K. R.; Bruck, M.; Huber, S.; Grittini, C.; Enemark, J. H.; Gable, R. W.; Wedd, A. G. *Inorg. Chem.* **1997**, *36*, 637–649.

- [99] Cospers, M. M.; Neese, F.; Astashkin, A. V.; Carducci, M. D.; Raitsimring, A. M.; Enemark, J. H. *Inorg. Chem.* **2005**, *44*, 1290–1301.
- [100] Lim, B. S.; Willer, M. W.; Miao, M.; Holm, R. H. *J. Am. Chem. Soc.* **2001**, *123*, 8343–8349.
- [101] Patchkovskii, S.; Ziegler, T. *J. Phys. Chem A* **2001**, *105*, 5490–5497.
- [102] Malkina, O. L.; Vaara, J.; Schimmelpfennig, B.; Munzarová, M.; Malkin, V. G.; Kaupp, M. *J. Am. Chem. Soc.* **2000**, *122*, 9206–9218.
- [103] Kaupp, M.; Reviakine, R.; Malkina, O. L.; Arbuznikov, A.; Schimmelpfennig, B.; Malkin, V. G. *J. Comp. Chem.* **2002**, *23*, 794–803.
- [104] Sunil, K. K.; Harrison, J. F.; Rogers, M. T. *J. Chem. Phys.* **1982**, *76*, 3087–3097.
- [105] Swann, J.; Westmoreland, T. D. *Inorg. Chem.* **1997**, *36*, 5348–5357.
- [106] Li, W.; Hong, M.; Cao, R.; Kang, B.; Liu, H. *J. Magn. Reson.* **1999**, *138*, 80–88.
- [107] Patchkovskii, S.; Ziegler, T. *J. Chem. Phys.* **1999**, *111*, 5730–5740.
- [108] Patchkovskii, S.; Ziegler, T. *J. Am. Chem. Soc.* **2000**, *122*, 3506–3516.
- [109] Arbuznikov, A. V.; Kaupp, M.; Malkin, V. G.; Reviakine, R.; Malkina, O. L. *Phys. Chem. Chem. Phys.* **2002**, *4*, 5467–5474.
- [110] Astashkin, A. V.; Neese, F.; Raitsimring, A. M.; Cooney, J. J. A.; Bultman, E.; Enemark, J. H. *J. Am. Chem. Soc.* **2005**, *127*, 16713–16722.
- [111] Arbuznikov, A. V.; Vaara, J.; Kaupp, M. *J. Chem. Phys.* **2004**, *120*, 2127–2139.
- [112] Remenyi, C.; Reviakine, R.; Arbuznikov, A. V.; Vaara, J.; Kaupp, M. *J. Phys. Chem. A* **2004**, *108*, 5026–5033.
- [113] Ahlrichs, R.; May, K. *Phys. Chem. Chem. Phys.* **2000**, *2*, 943–945.
- [114] Hess, B. A.; Marian, C. M.; Wahlgren, U.; Gropen, O. *Chem. Phys. Lett.* **1996**, *251*, 365–371.

- [115] Schimmelpfennig, B. *AMFI, Atomic Spin–Orbit Mean-Field Integral Program*; Stockholms Universitet: Stockholm, Sweden, 1996.
- [116] Sunil, K. K.; Rogers, M. T. *Inorg. Chem.* **1981**, *20*, 3283–3287.
- [117] Malkin, I.; Malkina, O. L.; Malkin, V. G.; Kaupp, M. *J. Chem. Phys.* **2005**, *123*, 244103.
- [118] Kaupp, M. In *EPR of Free Radicals in Solids – Trends in Methods and Applications*, Vol. 10; Lund, A.; Shiotani, M., Eds.; Springer: 2003.
- [119] Improta, R.; Barone, V. *Chem. Rev.* **2004**, *104*, 1231–1254.
- [120] Prisner, T.; Lyubenova, S.; Atabay, Y.; MacMillan, F.; Kröger, A.; Klimmek, O. *J. Biol. Inorg. Chem.* **2003**, *8*, 419–426.
- [121] Gesteland, R. F.; Atkins, J. F. *The RNA World*; Cold Spring Harbor Laboratory Press: New York, 1993.
- [122] Eckstein, F.; Lilley, D. M., Eds.; *Nucleic Acids and Molecular Biology. Catalytic RNA. Vol. 10*; Springer: Berlin, 1997.
- [123] Doherty, E. A.; Doudna, J. A. *Annu. Rev. Biophys. Biomol. Struct.* **2001**, *30*, 457–475.
- [124] Hammann, C.; Lilley, D. M. *ChemBioChem* **2002**, *3*, 690–700.
- [125] Fedor, M. J. *Curr. Opin. Struct. Biol.* **2002**, *12*, 289–295.
- [126] Scott, W. G.; Murray, J. B.; Arnold, J. R. P.; Stoddard, B. L.; Klug, A. *Science* **1996**, *274*, 2065–2069.
- [127] Horton, T. E.; Clardy, D. R.; DeRose, V. J. *Biochemistry* **1998**, *37*, 18094–18101.
- [128] Morrissey, S. R.; Horton, T. E.; Grant, C. V.; Hoogstraten, C. G.; Britt, R. D.; DeRose, V. J. *J. Am. Chem. Soc.* **1999**, *121*, 9215–9218.
- [129] Morrissey, S. R.; Horton, T. E.; DeRose, V. J. *J. Am. Chem. Soc.* **2000**, *122*, 3473–3481.
- [130] Horton, T. E.; DeRose, V. J. *Biochemistry* **2000**, *39*, 11408–11416.

- 
- [131] Munzarová, M.; Kaupp, M. *J. Phys. Chem. A* **1999**, *103*, 9966–9983.
- [132] Munzarová, M. L.; Kubáček, P.; Kaupp, M. *J. Am. Chem. Soc.* **2000**, *122*, 11900–11913.
- [133] Wittinghofer, A.; Waldmann, H. *Angew. Chem., Int. Ed.* **2000**, *39*, 4192–4214.
- [134] Barbacid, M. *Annu. Rev. Biochem.* **1987**, *56*, 779–827.
- [135] Rohrer, M.; Prisner, T. F.; Brüggmann, O.; Käß, H.; Spörner, M.; Wittinghofer, A.; Kalbitzer, H. R. *Biochemistry* **2001**, *40*, 1884–1889.
- [136] Tong, L.; deVos, A.; Milburn, M.; Brunger, A.; Kim, S.-H. *J. Mol. Biol.* **1991**, *217*, 503–516.
- [137] Pai, E.; Krenkel, U.; Goody, R.; Kabsch, W.; Wittinghofer, A. *EMBO J.* **1990**, *9*, 2351–2359.



*“The more progress physical sciences make, the more they tend to enter the domain of mathematics, which is a kind of centre to which they all converge. We may even judge the degree of perfection to which a science has arrived by the facility with which it may be submitted to calculation.”*

A. QUETELET, 1796–1874

## Chapter 6

# Publications

In this chapter the publications that have thus far originated from the authors’ doctoral studies are presented. Each section starts with a very brief introduction to the different manuscripts presenting the persons that have been involved as well as the complete citation of the work. Furthermore, the main objectives and/or results of the publications are described in very few sentences to give a general overview of the different research topics.

It should be noted here that the manuscript presented in Sections 6.8 has been submitted to *Inorg. Chem.*

The contributions of the author of this Ph.D. thesis to the different publications shall be clarified in the following. In almost all cases the computational work contained was performed by the author of this thesis independently. Furthermore, he was always involved in the interpretation of the theoretical results in the context of the experimental (EPR) data. In case of the work presented in Section 6.5 the CCSD(T) calculations were performed by S. Kacprzak and M. Kaupp. The studies in Sections 6.7 and 6.8 were carried out in close collaboration with M. Kaupp. Here, P. Hrobárik was instructed by the author of this thesis and performed many of the computations under his supervision.

All publications where the author of this thesis is first author were to large parts written by himself. In all other cases those parts of the manuscript dealing with computational methods or results were written by himself.



## 6.1 Synthesis, Structure and Magnetic Properties of a Novel Nitroxide Biradical. Theoretical Investigation of the Exchange Mechanisms

These studies were performed by Jörg Fritscher, Mario Beyer and Olav Schiemann and were published in *Chem. Phys. Lett.* **2002**, *364*, 393–401. They are mainly dealing with the synthesis and characterization of a nitroxide biradical. Its magnetic properties were measured and different mechanisms (e.g. through-bond or through-space) leading to the observed (and computed) exchange interaction were analyzed theoretically employing broken symmetry DFT methods. Thus, this work contributes to a deeper understanding of exchange interactions and especially the correlation of exchange coupling with structural parameters.

The experimental analysis of the structural and magnetic properties of the nitroxide biradical was already part of the author's diploma thesis ("*EPR-spektroskopische und quantentheoretische Untersuchungen an Nitroxid-Spinlabeln*", Jörg Fritscher, Diploma Thesis, Frankfurt am Main, 2000).



*Due to copyright restrictions the article manuscript is not included in the online version of this work.*



## 6.2 Synthesis of Novel Aromatic Nitroxides as Potential DNA Intercalators. An EPR Spectroscopic and DFT Computational Study

These studies were performed by Mario Beyer, Jörg Fritscher, Emiliano Feresin and Olav Schiemann and were published in *J. Org. Chem.* **2003**, *68*, 2209–2215. They are mainly dealing with the synthesis of aromatic nitroxides and a detailed spectroscopical and DFT computational analysis of their hyperfine coupling constants as well as their delocalized spin density distributions. In conclusion, the properties of several of these radicals render them promising candidates as DNA-intercalating spin probes.



*Due to copyright restrictions the article manuscript is not included in the online version of this work.*



### 6.3 Structural Investigations of a High-Affinity Mn<sup>II</sup> Binding Site in the Hammerhead Ribozyme by EPR Spectroscopy and DFT Calculations. Effects of Neomycin B on Metal–Ion Binding

These studies were performed by Olav Schiemann, Jörg Fritscher, Natalja Kisseleva, Snorri Th. Sigurdsson and Thomas F. Prisner and were published in *ChemBioChem* **2003**, *4*, 1057–1065. Here, a single high-affinity Mn<sup>2+</sup> binding site in the hammerhead ribozyme was investigated in order to gain structural information about the coordination of the metal ion. By using ESEEM and HYSCORE experiments in combination with DFT calculations it was possible to conclude that the Mn<sup>2+</sup> binding site found in frozen solution is very likely to be the same as the one found by X-ray crystallography.



*Due to copyright restrictions the article manuscript is not included in the online version of this work.*



## 6.4 Influence of Hydrogen Bond Geometry on Quadrupole Coupling Parameters: A Theoretical Study of Imidazole–Water and Imidazole–Semiquinone Complexes

These studies were performed by Jörg Fritscher and were published in *Phys. Chem. Chem. Phys.* **2004**, *6*, 4950–4956. In this publication DFT methods were used to investigate the dependence of  $^{14}\text{N}$  quadrupole coupling tensors of (methyl-)imidazole on the hydrogen bond geometry for imidazole–water and methylimidazole–benzosemiquinone complexes. Pronounced influences of the intermolecular arrangement on the electric field gradients were found allowing a characterization of specific hydrogen bonding interactions to the amino group of imidazole or histidine. Furthermore, implications of these results for the interpretation of experimental QC data of biologically relevant semiquinone–histidine systems were discussed.



*Due to copyright restrictions the article manuscript is not included in the online version of this work.*



## 6.5 Structure of the Nitrogen-Centered Radical Formed During Inactivation of *E. coli* Ribonucleotide Reductase by 2'-Azido-2'-deoxyuridine-5'-diphosphate: Trapping of the 3'-Ketonucleotide

These studies were performed by Jörg Fritscher, Erin Artin, Stanislaw Wnuk, Galit Bar, John H. Robblee, Sylwia Kacprzak, Martin Kaupp, Robert G. Griffin, Marina Bennati and JoAnne Stubbe and were published in *J. Am. Chem. Soc.* **2005**, *127*, 7729–7738. In this work sophisticated chemical, biochemical, spectroscopical and computational methods were combined to elucidate the structure of the nitrogen-centered radical that is generated upon incubation of RNR with the stoichiometric inhibitor N<sub>3</sub>UDP. It was possible to interpret the EPR data with the help of DFT calculations for a number of possible model structures thus correlating the experimental findings with molecular structure parameters. Identification of the structure of the nitrogen-centered radical that had been subject to debate for more than 20 years has furthermore for the first time provided evidence for the trapping of a 3'-ketonucleotide in the reduction process catalyzed by RNR.

**Erratum** In the original publication (*J. Am. Chem. Soc.* **2005**, *127*, 7729–7738) some minor mistakes can be found in Figure 2 (protonation state of C462 during proposed CNS generation process). A corrected version of this figure is provided below.

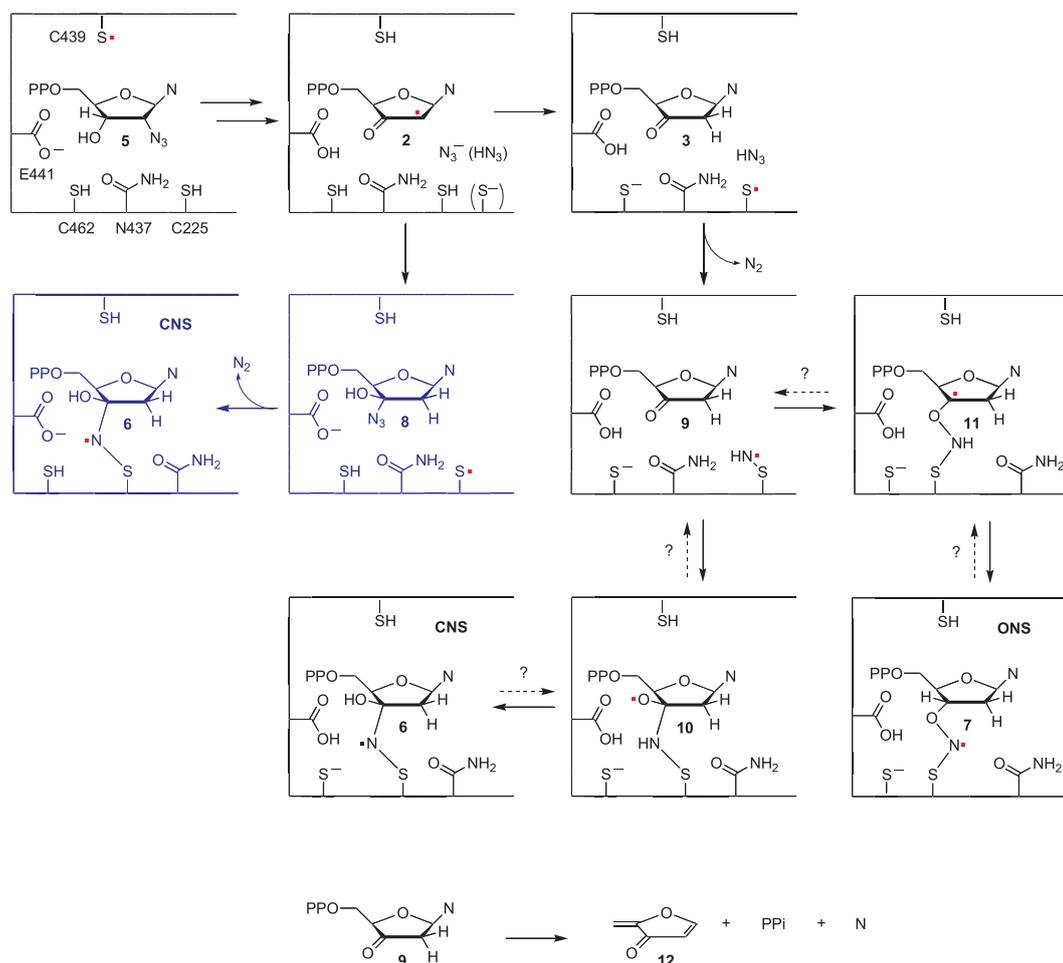


**Figure 2.** Two previously proposed structures for  $N^\bullet$  (6 and 7) and pathways for their generation. The blue pathway is proposed based on theoretical studies, while the black pathways were proposed by us. The major differences involve the timing of  $N_2$  release and the role of E441.

*Due to copyright restrictions the article manuscript is not included in the online version of this work.*



## 6.6 High-Frequency 94 GHz ENDOR Characterization of the Metal Binding Site in Wild-Type Ras•GDP and Its Oncogenic Mutant G12V in Frozen Solution

These studies were performed by Marina Bennati, Melanie M. Hertel, Jörg Fritscher, Thomas F. Prisner, Norbert Weiden, Roland Hofweber, Michael Spörner, Gudrun Horn and Hans-Robert Kalbitzer and were published in *Biochemistry* **2006**, *45*, 42–50. Here the  $\text{Mn}^{2+}$  binding sites in the wild-type Ras•GDP complex and the Ras(G12V)•GDP mutant were characterized using 94 GHz ENDOR spectroscopy. In this context DFT methods were employed to aid in the interpretation and simulation of the ENDOR spectra and to facilitate an assignment of the experimental hyperfine couplings to specific nuclei. In conclusion, no difference between the  $\text{Mn}^{2+}$  coordination spheres of the Ras(wt) and Ras(G12V) complexes could be detected.



*Due to copyright restrictions the article manuscript is not included in the online version of this work.*



## 6.7 Computational Studies of EPR Parameters for Paramagnetic Molybdenum Complexes.

### I. Method Validation on Small and Medium-Sized Systems

These studies were performed by Jörg Fritscher, Peter Hrobárik and Martin Kaupp and the corresponding manuscript has been accepted for publication in *J. Phys. Chem. B*. In this work a variety of DFT methods were tested for the calculation of EPR parameters of paramagnetic molybdenum systems such as the Mo atom, MoN as well as several Mo<sup>V</sup> complexes. A moderate-sized molybdenum basis set with a very good performance was developed and it was found that functionals incorporating 30-40% Hartree-Fock exchange yield the best results. Furthermore, the importance of spin-orbit corrections to the hyperfine coupling tensor and higher-order relativistic effects on the *g*-tensor were emphasized. It was found that the employed computational methods possess a very promising predictive power for the treatment of molybdenum species.



*Due to copyright restrictions the article manuscript is not included in the online version of this work.*



## 6.8 Computational Studies of EPR Parameters for Paramagnetic Molybdenum Complexes.

### II. Larger Mo<sup>V</sup> Systems Relevant to Molybdenum Enzymes

These studies were performed by Jörg Fritscher, Peter Hrobárik and Martin Kaupp and the corresponding manuscript has been submitted to *Inorg. Chem.* In this second part of the molybdenum validation study DFT methods were applied to a set of larger Mo<sup>V</sup> model complexes that were originally designed and synthesized to mimick molybdenum binding sites of various molybdoenzymes. In line with the results from the preceding work the good predictive power of DFT methods for the computation of EPR parameters of Mo<sup>V</sup> species was confirmed. Finally, implications for further computational studies of molybdoenzymes were discussed.



*Due to copyright restrictions the article manuscript is not included in the online version of this work.*



*“The electron is not as simple as it looks.”*

W. L. BRAGG, 1890–1971

## Chapter 7

# General Conclusions

In this thesis different EPR parameters such as electronic  $g$ -tensors  $\mathbf{g}$ , hyperfine coupling tensors  $\mathbf{A}$ , quadrupole coupling tensors  $\mathbf{Q}$  as well as exchange couplings  $J$  have been calculated for organic radicals or paramagnetic transition metal systems using modern DFT methods. Since all of these interaction parameters are strongly dependent on the structure of the paramagnetic species, a comparison of experimental EPR data with results from EPR parameter computations allows *a correlation between experimental spin Hamiltonian parameters and molecular structure*. Thus, valuable information about e.g. the constitution and conformation of radicals, their hydrogen bonding situation as well as metal complex symmetry and ligand sphere can be obtained using this approach. The structure–function paradigm of biology [1–3] renders this information even more important as it often leads to *further correlations of the three-dimensional molecular structures with the function of the systems under study*. This includes e.g. mechanisms of enzymatic catalytic reactions if paramagnetic intermediates are investigated or functions of proteins in a more general way if the investigation of the paramagnetic centers yields some information about protein structure. In this work DFT methods were applied to  $\text{Mn}^{2+}$  binding sites of the Ras protein and the hammerhead ribozyme,  $\text{Mo}^{\text{V}}$  complexes relevant to molybdoenzymes and a radical intermediate of the RNR inhibition reaction thereby demonstrating the large success and wide range of applicability of the quantum chemical methods.

Besides direct application to systems of biological relevance, another major advantage of quantum chemical calculations is the possibility to conduct systematic investigations of the interdependency of EPR parameters and structural features and to gain further insight into the physical origin of the observed mag-

netic interactions. Such type of data is usually not straightforward to obtain experimentally. In this thesis various examples like the systematic study of QC parameters of hydrogen-bonded imidazole complexes, the investigation of the properties of novel aromatic nitroxides as well as of the exchange mechanisms for a nitroxide biradical and the in-depth study of the magnetic properties of  $\text{Mo}^{\text{V}}$  complexes were presented. The results of these projects again emphasize the power of the theoretical methods.

Within this work it was furthermore shown what kind of demands concerning the computational model have to be considered when treating different kinds of systems and EPR parameters. Usually, best overall performance was achieved employing hybrid density functionals in combination with flexible (partially uncontracted) basis sets. The choice of the functional and basis set is critical for transition metal systems in general and calculations of Fermi contact interactions for all types of systems whereas the results of  $g$ - and dipolar HFC tensor computations for organic radicals are less dependent on the computational model. Often, one has to use increased amounts of Hartree–Fock exchange, include spin-orbit corrections to the HFC tensor or even employ relativistic two-component approaches for  $g$ -tensors in order to obtain accurate results for transition metals.

In conclusion, it was demonstrated in this thesis that the interplay of sophisticated experimental and quantum chemical methods represents a powerful and fruitful approach in the field of EPR spectroscopy and that it may be essential to employ EPR parameter computations to extract the full information content from EPR spectra. Therefore, great potential lies in future applications of DFT methods to the large number of systems where detailed and reliable experimental data is available but where an unequivocal correlation of these data with structural information is still lacking. Examples from research areas closely related to projects from this work are – amongst many others – e.g. quinone binding sites in different proteins such as bacterial reaction centers [4], other radical intermediates in RNR [5, 6] or molybdenum binding sites in enzymes such as polysulfide reductase [7].

However, it should also be mentioned in the end that a number of drawbacks and deficiencies are encountered when performing EPR parameter calculations using standard DFT approaches and/or when small or medium-sized models are used for much larger biological systems. One problem of standard DFT is that it cannot describe multi-determinantal low-spin states (e.g. open-shell singlet states). Thus, one has to use the broken symmetry formalism for

such electronic states. Different approximate formalisms can then be employed to extract exchange coupling constants or mapping procedures with spin projection methods have to be used to estimate other parameters such as HFC constants or  $g$ -values. Furthermore, a rigorous implementation of zero-field splittings in the DFT framework is not yet available even though a number of people are heavily working on this topic [8]. It was also shown (e.g. for  $\text{Mo}^{\text{V}}$  complexes in this work) that higher-order relativistic effects may be very important for an accurate prediction of  $g$ -shifts. These are e.g. accounted for in a recent two-component DFT treatment [9]. However, such methods can solely be applied to small systems due to their high computational efforts. Another property that is often difficult to predict quantitatively with DFT methods is the isotropic HFC constant. Thus, in all the described areas methodological developments are necessary in order to increase the reliability and predictive power of quantum chemical methods. This may either be achieved by efficiently including relevant algorithms and corrections in the DFT framework or by developing other methods that are comparable to DFT from the point of view of computational demands (e.g. the SORCI (spectroscopy oriented CI) approach for computations of  $J$  [10]).

Finally, it should also be mentioned that it is desirable and in many cases indispensable to include environmental effects into the EPR parameter calculations [11]. These may be solvent effects or influences by protein surroundings – e.g. different electrostatic influences on local electronic structures of paramagnetic centers and/or local structural changes due to constraints imposed by the surroundings. In this context continuum models [12, 13], QM/MM hybrid methods [13] or linear scaling approaches [13] can be used (cf. e.g. Ref. 14 for a recent example). Furthermore, it may also be interesting to include dynamic effects in the calculations to account for ensemble averaging leading to average EPR parameters in order to achieve better agreement with experimental values. Here, either Monte Carlo methods [13, 15, 16], classical molecular dynamics (MD) approaches [13, 15, 16] or Car–Parrinello (CP) quantum dynamics [17, 18] may be applied (cf. e.g. Refs. 19 and 20 for recent examples).

It seems to be very promising for the future that further methodological developments considering the abovementioned points together with increased computer speed will allow even more precise theoretical EPR parameter predictions and enlarge the field of applicability of quantum chemical methods. It is the hope that this would lead to an even more fruitful interaction of experiment and theory.

## References

- [1] Moulton, J.; Melamud, E. *Curr. Opin. Struct. Biol.* **2000**, *10*, 384–389.
- [2] Wright, P. E.; Dyson, H. J. *J. Mol. Biol.* **1999**, *293*, 321–331.
- [3] Uversky, V. N. *Cell. Mol. Life Sci.* **2003**, *60*, 1852–1871.
- [4] Lubitz, W.; Feher, G. *Appl. Magn. Reson.* **1999**, *17*, 1–48.
- [5] Persson, A. L.; Eriksson, M.; Katterle, B.; Pötsch, S.; Sahlin, M.; Sjöberg, B. M. *J. Biol. Chem.* **1997**, *272*, 31533–31541.
- [6] Lawrence, C. C.; Bennati, M.; Obias, H. V.; Bar, G.; Griffin, R. G.; Stubbe, J. *Proc. Natl. Acad. Sci. U.S.A.* **1999**, *96*, 8979–8984.
- [7] Prisner, T.; Lyubenova, S.; Atabay, Y.; MacMillan, F.; Kröger, A.; Klimmek, O. *J. Biol. Inorg. Chem.* **2003**, *8*, 419–426.
- [8] Neese, F. In *Calculation of NMR and EPR Parameters*; Kaupp, M.; Malkin, V. G.; Bühl, M., Eds.; Wiley-VCH: Weinheim, 2004.
- [9] Malkin, I.; Malkina, O. L.; Malkin, V. G.; Kaupp, M. *J. Chem. Phys.* **2005**, *123*, 244103.
- [10] Neese, F. *J. Chem. Phys.* **2003**, *119*, 9428–9443.
- [11] Improta, R.; Barone, V. *Chem. Rev.* **2004**, *104*, 1231–1254.
- [12] Ciofini, I. In *Calculation of NMR and EPR Parameters*; Kaupp, M.; Malkin, V. G.; Bühl, M., Eds.; Wiley-VCH: Weinheim, 2004.
- [13] Cramer, C. J. *Essentials of Computational Chemistry: Theories and Models*; Wiley: Chichester, 2002.
- [14] Schöneboom, J. C.; Neese, F.; Thiel, W. *J. Am. Chem. Soc.* **2005**, *127*, 5840–5853.
- [15] Allen, M. P.; Tildesley, D. J. *Computer Simulation of Liquids*; Clarendon Press: Oxford, 1987.
- [16] Frenkel, D.; Smit, B. *Understanding Molecular Simulation: From Algorithms to Applications*; Academic Press: San Diego, 2002.

- 
- [17] Car, R.; Parrinello, M. *Phys. Rev. Lett.* **1985**, *55*, 2471–2474.
- [18] Laasonen, K.; Sprik, M.; Parrinello, M.; Car, R. *J. Chem. Phys.* **1993**, *99*, 9080–9089.
- [19] Asher, J. R.; Doltsinis, N. L.; Kaupp, M. *J. Am. Chem. Soc.* **2004**, *126*, 9854–9861.
- [20] Asher, J. R.; Doltsinis, N. L.; Kaupp, M. *Magn. Reson. Chem.* **2005**, *43*, S237–S247.



# Appendix A

## Abbreviations

ACM	adiabatic connection method
AMFI	atomic (one-center) mean-field approximation to SO integrals
AO	atomic orbital
BITPAN	1,8-bis(3-ethynyl-2,2,5,5-tetramethyl-3-pyrroline-1-oxyl)-naphthalene
bRC	bacterial reaction center
BO	Born–Oppenheimer
BP	Breit–Pauli
BS	broken symmetry
CC	coupled cluster
CCSD(T)	coupled cluster theory with single and double excitations and a perturbative treatment of triple excitations
CGTO	contracted Gaussian-type orbital
CI	configuration interaction
CNDO	complete neglect of differential overlap
CP	Car–Parinello
CP(SCF)	coupled-perturbed (SCF)
CW	continuous wave
DF	density functional
DFT	density functional theory
DKH	Douglas–Kroll–Hess

---

DNA	deoxyribonucleic acid
DZ	double zeta
ECP	effective core potential
EFG	electric field gradient
ELDOR	electron–electron double resonance
ENDOR	electron–nuclear double resonance
EPR	electron paramagnetic resonance
ESEEM	electron spin-echo envelope modulation
ESR	electron spin resonance
GAP	GTPase activating protein
GD(T)P	guanosine-5'-di(tri)phosphate
GGA	generalized gradient approximation
GIAO	gauge-including atomic orbitals
GTO	Gaussian-type orbital
HF	Hartree–Fock
HFC	hyperfine coupling
HFCC	hyperfine coupling constant
HMO	Hückel molecular orbital
HOMO	highest occupied molecular orbital
HYSORE	hyperfine sublevel correlation
IGLO	individual gauge for localized orbitals
INDO	intermediate neglect of differential overlap
IR	infra-red
KS	Kohn–Sham
LCAO	linear combination of atomic orbitals
L(S)DA	local (spin) density approximation
MCSCF	multiconfiguration self-consistent field
MD	molecular dynamics
MO	molecular orbital
MP( <i>n</i> )	Møller–Plesset perturbation theory (of order <i>n</i> )
MRCI	multi-reference configuration interaction

---

NMR	nuclear magnetic resonance
NQR	nuclear quadrupole resonance
N <sub>3</sub> U(N)DP	2'-azido-2'-deoxyuridine(nucleoside)-5'-diphosphate
PGTO	primitive Gaussian-type orbital
PSII	photosystem II
QC	quadrupole coupling
QCC	quadrupole coupling constant
QED	quantum electrodynamics
QM/MM	quantum mechanics/molecular mechanics
R	restricted
Ras	rat sarcoma (protein)
RNA	ribonucleic acid
RNR	ribonucleotide reductase
RO	restricted open
SCF	self-consistent field
SH	spin Hamiltonian
SO(C)	spin-orbit (coupling)
SOMO	singly occupied molecular orbital
SOO	spin-other orbit
SORCI	spectroscopy oriented configuration interaction
SOS	sum-over-states
SQUID	superconducting quantum interference device
STO	Slater-type orbital
TF(D)	Thomas-Fermi(-Dirac)
TPA	3-ethinyl-2,2,5,5-tetramethyl-3-pyrroline-1-oxyl
TZ(VP)	triple zeta (valence polarized)
U	unrestricted
UV/Vis	ultra-violet/visible
VB	valence bond
ZFS	zero-field splitting
ZORA	zeroth-order regular approximation



# Appendix B

## Constants and Conversion Factors

A very good collection of all physical constants can be found at:

<http://physics.nist.gov/cuu/Constants/>

Conversion factors for energy equivalents are listed at:

<http://physics.nist.gov/cuu/Constants/energy.html>

Avogadro number	$N_A$	$= 6.022137 \cdot 10^{23} \text{ mol}^{-1}$
Bohr magneton	$\beta_e$	$= 9.274015 \cdot 10^{-24} \text{ A m}^2$
Boltzmann constant	$k$	$= 1.380658 \cdot 10^{-23} \text{ J K}^{-1}$
Electron rest mass	$m_e, m$	$= 9.109390 \cdot 10^{-31} \text{ kg}$
Elementary charge	$e$	$= 1.602177 \cdot 10^{-19} \text{ C}$
Fine structure constant	$\alpha$	$= 7.297353 \cdot 10^{-3}$
	$\alpha^{-1}$	$= 137.035999$
Free electron $g$ -value	$g_e$	$= 2.0023193043718$
Gas constant	$R$	$= 8.314472 \text{ J mol}^{-1} \text{ K}^{-1}$
Nuclear magneton	$\beta_N$	$= 5.050787 \cdot 10^{-27} \text{ A m}^2$
Permeability of vacuum	$\mu_0$	$= 1.256637 \cdot 10^{-6} \text{ V s A}^{-1} \text{ m}^{-1}$
Permittivity of vacuum	$\epsilon_0$	$= 8.854188 \cdot 10^{-12} \text{ A s V}^{-1} \text{ m}^{-1}$
Planck constant	$h$	$= 6.626076 \cdot 10^{-34} \text{ J s}$
	$\hbar$	$= h/2\pi = 1.054589 \cdot 10^{-34} \text{ J s}$
Proton/electron mass ratio	$m_p/m_e$	$= 1836.15$
Proton rest mass	$m_p$	$= 1.672623 \cdot 10^{-27} \text{ kg}$
Speed of light (vacuum)	$c$	$= 299792458 \text{ m s}^{-1}$

1 Hartree	=	$4.359744 \cdot 10^{-18}$	J
1 Hartree	=	627.5095	kcal/mol
1 Hartree	=	219474.6314	$\text{cm}^{-1}$
1 Hartree	=	27.211385	eV
1 eV	=	23.06037	kcal/mol
1 eV	=	8065.478	$\text{cm}^{-1}$
1 J	=	$7.242963 \cdot 10^{22}$	K
1 J	=	$5.386117 \cdot 10^{22}$	T
1 T	=	$1.856625 \cdot 10^{-23}$	J
$10^{-4} \text{ cm}^{-1}$	=	2.9979	MHz
1 G	=	2.802	MHz
1 G	=	$10^{-4}$	T
1 Bohr	=	0.5291772083	Å

# Acknowledgment

First of all I would like to express my gratitude to Prof. Thomas F. Prisner for the opportunity to work in his group and under his supervision. He provided excellent working conditions and all kinds of scientific and financial support necessary for carrying out my doctoral studies. Furthermore, he always encouraged me to work independently and offered me the possibility to accomplish my studies with a lot of freedom. Thanks to him I was able to get a deep insight into modern EPR methods.

Next, I am thankful to Prof. Martin Kaupp for his continuous help, for inspiring discussions and his patience in answering all of my questions as well as for collaboration in the molybdenum project where he introduced me to ‘higher levels’ of the interpretation of computational chemistry data. Thanks also for the opportunity to come to Würzburg several times.

Dr. Olav Schiemann is thanked for his constant support during my whole doctoral studies and for nice and fruitful collaboration at the beginning of my Ph.D. work as well as for interesting and motivating discussions – although you would have liked to get ‘rid’ of me much earlier...

I am grateful to Dr. Marina Bennati for inspiring debates (especially about rotations, coordinate systems, Euler angles and similar ‘confusing’ stuff) and much obliged to her for encouraging me to apply for the *Ernst award*. I would also like to thank her and Prof. JoAnne Stubbe for the beautiful RNR project.

Dr. Roman Reviakine must be thanked for all the technical support with MAG and Peter Hrobárik for the nice time during his stays in Frankfurt (‘molybdenum and beer hours’) and his collaboration in the molybdenum project.

I am thankful to Dr. Rainer Hegger who has always been helpful in many different situations but who was of course often my ‘last rescue’ concerning problems with linux administration and networking. PD Dr. Thomas Müller, Prof. Frank Neese, Dr. Andreas Dreuw and Prof. Max Holthausen are thanked for their

help with Gaussian, Q-Chem, ORCA,... and all kinds of general computational chemistry questions.

Thanks to Olga Frolov and Maja Kobus for their help during their (extended) ‘Arbeitskreispraktika’ – you were the only ones brave enough to deal with the computer mysteries and EPR in parallel.

Without Sigrid Kämmerer I would have spent many more hours in libraries and in front of copy machines and Hildegard Mathis was always very flexible when it came to planning holidays.

I would like to thank Dr. Marina Bennati, Bela Bode, Dr. Stéphane Grimaldi, Melanie Hertel, Natalie Kisseleva ( $h = Q \cdot [12 + (3s/8)]$ ), Sevdalina Lyubenova, Dr. Fraser MacMillan, Dr. ‘Doc’ Thorsten Maly, Dr. Veronica Mugnaini, Dr. Olav Schiemann and Dr. Axel Weber for the nice time, interesting discussions, conference evenings and bed-sharing, beer hours, computer admin sessions, whisky and cigars, music, wine and cooking debates,... All of this made work really enjoyable.

Furthermore, my work was supported by the *Fonds der Chemischen Industrie* (Doktorandenstipendium), the *Deutsche Forschungsgemeinschaft* (SFB 472 and 579, SPP 1071), the *Hermann-Willkomm-Stiftung*, the *Fachgruppe Magnetische Resonanz* of the GDCh and the *Frankfurt Center for Scientific Computing*.

I am much obliged to my parents who laid the basis for my ‘scientific career’ by enabling me to study chemistry without having to bother about unimportant things. Thanks for your support.

I am also grateful to my parents-in-law for providing everything you need to finish your dissertation: a place to work, babysitting (=time), lunch,...

This thesis is especially dedicated to my wife Dorothee and my daughter Philine Marie who have – fortunately – distracted me from my work at every opportunity thereby giving me the strength to carry on. However, without knowing much about physics they have managed to undermine one of the basic principles of the theory of relativity by providing me with a *unique frame of reference!*

PS: ‘Grüner Wackelpudding mit Vanillesauce’ should certainly be on the first place of the all time greatest ranking for mensa desserts. Sorry, Thorsten!

# Lebenslauf

## **Persönliche Daten**

Vorname: Jörg  
Nachname: Fritscher  
Adresse: Kettelerstr. 11  
63579 Freigericht–Neuses  
Deutschland  
Geburtsdatum: 22.01.1975  
Geburtsort: Fulda  
Nationalität: deutsch  
Familienstand: verheiratet mit Dorothee Fritscher, geb. Dornhecker,  
seit September 2003  
Kinder: Philine Marie Fritscher, geb. am 20.02.2005  
Eltern: Leo Fritscher und Doris Fritscher, geb. Acker  
Geschwister: Katja Fritscher  
Judith Fritscher  
Johanna Fritscher

## **Ausbildung (Schule)**

1981 – 1985 Grundschule, Hasselroth–Neuenhaßlau  
1985 – 1994 Kopernikusschule Freigericht (Europaschule), Freigericht–Somborn  
(Gymnasium und Gymnasiale Oberstufe)  
1994 Abitur

## **Zivildienst**

1994 – 1995 Altersheim, Rodenbach

### Ausbildung (Universität)

- 1995 – 2000      Chemiestudium an der Johann Wolfgang Goethe-Universität in Frankfurt a. M.
- 2000              Diplomarbeit “*Quantenchemische und EPR-spektroskopische Untersuchungen von Nitroxid-Spinlabeln*”  
in der Arbeitsgruppe von Prof. T. F. Prisner
- 2000 – 2006      Doktorarbeit in der Arbeitsgruppe von Prof. T. F. Prisner

### Stipendien und Auszeichnungen

- 2001 – 2003      Doktorandenstipendium  
des Fonds der Chemischen Industrie
- 2005              *Ernst Award* der Fachgruppe Magnetische Resonanz  
der GDCh

### Akademische Lehrer

N. Auner, M. Bennati, B. Brutschy, F. J. Comes, E. Egert, J. W. Engels, H. Falsold, S. Glaser, M. Göbel, C. Griesinger, K. Hensen, M. C. Holthausen, B. Lüthi, M. Kaupp, W. Koch, G. Kohlmaier, B. Kolbesen, P. Pickel, T. F. Prisner, D. Rehm, E.-A. Reinsch, O. Schiemann, F. Schüth, H. Schwalbe, and G. Stock

### Publikationsliste

1. Fritscher, J.; Beyer, M.; Schiemann, O. *Chem. Phys. Lett.* **2002**, *364*, 393–401.
2. Schiemann, O.; Fritscher, J.; Kisseleva, N.; Sigurdsson, S. T.; Prisner, T. F. *ChemBioChem* **2003**, *4*, 1057–1065.
3. Beyer, M.; Fritscher, J.; Feresin, E.; Schiemann, O. *J. Org. Chem.* **2003**, *68*, 2209–2215.
4. Schiemann, O.; Plackmeyer, J.; Fritscher, J.; Pebler, J.; Elschenbroich, C. *Appl. Magn. Reson.* **2004**, *26*, 171–182.
5. Fritscher, J. *Phys. Chem. Chem. Phys.* **2004**, *6*, 4950–4956.

6. Fritscher, J.; Artin, E.; Wnuk, S.; Bar, G.; Robblee, J. H.; Kacprzak, S.; Kaupp, M.; Griffin, R. G.; Bennati, M.; Stubbe, J. *J. Am. Chem. Soc.* **2005**, *127*, 7729–7738.
7. Bennati, M.; Hertel, M. M.; Fritscher, J.; Prisner, T. F.; Weiden, N.; Hofweber, R.; Spörner, M.; Horn, G.; Kalbitzer, H.-R. *Biochemistry* **2006**, *45*, 42–50.
8. Fritscher, J.; MacMillan, F.; Prisner, T. F. *Appl. Magn. Reson.* **2006**, *30*, 251–268.
9. Fritscher, J.; Hrobárik, P.; Kaupp, M. *J. Phys. Chem. B* **2007**, *Computational Studies of EPR Parameters for Paramagnetic Molybdenum Complexes. I. Method Validation on Small and Medium-Sized Systems*, accepted.
10. Fritscher, J.; Hrobárik, P.; Kaupp, M. *Inorg. Chem.* **2007**, *Computational Studies of EPR Parameters for Paramagnetic Molybdenum Complexes. II. Larger Mo<sup>V</sup> Systems Relevant to Molybdenum Enzymes*, submitted.